CHAPTER THIRTY-SEVEN

ACTINIDE CHALCOGENIDE COMPOUNDS

Emmanouil Manos, Mercouri G. Kanatzidis, and James A. Ibers

37.1 INTRODUCTION

This chapter describes the preparation, structures, and physical properties of the known binary, ternary, and quaternary actinide chalcogenide compounds. In discussing structures we rely almost exclusively on X-ray or neutron diffraction results from single crystals rather than from powders. Owing to the dearth of measurements on single crystals, in discussions of physical properties we must rely as well on the results from powders. In doing so we note the caveat that physical properties of solid-state materials are often very sensitive to the presence of impurities, defects, and related phenomena that are often difficult to detect by powder diffraction methods. For convenience the article is subdivided according to composition (e.g. binary, ternary and multinary compounds).

37.2 BINARY ACTINIDE CHALCOGENIDES

The binary Th and U chalcogenides have been discussed earlier in Sections 3.7.5 and 5.7.5 of this series, respectively. A number of binary chalcogenides of Np and Pu have been reported, many on the basis of the similarities of their X-ray powder diffraction patterns to those of known U compounds. Table 37.1 summarizes the known, structurally-characterized binary actinide chalcogenide stoichiometries, along with selected references. We will discuss these stoichiometries in turn.

Table 37.1 *Binary chalcogenide compounds of An = Th[a], U[b], Np, and Pu.*

	Th	*U*	*Np*	*Pu*	*Representative references*
An_4Q_3		S			Zumbusch, 1940
AnQ	S, Se, Te	S, Se, Te	S, Se	S, Se, Te	d'Eye *et al.*, 1952; d'Eye and Sellman, 1954; Ferro, 1955; Kruger and Moser, 1967; Olsen *et al.*, 1988; Dabos-Seignon *et al.*, 1990; Wastin *et al.*, 1995
AnQ_{Hx}		S, Se, Te			Noel and le Marouille, 1984; Beck and Dausch, 1988, 1989a
$An_{3-x}Q_4$		Se, Te			Szytula and Suski, 1973; Noel, 1985b; Shlyk *et al.*, 1995a
An_2Q_3	S, Se, Te	S, Se, Te	S, Se	S, Se, Te	Zachariasen, 1949a; Khodadad, 1961; Tougait *et al.*, 1998a; Tougait *et al.*, 2001
An_3Q_5		S, Se, Te	S		Moseley *et al.*, 1972; Potel *et al.*, 1972; Tougait *et al.*, 1998c; Tougait *et al.*, 2001;
An_7Q_{12}	S, Se	Se, Te			Zachariasen, 1949c; d'Eye, 1953;Tougait *et al.*, 1998b
AnQ_{2-x}		S, Te			Haneveld and Jellinek, 1969;Noel *et al.*, 1996
AnQ_2	S, Se, Te	S, Se, Te		S, Se, Te	d'Eye, 1953; Marcon and Pascard, 1966; Suski *et al.*, 1972;Mooney-Slater, 1977; Amoretti *et al.*, 1984; Beck and Dausch, 1989a; Daoudi *et al.*, 1996a; Noel *et al.*, 1996; Kohlmann and Beck, 1997
An_2Q_5	S, Se	Te	S	S	Noel and Potel, 1982; Kohlmann and Beck, 1999;Stöwe, 1996b; Tougait *et al.*, 1997a
AnQ_3	Te	S, Se, Te	S, Se	Te	Ben Salem *et al.*, 1984; Noel and Levet, 1989; Stöwe, 1996a; Kwak *et al.*, 2006
AnQ_{3+x}		Te			Stöwe, 1997
AnQ_5		Te			Noel, 1984;Noel 1985a

[a]Also see Section 3.7.5.
[b]also see Section 5.7.5.

37.2.1 The U_4S_3 compound

From X-ray powder diffraction data U_4S_3 has been described as a "defect" AnS phase (An = actinide) wherein the primitive cubic cell, similar to that of US, has an empty body center (normally filled in US) (Zumbusch, 1940). This creates a structure similar to that of perovskite with octahedra of US_6 that are corner-shared with U atoms in the square-planar open faces as if they were face-centered on a cube (Fig. 37.1). The U−S distance is 2.747(1) Å.

37.2.2 The actinide monochalcogenides AnQ

The phase diagrams of the binary actinide chalcogenides are particularly rich, showing regions of solid solutions near stoichiometric $AnQ_{1\pm x}$ and $AnQ_{2\pm x}$, where throughout this chapter we use the symbol Q = S, Se, or Te. The formal oxidation states of the actinides in these compounds are open to question and have been the subject of EXAFS studies that compare the binary oxides with their chalcogenide counterparts (Conradson *et al.*, 2004a; Conradson *et al.*, 2004b; Conradson *et al.*, 2005).

Actinide monochalcogenides have been extensively studied. Nearly all crystallize in the rock-salt (NaCl) structure type. Interatomic distances within the AnQ_6 octahedra are 2.841 Å in ThS, 2.742 Å in US, 2.768 Å in PuS, (Zachariasen, 1949d), 3.195 Å in UTe, and 3.089 Å in PuTe (Kruger and Moser, 1967). ThTe forms in the CsCl structure type. The Th−Te distance in the $ThTe_8$ cube is 3.312 Å (d'Eye and Sellman, 1954; Haessler *et al.*, 1976).

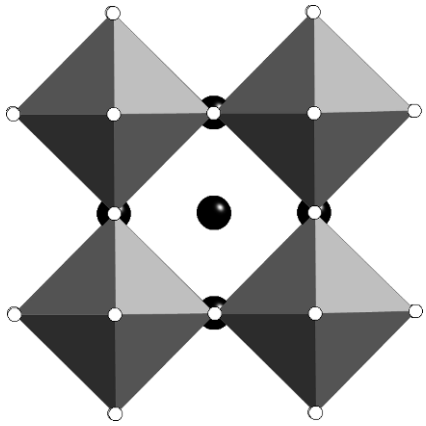

Fig. 37.1 *Structure of U_4S_3 (U: black balls; US_6: gray polyhedra; S: white balls).*

The synthesis of single crystals of US is noteworthy (Van Lierde and Bressers, 1966). It was carried out by the reaction of U metal powder with the stoichiometric amount of H_2S gas at 500°C according to

$$U_{(s)} + H_2S_{(g)} \rightarrow {}^1\!/_2US_{2(s)} + {}^1\!/_2U_{(s)} \tag{37.1}$$

This mixture then was reacted at 1,900°C to give US according to

$${}^1\!/_2US_{2(s)} + {}^1\!/_2U_{(s)} \rightarrow US_{(s)} \tag{37.2}$$

Because the melting points of US_2 (1,560°C) and US (2,460°C) are very different, US can be prepared in single-crystal form by slow decomposition of a melt of US_{1+x}. To do this, reaction (37.1) is carried out with about 15% H_2S in excess to give a black nonreactive powder with a low melting point consisting of a complex mixture of uranium polysulfides and free U. The temperature then is raised to 1,700°C; reaction (37.2) proceeds slowly and is mainly controlled by the evaporation of excess S. This evaporation first occurs on the free surface of the melt, where a few US crystals are nucleated. Large crystals with a gold–silver luster develop from the surface inside the melt, up to complete transformation into US as the temperature is raised further to 1,900°C.

It is interesting that US was studied as a unique form of nuclear fuel in the 1960s and 1970s, as well as an additive to uranium carbide ceramics for fuel elements and as molten salts for nuclear fuel (Neimark and Carlander, 1964; Handwerk *et al.*, 1965; Dell *et al.*, 1967; Handwerk and Kruger, 1971; Lovell *et al.*, 1973; Kikuchi and Fukuda, 1974; Lovell and Van Tets, 1979).

The high-melting compounds NpQ and PuQ (Q = S, Se, Te) have been grown as single crystals by means of the Czochralski crystal growth technique (Wastin *et al.*, 1995). Crystals of these monochalcogenides have also been grown by heating their pressed pellets sealed in W crucibles to temperature ~50°C below their melting points for several weeks (Mattenberger *et al.*, 1984).

US, USe, and UTe were found to order ferromagnetically with Curie temperatures between 180 and 104 K. The properties seem to depend on the orientation of the applied magnetic field. The [111] direction of the lattice is the easy magnetic axis (Wedgwood and Kuznietz, 1972; Busch and Vogt, 1978; Mattenberger and Vogt, 1992; Vogt *et al.*, 2001).

37.2.3 The compounds between AnQ and AnQ_2

A relatively large number of structurally-characterized compounds reside between the AnQ cubic compounds and the chalcogen-rich AnQ_2 compounds. The An_3Q_4 body-centered cubic compound (Th_3P_4 structure type) is known for U selenides and tellurides. Single crystals of U_3Se_4 were prepared by the thermal decomposition of α-USe_2 at 1,400°C. Its structure comprises USe_8 polyhedra that are face-sharing in a three-dimensional structure; U–Se distances range from 2.980(2) to 3.128(2) Å (Szytula and Suski, 1973; Noel, 1985b). Figure 37.2

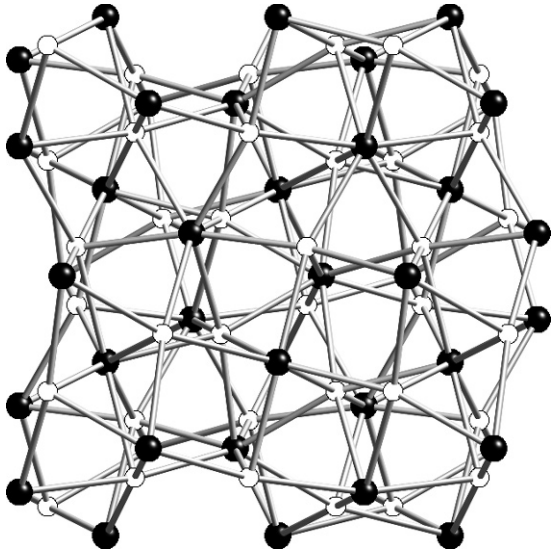

Fig. 37.2 *Structure of U_3Se_4 (U: black; Se: white).*

shows a rendering of the complex three-dimensional structure. No X-ray single crystal structure has been reported for U_3Te_4, but its structure was identified to be of the Th_3P_4 structure type by powder X-ray diffraction measurements (Ferro, 1954). The crystal structure of $U_{2.87}Te_4$ (also Th_3P_4 structure type) was, however, determined from single-crystal diffraction data (Shlyk *et al.*, 1995a). Np_3Q_4 (Q = Se, Te), Am_3Q_4 (Q = Se, Te), and Pu_3S_4 are also known, but only powder diffraction data have been reported for these compounds (Mitchell and Lam, 1970, 1971).

Several different sesquichalcogenide compounds are known for the An_2Q_3 solids. The α compounds of Th_2S_3, U_2S_3, and Np_2S_3 are isostructural (Fig. 37.3). In this structure the actinide is in a seven-coordinate monocapped trigonal-prismatic S environment (Zachariasen, 1949d). U_2Se_3 adopts the U_2S_3 structure type, as deduced from powder diffraction data (Khodadad, 1959). Single crystals of U_2Te_3, which have been prepared from a low-temperature (700°C) stoichiometric reaction between the elements mixed with a small quantity of CsCl, display the same structure type (Tougait *et al.*, 1998a). Magnetic measurements on a polycrystalline sample of U_2Te_3 (of high purity as deduced by Rietveld analysis) revealed a complex magnetic behavior with a ferromagnetic ordering around 110 K and spin reorientations in the range of 85–105 and at 45 K.

In the cubic γ compounds Ac_2S_3, Pu_2S_3, and Am_2S_3 (Ce_2S_3 structure type) the actinide is bound in a distorted square-antiprismatic Q coordination (Fig. 37.4)

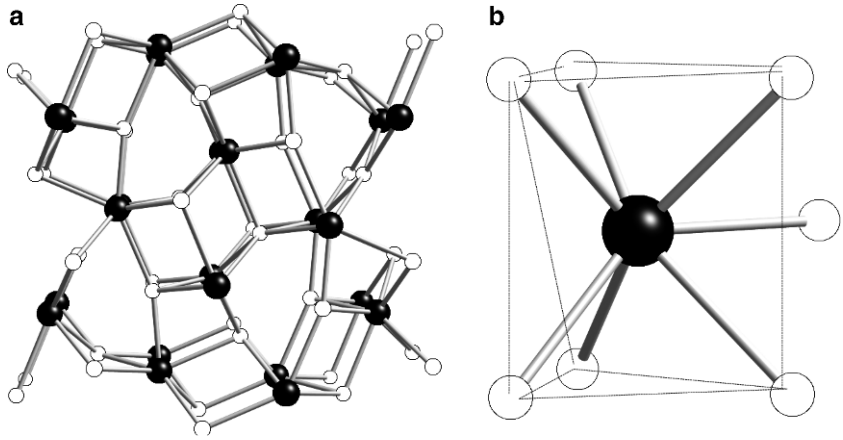

Fig. 37.3 (*a*) *Structure of* α-Th_2S_3 (*Th: black; S: white*); (*b*) *coordination environment of Th.*

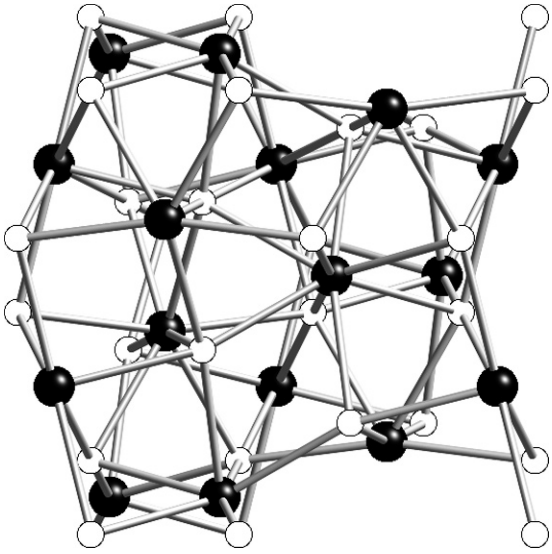

Fig. 37.4 *Structure of* γ-Pu_2S_3 (*Pu: black; S: white*).

(Zachariasen, 1949a). Orthorhombic η-Pu_2Te_3 and η-Np_2Te_3 compounds have been reported from powder diffraction data (Damien, 1973, 1974).

An_3Q_5 is a peritectic phase. For example, U_3S_5 decomposes into U_2S_3 and S above 1,800°C. In the U_3S_5 structure, U is in two distinct coordination environments (seven- and eight-coordinate) with interatomic U−S distances ranging

from 2.662(3) to 3.033(3)Å. Figure 37.5 shows the coordination environments of the two U atoms that form a network of edge-sharing distorted square antiprisms and monocapped trigonal prisms (Potel *et al.*, 1972; Noel and Prigent, 1980). U_3Se_5 has the same structure. See also Section 37.3.13.

The An_7Q_{12} compound contains two crystallographically distinct An atoms in a nearly hexagonal close-packed network of Q atoms in layers along the hexagonal axis (Zachariasen, 1949c; d'Eye, 1953; Tougait *et al.*, 1998b). One An atom resides in a bicapped trigonal-prismatic coordination site that creates a network with nearly perfect hexagonal holes along the *c*-axis. Figure 37.6a shows a view of the structure of U_7Te_{12} down the *c*-axis, where one unique U atom has been removed. The missing U atoms are 50% present in trigonal-planar

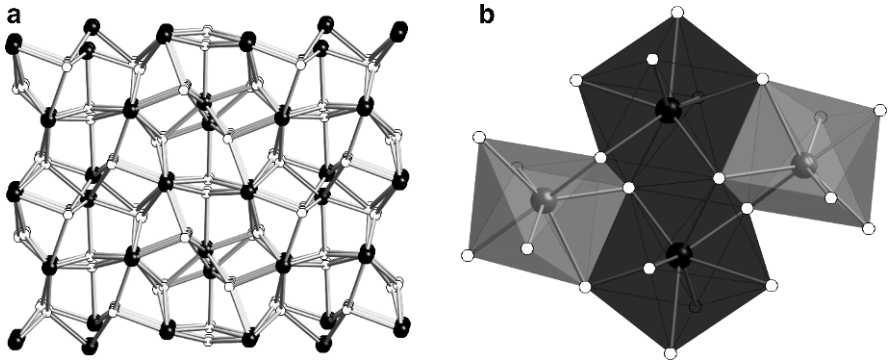

Fig. 37.5 (*a*) *Structure of* U_3S_5 (*U: black; S: white*); (*b*) *the coordination environment of the two U atoms. The* 7- *and* 8-*coordinated U atoms are shown as gray and black balls, respectively.*

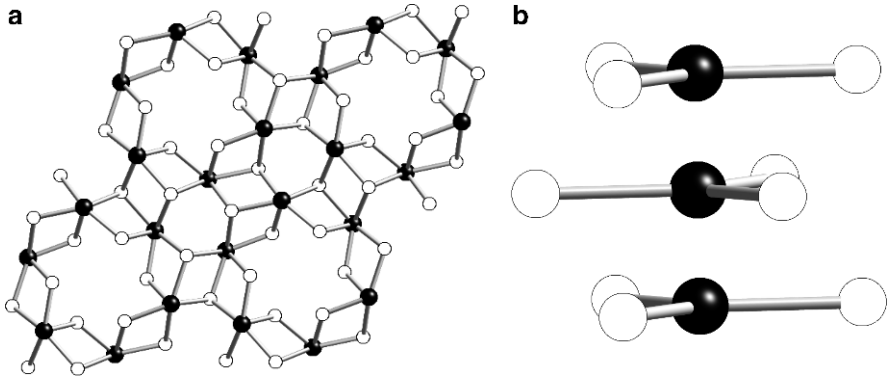

Fig. 37.6 (*a*) *A view of* U_7Te_{12} *along the c-axis where U*(1) *sites are shown empty;* (*b*) *a view of the* 50%*-occupied U*(1) *sites perpendicular to the c-axis. Only the equatorial U−Te bonds are shown* (*U: black; Te: white*).

sites along distinct chains (Fig. 37.6b). These sites along the *c*-axis are separated by about 2.1 Å, leading to nine-coordination of the U atom.

37.2.4 The AnQ_2 and AnQ_{2-x} compounds

The AnQ_2 compounds, and their respective defect structures, AnQ_{2-x}, are very numerous. They crystallize in α (tetragonal), β (orthorhombic), and γ (hexagonal) structures (d'Eye, 1953; Marcon and Pascard, 1966; Suski *et al.*, 1972; Mooney-Slater, 1977; Amoretti *et al.*, 1984; Noel *et al.*, 1996; Daoudi *et al.*, 1996a; Kohlmann and Beck, 1997). US_2 is a line phase up to about 1,100°C where it begins to lose S to form US_{2-x}, which melts above 1,800°C; moreover, it forms a eutectic with U_3S_5 just above 1,700°C (Noel *et al.*, 1996). The solid US_{2-x} may be isolated at temperatures below 1,200°C in the α-phase, whereas $UTe_{1.87}$ has a primitive tetragonal structure. The structure of $UTe_{1.87}$ is reminiscent of layered tellurides in the rare-earth series where a double layer of U and Te atoms in a pseudo-NaCl arrangement reside between square-planar layers of Te atoms that are not fully occupied and have close Te–Te interactions (3.0 Å), Fig. 37.7 (Haneveld and Jellinek, 1969).

The α phases of UQ_2 (Q = S, Se) crystallize in a primitive tetragonal unit cell that contains two crystallographically unique U atoms. The preparation of single crystals of these compounds was performed by the gas-phase transport method with bromine as transporting agent at 840–930°C. α-USe_2, Fig. 37.8a, crystallizes in a twinned $SrBr_2$-type structure (Beck and Dausch, 1989a). Each of the two unique U atoms, U(1) and U(2), is bonded to eight Se atoms. The coordination of the U(1) atom is described as a distorted square antiprism with interatomic distances ranging from 2.880 to 3.133 Å (Fig. 37.8b), whereas the

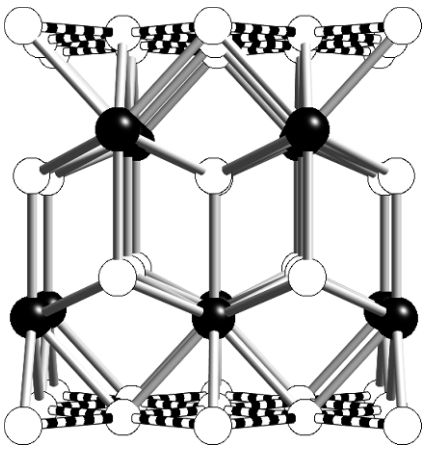

Fig. 37.7 *Structure of* $UTe_{1.87}$ (*U: black; Te: white*). *The Te–Te bonds are represented as horizontal multi-banded bonds.*

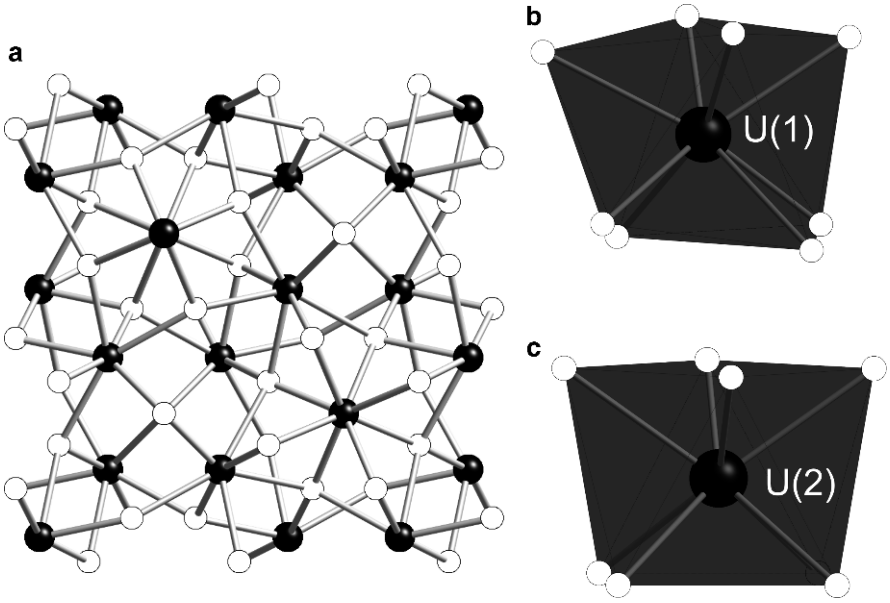

Fig. 37.8 (*a*) *Structure of* α-USe_2; (*b*) *the distorted antiprismatic coordination of atom U*(1); *and* (*c*) *the regular square antiprismatic coordination of atom U*(2) (*U: black; Se: white*).

U(2) atom is in a regular square-antiprismatic geometry with distances ranging from 2.908 to 2.952 Å. An earlier single-crystal refinement of α-US_2 and α-USe_2 (Noel and le Marouille, 1984) led to partial occupancy and a composition $UQ_{1.82}$. This result may be in doubt given the tendency of these compounds to be twinned.

Single crystals of β-UQ_2 (Q = S, Se) were also prepared with the vapor transport method with bromine as the carrier gas (Noel *et al.*, 1996). In addition, the reaction of UCl_4, Al, and H_2S at temperatures above 400°C was reported as a practical high-yield preparation of β-US_2 (Yoshihara *et al.*, 1967). β-UQ_2 (Q = S, Se), Fig. 37.9a, crystallize in an orthorhombic unit cell (Suski *et al.*, 1972; Noel *et al.*, 1996). The one crystallographically unique U atom is coordinated by nine Q atoms in a tricapped trigonal prism (Fig. 37.9b).

The U mixed chalcogenides [USSe, USTe, USeTe, $USe_{2-x}Te_x$ (x = 0.24, 0.72)] isostructural to the β-UQ_2 phases also have been reported (Troc *et al.*, 1994; Noel *et al.*, 1996). Magnetic measurements for single crystals of β-US_2 revealed Curie–Weiss behavior in the temperature range 50–400 K and an effective magnetic moment of ∼3.1 μ_B. Deviation from the Curie–Weiss law was observed at temperatures below 50 K (Suski *et al.*, 1972). Single-crystal magnetization studies of β-USe_2 revealed ferromagnetism with a $T_c \sim 14$ K (Shlyk *et al.*, 1995b). Interestingly, magnetic studies on single crystals of the mixed

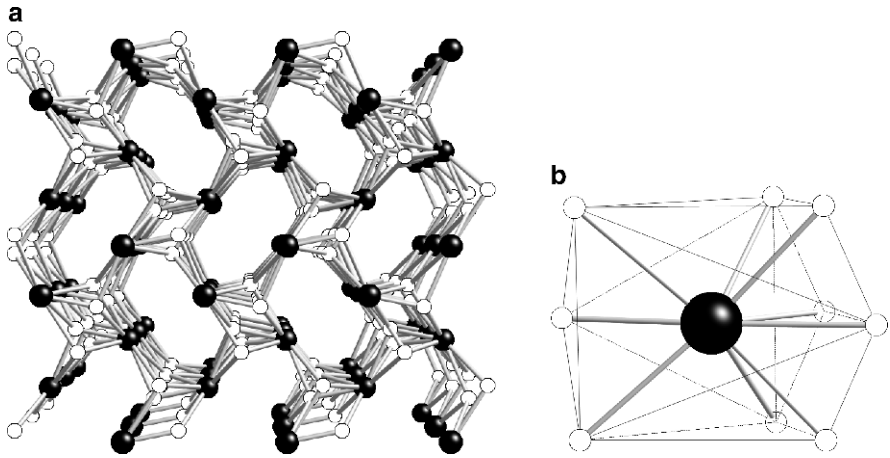

Fig. 37.9 (*a*) *Structure of β-US_2;* (*b*) *the coordination of the U atom with nine S atoms* (*U: black; S: white*) *in a tricapped trigonal prism.*

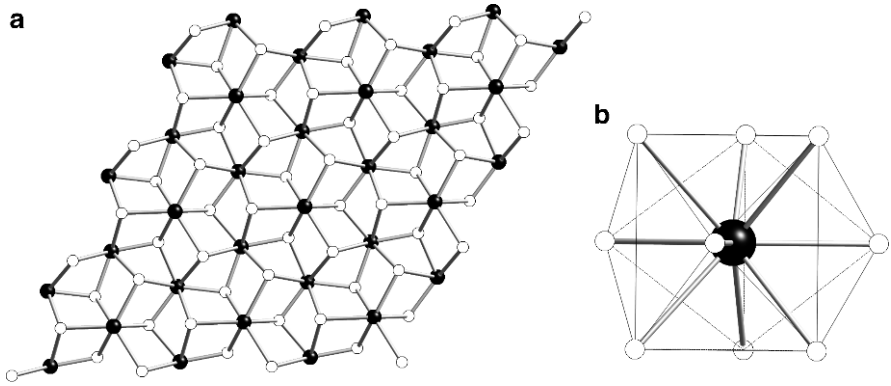

Fig. 37.10 (*a*) *Structure of γ-UQ_2* (*Q = S, Se*)*;* (*b*) *the coordination of U atoms with nine Q atoms in a tricapped trigonal prism* (*U: black; Q: white*)*.*

U chalcogenides revealed much higher Curie temperatures in the range 24–85 K (Troc *et al.*, 1994; Noel *et al.*, 1996).

γ-US_2 and γ-USe_2 have hexagonal structures (Daoudi *et al.*, 1996a; Kohlmann and Beck, 1997). These compounds were prepared by a gas–solid reaction of the binary U_3Q_5 (Q = S, Se) and H_2S at 410°C or with a solid-state reaction of stoichiometric amounts of U_3Q_5 and elemental Q in a sealed fused-silica tube at the same temperature. In γ-UQ_2, Fig. 37.10a, both crystallographically unique U atoms are bound to nine Q atoms in a tricapped trigonal prism (Fig. 37.10b).

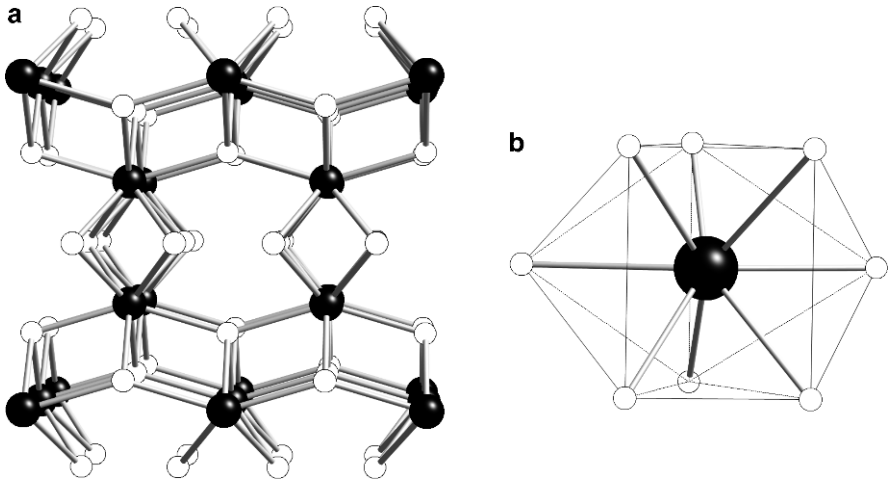

Fig. 37.11 (*a*) *Structure of α-UTe_2;* (*b*) *the coordination of U atom in a bicapped trigonal prism* (*U: black; Te: white*).

In contrast to these multiple structures of the UQ_2 (Q = S, Se) compounds, UTe_2 crystallizes only in a body-centered orthorhombic cell that contains UTe_8 bicapped trigonal prisms with U−Te distances of 3.201 and 3.076 Å, Fig. 37.11 (Beck and Dausch, 1988).

37.2.5 The An_2Q_5 compounds

The An_2Q_5 compounds crystallize in a monoclinic or a pseudo-tetragonal orthorhombic cell (Noel and Potel, 1982; Stöwe, 1996b; Tougait *et al.*, 1997a; Kohlmann and Beck, 1999). In monoclinic U_2Te_5 slabs of "UTe_2" are stacked with a van der Waals gap between, as shown in Fig. 37.12. The Te–Te bonding leads to a U(IV) compound of formula $U_2Te_3(Te_2)$. Electrical resistivity measurements on single crystals of U_2Te_5 indicate semiconducting behavior (Tougait *et al.*, 1997a).

In the orthorhombic (pseudotetragonal) phase of Th_2S_5 (Noel and Potel, 1982), Fig. 37.13a, a three-dimensional interconnected network of ThS polyhedra edge share and face share. These polyhedra are distorted tricapped trigonal prisms with one of the normal capping sites replaced by an S−S dimer, Fig. 37.13b. The interatomic Th–S distances range from 2.861(4) to 2.983(4) Å. The long interactions to the S–S dimer are 3.123(4) and 3.163(4) Å. The S–S distance is 2.117(7) Å, a normal single-bond distance.

37.2.6 The AnQ_3 compounds

There are a number of AnQ_3 compounds: monoclinic α- and orthorhombic *β*-UTe_3 and a monoclinic $ZrSe_3$-type phase for $ThTe_3$, USe_3, and US_3 (Ben Salem *et al.* 1984; Noel and Levet, 1989; Stöwe, 1996a; Kwak *et al.*, 2006).

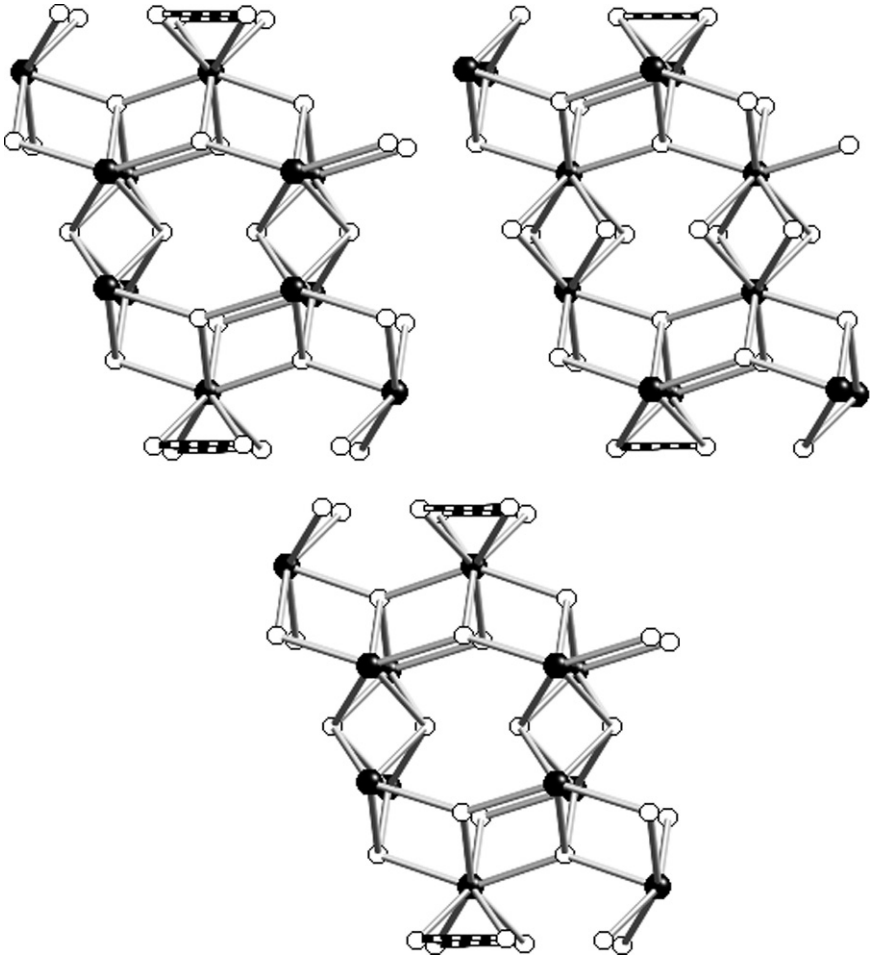

Fig. 37.12 *The structure of U_2Te_5 showing the stacking of U/Te slabs (U: black; Te: white). Te–Te bonds are shown as horizontal multi-banded bonds.*

The UQ_3 (Q = S, Se, Te) compounds with the $ZrSe_3$-structure type have been grown from chemical vapor-transport reactions with I_2 as the transport agent (Noel, 1986). β-UTe_3 was prepared by a sealed-tube reaction of U and Te in a 1:4 molar ratio at 700°C. Crystals were obtained with the chemical vapor-transport technique with the use of UBr_4 (Noel and Levet, 1989). The α-UTe_3 phase, Fig. 37.14a, is related to the $ZrSe_3$ phase in that it contains edge-sharing UTe_8 bicapped trigonal prisms with Te–Te distances of 2.751Å along two short edges. These trigonal prisms are arranged in layers that are capped on the top and bottom by Te networks, Fig. 37.14b (Stöwe, 1996a). The β-UTe_3 structure is also layered, Fig. 37.15a, but the U atom is in a distorted tricapped trigonal

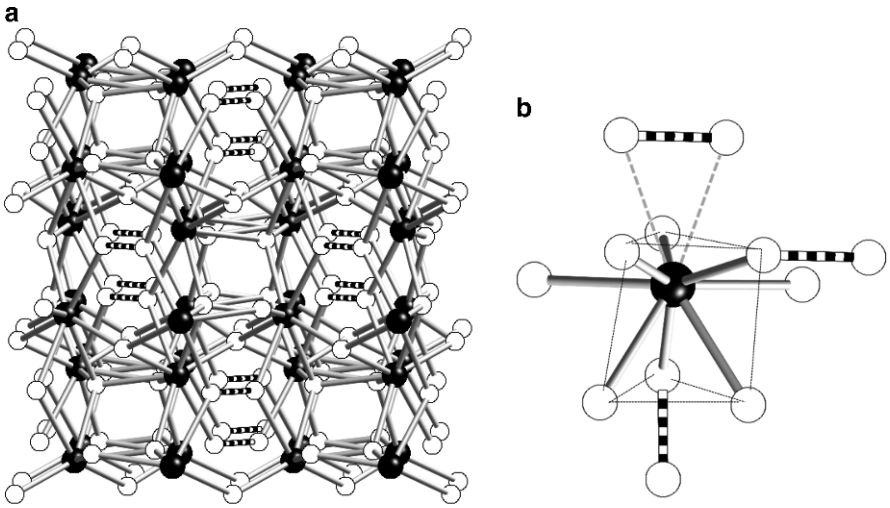

Fig. 37.13 (*a*) *Structure of the orthorhombic* Th_2S_5. *S–S bonds are shown as horizontal multi-banded bonds);* (*b*) *a view of the Th coordination environment that shows how the* S_2 *group is bound to the Th* (*Th: black; S: white*).

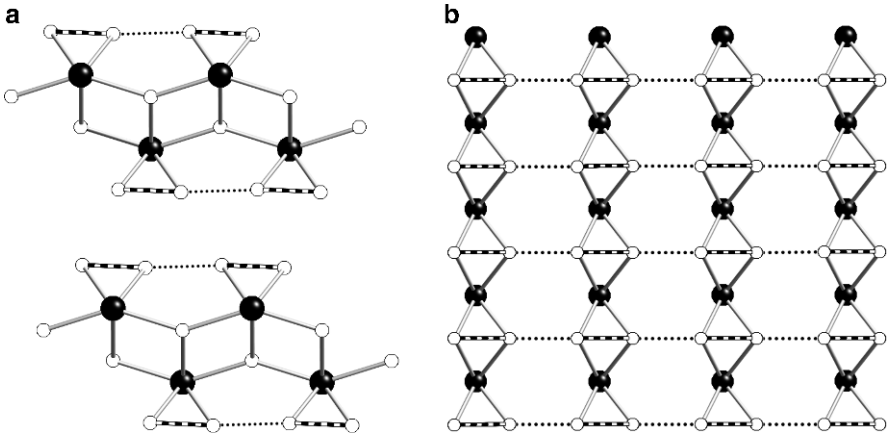

Fig. 37.14 (*a*) *A view parallel to the layers in* α-UTe_3 (*monoclinic*); (*b*) *a view perpendicular to the layers showing the Te–Te network connected through U atoms* (*U: black; Te: white*). *Te−Te bonds are shown as horizontal multi-banded bonds. Long Te−Te interactions* (3.35 Å) *are indicated with dotted lines.*

prism with the longer Te–Te distance of 3.067 Å between one edge of the trigonal prism and two capping atoms that are part of a network of Te atoms, Fig. 37.15b. This arrangement is similar to that found in $NbSe_3$ (Noel and Levet, 1989). The USe_3 and monoclinic $ZrSe_3$ structures are closely related,

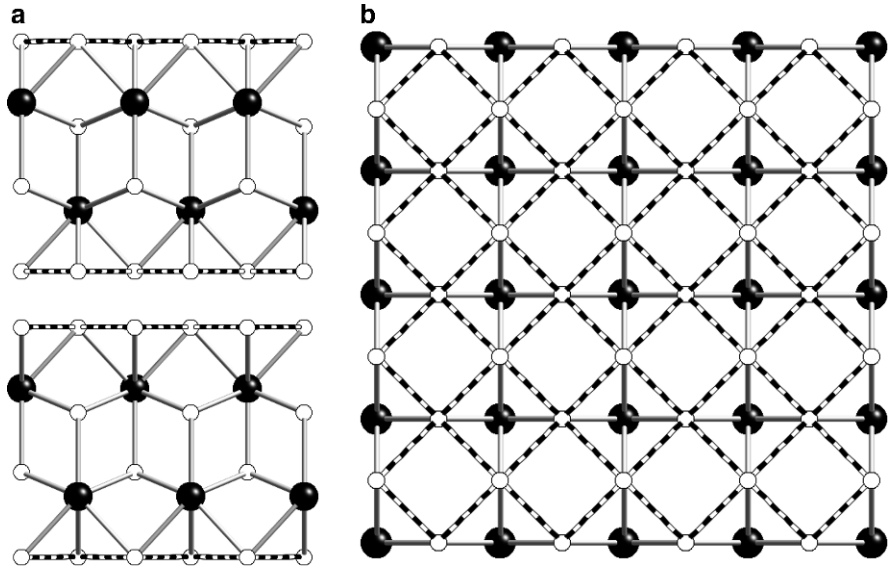

Fig. 37.15 (*a*) *A view parallel to the layers in β-UTe_3* (*orthorhombic*)*;* (*b*) *a view perpendicular to the layers showing the Te–Te network connected through U atoms* (*U: black; Te: white*)*. Te–Te bonds are shown as horizontal multi-banded bonds.*

Fig. 37.16. For reference, in USe_3 the Se–Se bond distance is 2.363(1) Å, a typical single bond.

The magnetic properties of UQ_3 (Q = S, Se, Te) measured on single-crystal samples show that they have similar magnetic susceptibilities characterized by a large anisotropy consistent with their anisotropic structure. They show antiferromagnetic transitions at 50, 45, and 5 K for the S, Se, and Te compounds, respectively (Noel, 1986).

37.2.7 UTe_5

The UTe_5 compound (Noel, 1984) forms a layered structure (Fig. 37.17a) that is not related to that of UTe_3. This compound was prepared by a sealed-tube reaction of the elements at 450°C for 3 weeks. Single crystals were grown with chemical vapor transport with I_2 as the transport agent. This structure comprises a network of highly-distorted bicapped UTe_8 trigonal prisms in which there is a zigzag chain of Te atoms with a Te–Te distance of 3.140(1) Å. The Te atoms are in linear and right-angle geometries, Fig. 37.17b. Along with the quasi-infinite chains of Te running through the structure, a Te_3^{2-} unit [Te–Te is 2.803(2) Å] is also bound to U. Finally, there is a long U–Te interaction [3.202 (2) Å] that links the chains, as shown in Fig. 37.17b, with the next set of chains in the layer and completes the ninth coordination position around U.

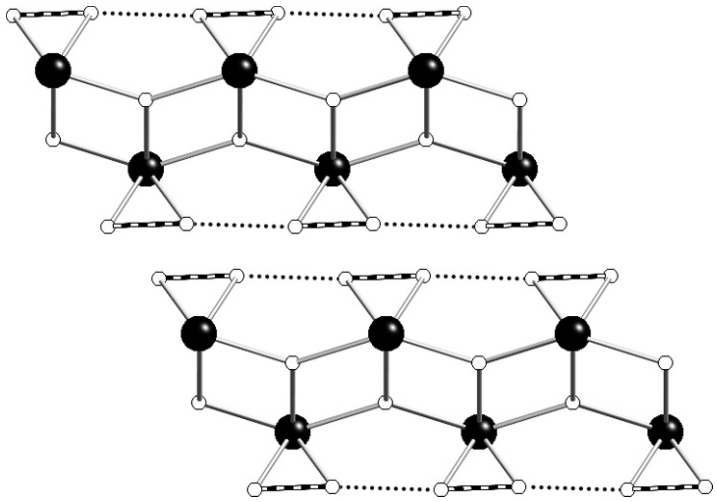

Fig. 37.16 *A view of the structure of USe_3 for comparison to the α- and β-UTe_3 structures (U: black; Se: white). Se−Se bonds are shown as horizontal multi-banded bonds. Long Se−Se interactions* (3.294 *Å*) *are indicated with dotted lines.*

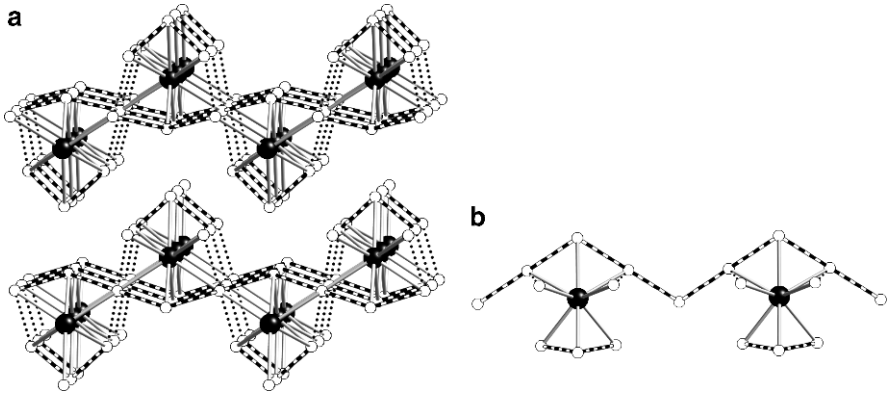

Fig. 37.17 (*a*) *A view of the layered structure of UTe_5;* (*b*) *a view of the coordination environment around U atoms and the quasi-infinite chains of Te* (*U: black; Te: white*). *Te−Te bonds are shown as horizontal multi-banded bonds. Long Te−Te interactions* (3.428 *Å*) *are indicated with dotted lines.*

37.3 TERNARY ACTINIDE CHALCOGENIDES

This subject was reviewed in less extensive form a decade ago (Narducci and Ibers, 1998b).

37.3.1 AnMQ compounds

Compounds of the AnMQ type are found for almost all permutations of An = U, Th; M = O, N–Bi, Si–Sn; and Q = S, Se, Te, as well as for NpOS. Table 37.2 lists the compounds of this type whose structures have been determined from single-crystal diffraction data. Generally, these compounds form from stoichiometric reactions of the elements or from reactions of suitable binaries with chalcogens at temperatures between 600°C and 1,050°C.

There are two distinct subtypes of this group, both of which are related to the PbFCl structure type. Both subtypes include nine-coordinate An cations in a capped square-antiprismatic environment. Four M atoms form the ''bottom'' square face, whereas 4 + 1 Q atoms make up the top face and cap. The prisms share edges and corners to form layers that stack with an atom sequence M–An–Q–Q–An–M. The two subgroups adopt either the anti-Ti_2Bi structure type (UGeTe) or the PbFCl structure type. The difference between the two structures lies in the way the antiprisms are connected. For the former, the antiprisms stack directly on top of one another, sharing 4M faces (Fig. 37.18a). For the latter, the true PbFCl structure (Fig. 37.18b), the slabs formed by these antiprisms are offset so that they share edges of the 4M faces. Which structure type a given compound will possess is dependent on the radius ratio r_M:r_Q and the size of An. If r_M:r_Q is small and An is large the compound will adopt the anti-Ti_2Bi structure type. If the situation is reversed, An is small and r_M:r_Q is large, the compound will adopt the PbFCl structure type.

Physical properties of some of these AnMQ compounds have been measured, usually on powders. Neutron diffraction measurements at 4.2 K on powders of UAsSe and USbSe (Leciejewicz and Zygmunt, 1972) show these compounds to have a simple uniaxial ferromagnetic structure with the magnetic moment of 1.5(1) μ_B of U aligned along the fourfold axis. Specific heat measurements on UAsS, UAsSe, and UAsTe indicate ferromagnetic ordering at 125.8, 108.8, and 62.8 K, respectively (Blaise *et al.*, 1980). Magnetization measurements on UAsS, UAsSe, and UAsTe have also been performed (Bazan and Zygmunt, 1972).

From measurements on single crystals it was found that UPS orders ferromagnetically in a similar manner below 118 K (Kaczorowski *et al.*, 1994). Both in the ordered and paramagnetic regions UPS exhibits considerable magnetic anisotropy. Above T_c the electrical resistivity decreases logarithmically with increasing temperature. ^{31}P NMR Knight shift measurements confirm axial symmetry of the P environment in UPS, but indicate that the environments are lower in UPSe and UPTe (Zogal and Zygmunt, 1982). Electrical resistance and thermoelectric power measurements on ThPS show it to be a metallic conductor (Wawryk *et al.*, 2005).

A powder neutron diffraction study shows ferromagnetic ordering of UNSe below 52 K with a magnetic moment for U of 0.85(16) μ_B aligned along the fourfold axis. Heat capacity measurements on UNTe and UNSe were also performed (Amoretti *et al.*, 1986).

Table 37.2 *Structure types of known AnMQ compounds.*

ThMQ	*Structure type*	*References*	UMQ	*Structure type*	*References*
ThOS[a]	PbFCl	Zachariasen, 1949d	UOS[a]	PbFCl	Zachariasen, 1949d; Ellert *et al.*, 1974; Sato *et al.*, 1999
ThOSe[a]	PbFCl	d'Eye *et al.*, 1952	UOSe[b]	PbFCl	Ferro, 1954; Mansuetto *et al.*, 1993; Kaczorowski *et al.*, 1993
ThOTe[b]	PbFCl	d'Eye and Sellman, 1954; Beck and Dausch, 1989b	UOTe[c]	PbFCl	Ferro, 1955; Trzebiatowski *et al.*, 1961; Haneveld and Jellinek, 1964
ThSiS[a]	anti-Ti_2Bi	Stocks *et al.*, 1981	USiS[c]	PbFCl	Hulliger, 1968
ThSiSe[a]	anti-Ti_2Bi	Stocks *et al.*, 1981	USiSe[a]	PbFCl	Hulliger, 1968
ThSiTe[a]	anti-Ti_2Bi	Stocks *et al.*, 1981	UGeS[c]	PbFCl	Hulliger, 1968; Haneveld and Jellinek, 1969; Ptasiewicz-Bak *et al.*, 1978
ThGeS[b]	anti-Ti_2Bi	Stocks *et al.*, 1981	UGeSe[c]	Anti-Ti_2Bi	Hulliger, 1968; Haneveld and Jellinek, 1969; Ptasiewicz-Bak *et al.*, 1978
ThGeSe[a]	anti-Ti_2Bi	Stocks *et al.*, 1981	UGeTe[c]	Anti-Ti_2Bi	Hulliger, 1968; Haneveld and Jellinek, 1969; Ptasiewicz-Bak *et al.*, 1978
ThGeTe[a]	anti-Ti_2Bi	Stocks *et al.*, 1981	USnTe[c]	PbFCl	Hulliger, 1968; Haneveld and Jellinek, 1969
ThNSe[a]	PbFCl	Amoretti *et al.*, 1986	UNSe[a]	PbFCl	Amoretti *et al.*, 1986
ThNTe[a]	PbFCl	Amoretti *et al.*, 1986	UNTe[c]	PbFCl	Amoretti *et al.*, 1986
ThPS	PbFCl	Hulliger, 1968;Wawryk *et al.*, 2005	UPS[b]	PbFCl	Kaczorowski *et al.*, 1994
ThPSe[a]	PbFCl	Hulliger, 1968	UPSe[b]	PbFCl	Hulliger, 1968; Zygmunt *et al.*, 1974a;Henkie *et al.*, 1998
ThAsS[a]	PbFCl	Hulliger, 1968	UPTe[c]	Anti-Ti_2Bi	Zygmunt *et al.*, 1974b

Table 37.2 (*Contd.*)

ThMQ	*Structure type*	*References*	UMQ	*Structure type*	*References*
ThAsSe[b]	PbFCl	Hulliger, 1968	UAsS[b]	PbFCl	Hulliger, 1968; Pietraszko and Lukaszewicz, 1975;
ThAsTe[b]	PbFCl	Hulliger, 1968	UAsSe[b]	PbFCl	Hulliger, 1968; Pietraszko and Lukaszewicz, 1975; Henkie *et al.*, 1998
ThSbSe[a]	PbFCl	Hulliger, 1968	UAsTe[b]	Anti-Ti_2Bi	Ferro, 1954; Zygmunt *et al.*, 1974b; Pietraszko and Lukaszewicz, 1975; Pearson, 1985
ThSbTe[a]	PbFCl	Hulliger, 1968	USbS[a]	PbFCl	Hulliger, 1968
ThBiTe[a]	PbFCl	Hulliger, 1968	USbSe[b]	PbFCl	Hulliger, 1968;Leciejewicz and Zygmunt, 1972
			USbTe[b]	PbFCl	Hulliger, 1968; Haneveld and Jellinek, 1969
NpOS[a]	PbFCl	Zachariasen, 1949d	UBiTe[a]	PbFCl	Hulliger, 1968

[a] Unit cell from powder data only.
[b] Single crystal structure data.
[c] Structure from powder data only.

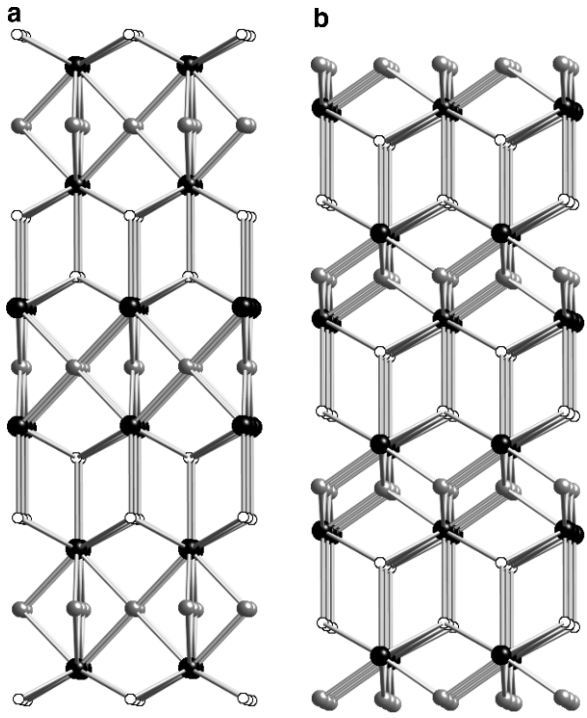

Fig. 37.18 (*a*) *Structure of AnMQ with the anti-Ti_2Bi structure;* (*b*) *structure of AnMQ with the PbFCl structure* (*An: black; Q: white; M: gray*).

A powder neutron diffraction study of UGeS, UGeSe, and UGeTe (Ptasiewicz-Bak *et al.*, 1978) indicates that the magnetic moments in these compounds align ferromagnetically at 88, 73, and 40 K with magnetic moments for U of 1.26, 1.50, and 0.26 μ_B, respectively. Interestingly, the UGeSe and UGeTe magnetic cells coincide with the chemical unit cells, whereas the magnetic cell of UGeS is doubled along the fourfold axis.

Measurements on single crystals showed that UOSe orders antiferromagnetically at T_N = 100(2) K and exhibits very strong anisotropy in its susceptibility vs. temperature dependence (Kaczorowski *et al.*, 1993). A later study (Amoretti *et al.*, 1995) found T_N = 55 K. Magnetic measurements on polycrystalline samples of NpOS and NpOSe indicate antiferromagnetic ordering below 2 and at 11 K, respectively (Amoretti *et al.*, 1989).

37.3.2 $AnMQ_2$ compounds

In a study of the phase relationships in the US-CaS, US-SrS, and US-BaS systems (Komac *et al.*, 1971) the compounds UMS_2, M = Ca, Sr, Ba, were found. From powder diffraction data $UCaS_2$ and $USrS_2$ were assigned to

space group $I\bar{4}3d$ of the cubic system. The proposed structure leads to some unlikely interatomic distances. $NpCuSe_2$ (Wells *et al.*, 2009) crystallizes in the $LaCuS_2$ structure type (Julien-Pouzol *et al.* 1981). The structure comprises stacking of $CuSe_4$ tetrahedral layers and double layers of $NpSe_7$ monocapped trigonal prisms.

37.3.3 $AnMQ_3$ compounds

Many compounds of this formula are known (Table 37.3). All form at high temperatures from stoichiometric reactions of the elements in their pure states, or more commonly from the binary chalcogenides. In order to grow single crystals, I_2 is typically used as a transport agent. These compounds all possess the basic elements of the perovskite (ABQ_3) structure; namely, chains of corner-shared BQ_6 octahedra, with A cations in the interstitial sites. Typically U or Th occupies the eight-coordinate A interstitial site with the smaller metal centering the BQ_6 octahedron. In $BaUS_3$, Ba occupies the A site and U the B site as Ba^{2+} has a larger crystal radius than U^{4+} (1.3 Å vs 0.89 Å).

There are two main subclasses of this structure type. Most of the ABQ_3 compounds crystallize in a three-dimensional structure (space group *Pnma*); however when B = Sc, Fe, or Mn the compounds crystallize in a layered structure (space group *Cmcm*). The former structure, as illustrated by that of

Table 37.3 *Known $AnMQ_3$ structures.*

Compound	*References*	*Structure type*
$ThMgTe_3$	Narducci and Ibers, 2000	*Cmcm*
$ThMnSe_3$	Ijjaali *et al.*, 2004	*Cmcm*
$ThMnTe_3$	Narducci and Ibers, 2000	*Cmcm*
$UBaS_3$	Brochu *et al.*, 1970b; Lelieveld, 1980	*Pnma*
$UCoS_3$	Noel *et al.*, 1971;Chenevier *et al.*, 1981	*Pnma*
$UCoSe_3$	Noel, 1974	*Pnma*
$UCrS_3$	Noel, 1973; Noel *et al.*, 1975b	*Pnma*
$UCrSe_3$	Noel, 1974	*Pnma*
$UFeS_3$	Noel *et al.*, 1971; Noel and Padiou, 1976b	*Cmcm*
$UFeSe_3$	Noel, 1974	*Cmcm*
$UKSe_3$	Padiou and Guillevi, 1969	*unknown*
$UMnSe_3$	Noel, 1974; Ijjaali *et al.*, 2004	*Cmcm*
$UNiS_3$	Noel *et al.*, 1971	*Pnma*
$UNiSe_3$	Noel, 1974	*Pnma*
$UPdSe_3$	Daoudi and Noel, 1989	*Pnma*
$URhS_3$	Daoudi and Noel, 1987	*Pnma*
$URuS_3$	Daoudi and Noel, 1987	*Pnma*
$UScS_3$	Julien *et al.*, 1978	*Cmcm*
$UTl_{0.56}Te_3$	Tougait *et al.*, 1997b	*Cmcm*
UVS_3	Noel, 1973	*Pnma*
$UVSe_3$	Noel, 1974	*Pnma*

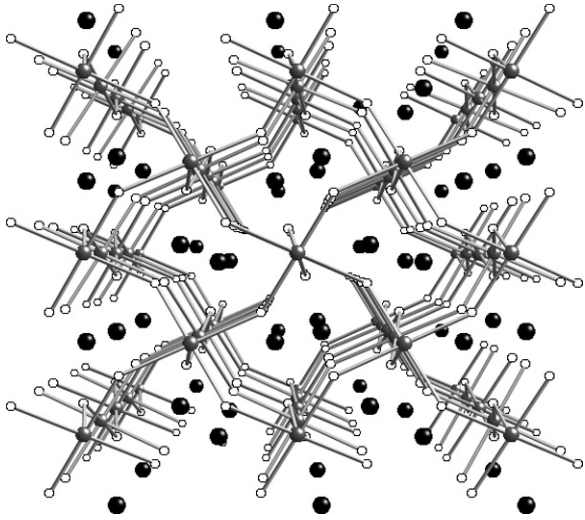

Fig. 37.19 *Structure of $UCrS_3$ (U: black; Cr: gray; S: white).*

$UCrS_3$ (Fig. 37.19), comprises chains of corner-shared BQ_6 octahedra; these chains are then linked together through corners of the octahedra to form a three-dimensional structure. In the normal perovskite ($CaTiO_3$) structure, the A cations (Ca) are coordinated to 12 anions at the corners of a cuboctahedron. However, in the related U and Th compounds the environment of the A sites is distorted in such a way that A is coordinated to eight anions at the corners of a bicapped trigonal prism. This distortion arises from tilting of the BQ_6 octahedra, which is necessary to accommodate the smaller size of the A cation. $PdUSe_3$ (Fig. 37.20) offers an interesting exception to the usual perovskite structure. Because Pd prefers square-planar coordination, the B octahedral site is distorted in such a way that the two apical Se atoms are removed from the coordination sphere of Pd.

The reason for the formation of layered (*Cmcm*) structures for the Sc, Fe, and Mn compounds has never been adequately addressed. These compounds (Fig. 37.21) form slabs of BQ_6 octahedra sharing corners in one direction and edges along the other. The U or Th atoms, still with the eight-coordinate bicapped trigonal-prismatic coordination environment, occupy the interlayer sites.

A limited number of measurements of the physical properties of these $AnMQ_3$ compounds have been made. $UMnSe_3$ (Ijjaali *et al.*, 2004) is a ferromagnet with T_c = 62 K. $ThMnTe_3$ is also a ferromagnet with T_c = 70 K (Narducci and Ibers, 2000). $UPdSe_3$ is an antiferromagnet with a Néel temperature T_N of 11 K (Daoudi and Noel, 1989). Neutron diffraction measurements on powders of $UCrSe_3$ and UVS_3 (Wolfers and Fillion, 1977) found significant

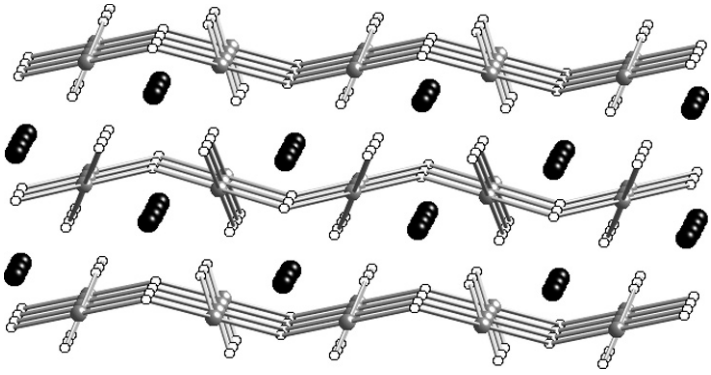

Fig. 37.20 *Structure of $UPdSe_3$ (U: black; Pd: gray; S: white).*

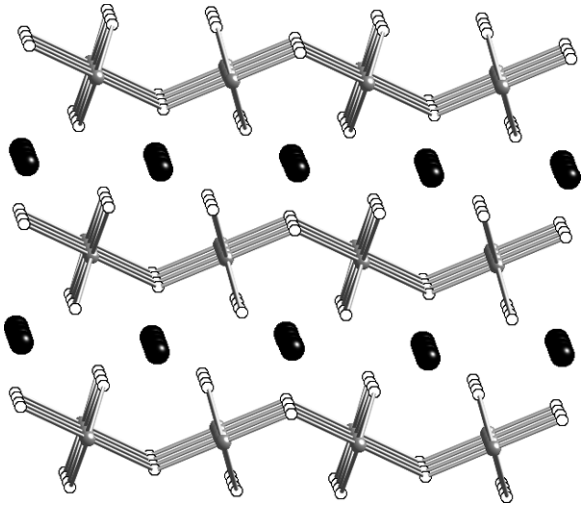

Fig. 37.21 *Structure of $UFeS_3$ (U: black; Fe: gray; S: white).*

spin density located more than 2 Å from any atom. This was attributed to an extended $6d_{z^2}$ orbital of U.

37.3.4 $AnMQ_6$ compound

The only compound of this stoichiometry is $CsUTe_6$ (Cody and Ibers, 1995) (Fig. 37.22). It was formed in an attempt to synthesize a quaternary Cs/Ag/U/Te compound by reacting elemental Ag, U, and Te with a Cs_2Te_3 flux. The compound has a one-dimensional structure unique to the ternary uranium

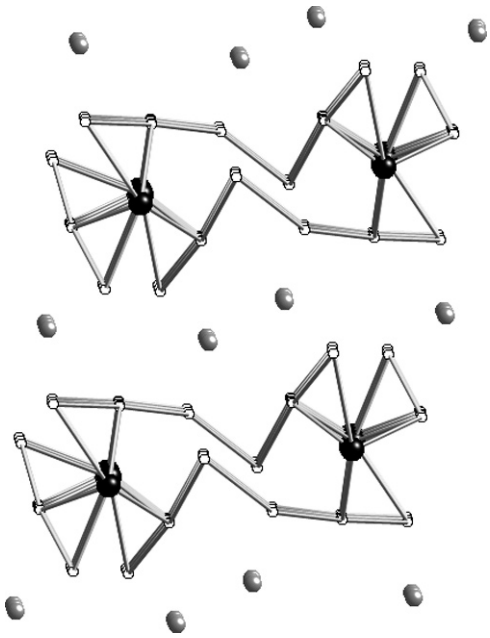

Fig. 37.22 *Structure of $CsUTe_6$ (U: black; Te: white; Cs: gray).*

chalcogenides. U atoms are coordinated to nine Te atoms in a tricapped trigonal prismatic environment. These UTe_9 prisms share triangular faces to form infinite chains. Two capping Te atoms from neighboring chains are bound by a distance of 2.795(9) Å to link two chains together. Cs atoms are situated between the $^1_\infty[U_2Te_{12}]^{2-}$ chains, coordinated to nine Te atoms.

37.3.5 AnM_2Q_2 compound

The mixed halide chalcogenide compound ThI_2Te_2 forms from the reaction of the elements at 500°C (Rocker and Tremel, 2001). It has the $NbCl_2S_2$ structure type. Binuclear $[Th_2(Te_2)_2]^{4+}$ units with square antiprismatically coordinated Th atoms are linked together by I^- anions to form sheets, Fig. 37.23.

37.3.6 AnM_2Q_3 compound

The compound K_2UTe_3 (Stöwe and Appel-Colbus, 1999) was prepared by the reaction of U and K_2Te_3 at 600–800°C. The structure contains regular UTe_6 octahedra, Fig. 37.24. The structure is layered with anionic slabs of $[UTe_3]^{2-}$, which adopt the same motif as $AlCl_3$. The K cations are found between the

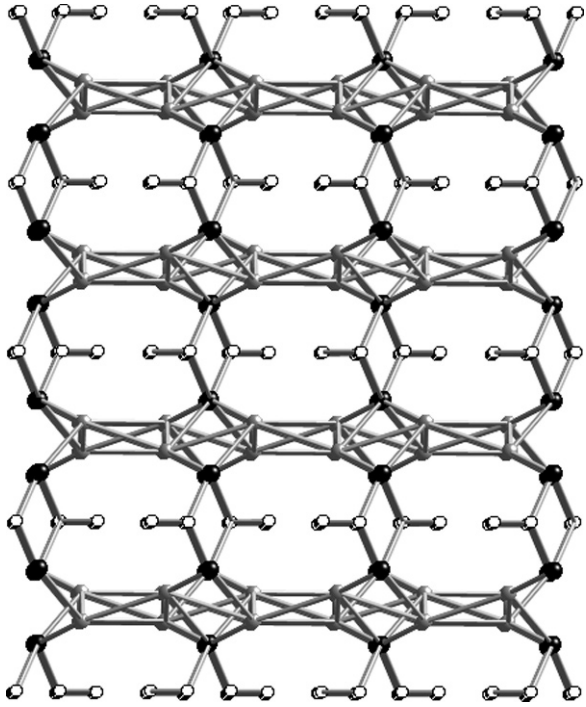

Fig. 37.23 *Structure of ThI_2Te_2 (Th: black; Te: white; I: gray).*

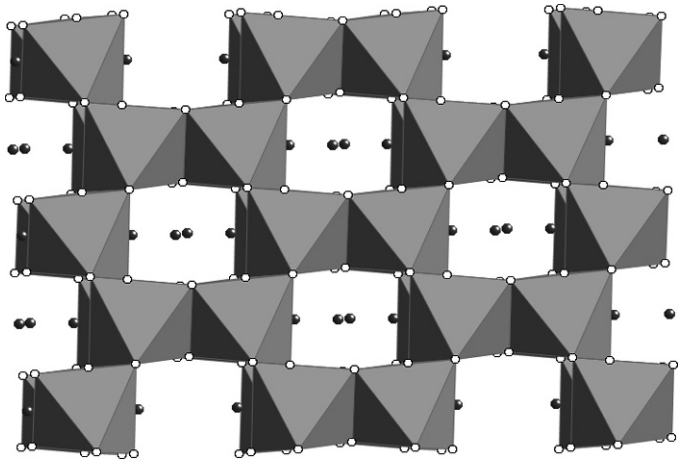

Fig. 37.24 *Structure of K_2UTe_3 (UTe_6: gray polyhedra; K: black balls).*

layers. Alternatively, K_2UTe_3 can be viewed as an ordered low-symmetry variant of the NaCl structure (e.g. $[K_{0.67}U_{0.33}]Te$).

37.3.7 AnM_2Q_4 compound

UPd_2S_4 (Daoudi and Noel, 1985) forms from the stoichiometric reaction of US_2 with elemental Pd and S at 900°C. Its structure contains a three-dimensional connected network of square-planar PdS_4 units and US_8 polyhedra that can best be described as deformed square antiprisms (Fig. 37.25).

37.3.8 AnM_2Q_6 compound

The compound ThP_2S_6 is a simple salt of Th^{4+} and the ethane-like thiohypophosphate anion $[P_2S_6]^{4-}$ (Fig. 37.26). It was prepared from the stoichiometric mixture of the elements at 500°C (Simon *et al.*, 1982). The compound UP_2S_6 (Do *et al.*, 1993) is isostructural with ThP_2S_6.

37.3.9 AnM_3Q_4 compound

UPd_3S_4 (Daoudi and Noel, 1986a) was prepared from the stoichiometric reaction of US_2 with elemental Pd and S at 900°C. Its structure (Fig. 37.27) is of the platinum–bronze structure type. It comprises cubic US_8 units stacked along the corners of the unit cell, stitched together through square-planar PdS_4 units.

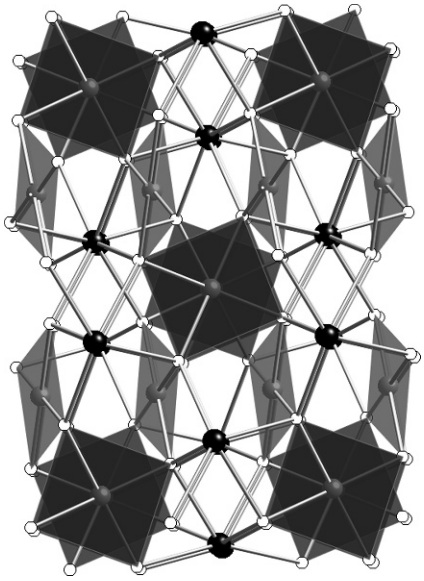

Fig. 37.25 *Structure of UPd_2S_4 (U: black; Pd: gray; S: white).*

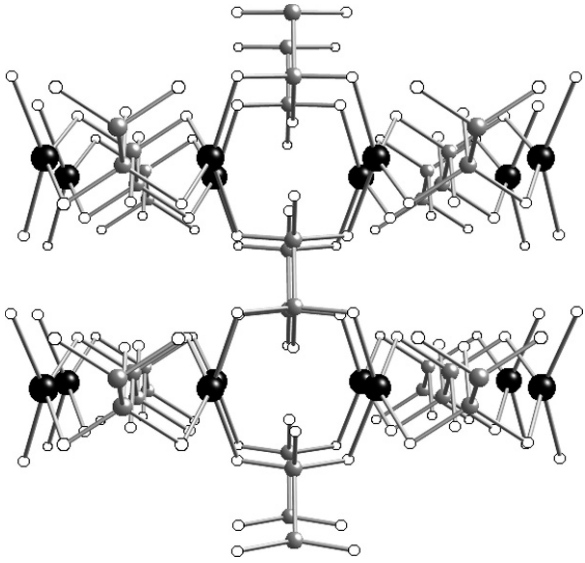

Fig. 37.26 *Structure of* ThP_2S_6 (*Th: black; P: gray; S: white*).

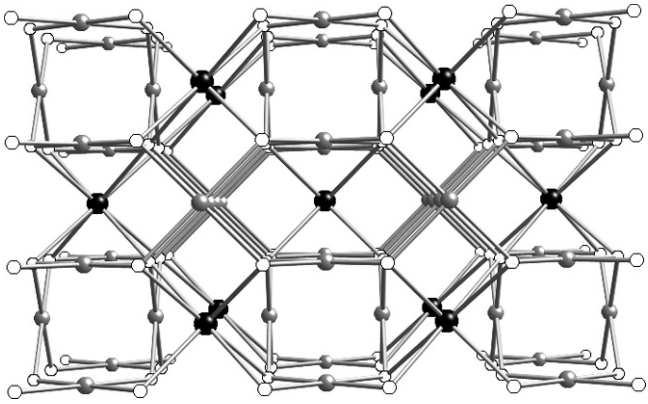

Fig. 37.27 *Structure of* UPd_3S_4 (*U: black; Pd: gray; S: white*).

37.3.10 AnM_4Q_8 compound

The only example of this stoichiometry is the compound K_4USe_8 (Sutorik and Kanatzidis, 1997a), which was prepared by the reaction of U, K_2Se, and Se at 300°C. The structure comprises a single $[U(Se_2)_4]^{4-}$anion (Fig. 37.28) separated by K^+ cations. The anion has pseudo-D_{2d} symmetry.

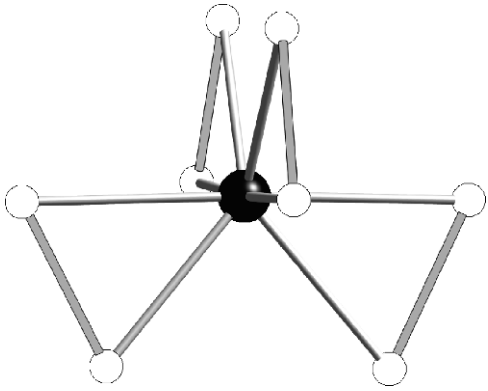

Fig. 37.28 *Structure of the* $[U(Se_2)_4]^{4-}$ *anion* (*U: black; Se: white*).

The material displays paramagnetic behavior from 120 K upwards, with $\mu_{eff} = 3.82\ \mu_B$ at 300 K, consistent with a formal oxidation state of U of +4. A magnetic transition is observed at about 90 K, followed by antiferromagnetic ordering at 65 K.

37.3.11 AnM_6Q_8 compounds

These compounds (An = U, Th) (Daoudi *et al.*, 1996b), which are non-stoichiometric, were synthesized by stoichiometric reactions of AnQ_2, MoQ_2, and Mo powder at approximately 1,300°C. They crystallize with the typical Chevrel-phase structure (Chevrel *et al.*, 1971) with Mo_6 octahedra capped by eight Q atoms on each face and An atoms coordinated by eight Q atoms in the cubic vacancies (Fig. 37.29).

Valence electron counts for typical Chevrel phases show that the Mo_6 core has 20 e^-. Subsequent filling of the vacancies by metal atoms leads to charge transfer from the metal to the Mo_6 core, up to a total of 24 e^-. No compounds are known that have a total count of exactly 24 e^-. U^{4+} and Th^{4+} ions should supply exactly 4 e^- per cluster. However, from single-crystal determinations the actual compositions are $U_{0.82}Mo_6Se_8$ and $Th_{0.81}Mo_6S_8$.

The compounds $Np_{1+x}Mo_6Se_8$ (Damien *et al.*, 1981; de Novion *et al.*, 1981) and $An_{1+x}Mo_6Se_8$ (An = Pu, Am) (de Novion *et al.*, 1981) were prepared by reacting $NpSe_3$ or $AnSe_2$ (An = Pu, Am) with Mo and Se powders. Whereas the Np compound displays a superconducting critical temperature at 5.6(1) K the Pu and Am compounds show no superconducting transitions down to 2.5 and 3.5 K, respectively.

37.3.12 An_2MQ_4 compound

The compound U_2PdS_4 (Daoudi and Noel, 1986b) forms from the stoichiometric reaction of US_2 with elemental Pd and S at 900°C. Its structure

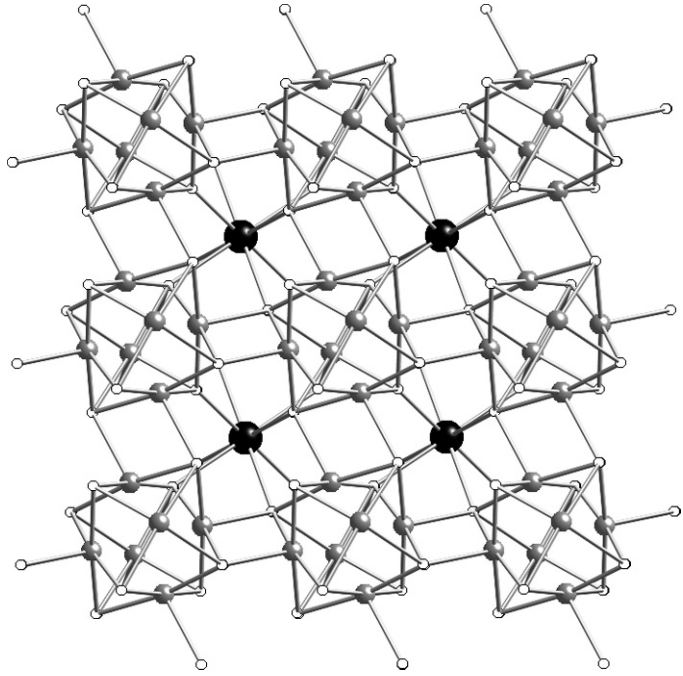

Fig. 37.29 *Structure of $AnMo_6Q_8$ (An: black; Mo: gray; Q: white).*

(Fig. 37.30a) contains seven-coordinate U atoms in irregular polyhedra. The U atoms are coordinated to three S atoms of a triangular face and four additional S atoms of the opposite square face (Fig. 37.30b). Pd atoms occupy the centers of highly distorted S_4 tetrahedra (Fig. 37.30c) formed from the S atoms of the triangular faces of the US_7 units.

37.3.13 AnM_2Q_5 and An_2MQ_5 compounds

Most of the $AnMQ_3$ compounds (Section 37.3.3) decompose into an AnM_2Q_5 phase upon heating at temperatures above 1,200°C. These AnM_2Q_5 compounds can be synthesized in a rational manner by reactions of the binary metal chalcogenides at 800–1,300°C. Ternary compounds of the type AnM_2Q_5 and An_2MQ_5 (An = U; Q = S, Se) are found for M = La–Gd (Tien *et al.*, 1975; Noel and Prigent, 1980; Slovyanskikh *et al.*, 1984), Ca, Ba, Sr, Pb (Brochu *et al.*, 1970a, Brochu *et al.*, 1972, Potel *et al.*, 1975), as well as Ti, Zr, Fe, Co, and Ni (Noel *et al.*, 1971, Noel, 1973, Noel, 1974, Noel and Padiou, 1976a). It has been postulated that, owing to ionic sizes involved, only the lighter lanthanides will form this structure type (Noel and Prigent, 1980). Most of these compounds are isostructural with the U_3Q_5 parent structure (see Section 37.2.3). However the

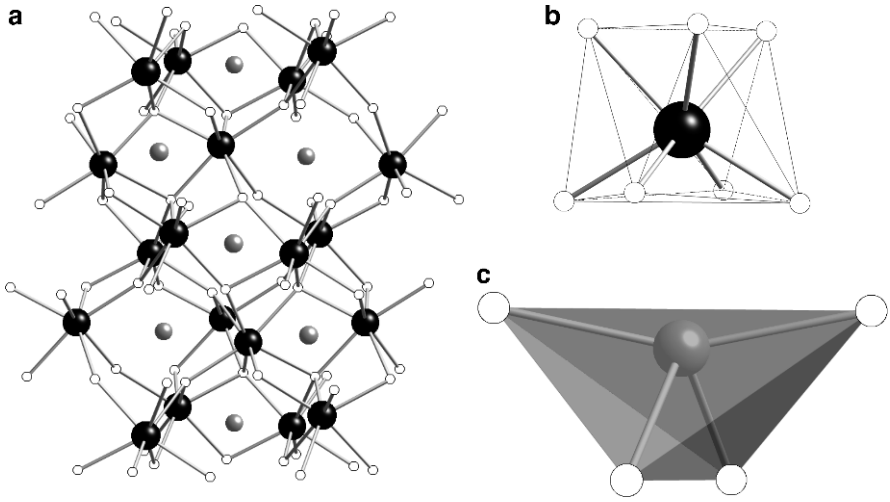

Fig. 37.30 *Views of* (*a*) *the structure of* U_2PdS_4 *with bonds to Pd atoms removed for clarity;* (*b*) US_7 *polyhedron;* (*c*) PdS_4 *squashed tetrahedron* (*U: black; Pd: gray; S: white*).

Fe, Co, and possibly Ni compounds form structures, shown in Fig. 37.31, that are more closely related to those of the $AnMQ_3$ compounds.

The U_3Q_5 structure (Potel *et al.*, 1972) (Fig. 37.5) possesses two crystallographically independent U sites, one monocapped octahedral and one bicapped trigonal prismatic. The formal charges can be assigned as $U^{4+}(U^{3+})_2(Q^{2-})_5$, because there are no Q–Q bonds. The U^{3+} cations occupy the bicapped trigonal prismatic sites. Both divalent and trivalent metal ions can be substituted into the U_3Q_5 structure to form compounds of formula $M_xU_{3-x}Q_5$. For the divalent cations the maximum value of x is 1, because as M^{2+} substitutes for U^{3+} another U^{3+} converts to U^{4+}. Such a substitution reduces the symmetry of the structure from orthorhombic to monoclinic (with $\beta = 90°$), with subsequent splitting of the bicapped trigonal prismatic site into two crystallographically distinct positions. The non-uranium metal atoms always substitute into one of the bicapped trigonal prismatic sites, perhaps because of their larger ionic radii, greater than 1.00 Å in most cases. The same situation is observed in the only structurally characterized and related Th compound, Th_2SrSe_5 (Fig. 37.32) (Narducci and Ibers, 1998b). For the trivalent cations the maximum value of x is 2, corresponding to the formula M_2UQ_5, and to substitution of the U^{3+} site $[(M^{3+})_2U^{4+}(Q^{2-})_5]$. In this instance the structure remains orthorhombic and isostructural with U_3Q_5.

The unusual structure of U_2PbSe_5 is shown in Fig. 37.33. It comprises a network of one-dimensional corner-sharing $PbSe_4$ trigonal bipyramids, with the lone pair on Pb occupying one of the equatorial positions. These chains penetrate a three-dimensionally connected network of USe_6 distorted octahedra

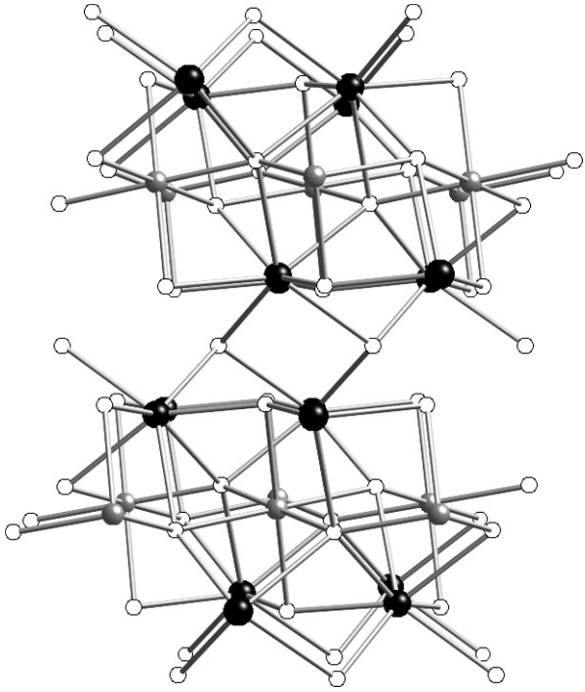

Fig. 37.31 *Structure of An_2MQ_5 for M = Fe, Co, and possibly Ni (An: black; M: gray; S: white).*

sharing corners and edges as well as a set of bicapped trigonal prismatic USe_8 polyhedra (Potel *et al.*, 1975).

37.3.14 An_2AQ_6 compounds

The actinide compounds of formula An_2AQ_6 (A = alkali metal or Tl) have generally been prepared by the reactions of the elements or by the reaction of the actinide with the appropriate polychalcogenide flux. These compounds present interesting problems in chemical bonding and formal oxidation states. When Q = Te, the known compounds $CsTh_2Te_6$ (Cody and Ibers, 1996), $Tl_{1.12}U_2Te_6$ (Tougait *et al.*, 1997b), and KTh_2Te_6 (Wu *et al.*, 1997) crystallize in space group *Cmcm* of the orthorhombic system. These compounds are isostructural; the layered structure features not only isolated Te^{2-} species but linear, infinite one-dimensional Te chains with Te−Te distances approximately 0.35 Å longer than that of a typical Te−Te single bond. When Q = Se, the known compounds KTh_2Se_6 (Choi *et al.*, 1998), $RbTh_2Se_6$ (Choi *et al.*, 1998), CsU_2Se_6 (Chan *et al.*, 2004), and KU_2Se_6 (Mizoguchi *et al.*, 2006) crystallize in space group *Immm* of the orthorhombic system. These compounds, which are isostructural, have a

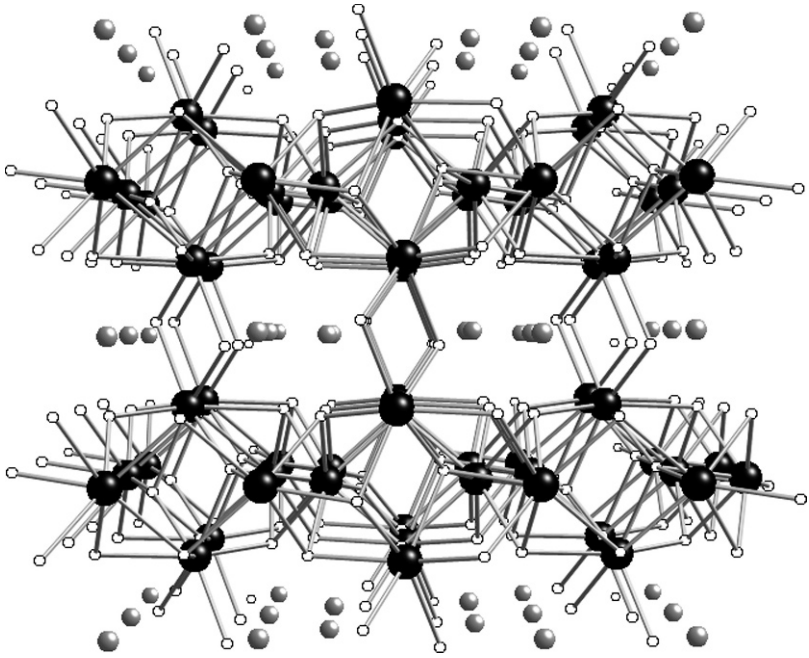

Fig. 37.32 *Structure of Th_2SrSe_5. Bonds to the Sr atoms have been removed for clarity. The Sr atoms sit in the eight-coordinate bicapped trigonal-prismatic sites* (*Th: black; Sr: gray; S: white*).

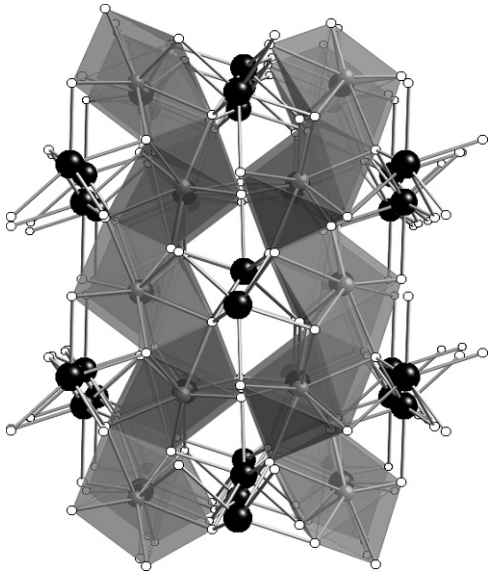

Fig. 37.33 *Structure of U_2PbSe_5 viewed down to the a-axis.* (*U: black; Pb: gray; Se: white*). *$PbSe_4$ trigonal pyramids are depicted as a polyhedral representation.*

layered structure that differs in its stacking pattern from that of the *Cmcm* structure. The *Immm* structure contains discrete Se^{2-} species and infinite one-dimensional Se chains with Se–Se distances about 0.35 Å longer than a typical Se–Se single bond. The only known S analogue is $K_{0.91}U_{1.79}S_6$ (Mizoguchi *et al.*, 2006). In this compound the infinite S chains display alternating S–S distances of 2.097(5) Å (a single bond distance) and 3.295(5) Å (a nonbonding distance).

The An_2AQ_6 structure is closely related to those of UTe_2 (Beck and Dausch, 1988) and $ZrSe_3$ (Furuseth *et al.*, 1975, Furuseth and Fjellvag, 1991). In these two binaries, metal atoms are again coordinated by eight Q atoms in a bicapped trigonal prism. These prisms link together by sharing vertices and capping Q atoms to form infinite chains. In UTe_2 these chains form a three-dimensional network by sharing the uncapped faces of the MQ_8 prisms, as shown in Fig. 37.34a. In $ZrSe_3$ the layers are separated by a van der Waals gap (Fig. 37.34b). In the An_2AQ_6 structure, these A cations force the layers apart by weakly coordinating to the eight Q atoms of the uncapped faces (Fig. 37.35a.). The isostructural compounds Th_2CuTe_6 (Narducci and Ibers, 1998b) and $U_2Cu_{0.78}Te_6$ (Huang and Ibers, 2001) are also known. They possess a three-dimensional structure with the Cu atoms formally bound tetrahedrally to four Te atoms, two from each uncapped face (Fig. 37.35b).

It has been postulated that in the Th_2ASe_6 (A = K, Rb) compounds the Se atoms in the $[Th_2Se_6]$ layers accept extra electrons from the A atoms, thereby breaking one out of four Se_2^{2-} bonds (Choi *et al.*, 1998). This picture is supported by a variety of physical measurements on these compounds (Choi *et al.*, 1998). This formulation leaves Th with the expected formal oxidation state of +4. On the basis of XPS measurements on a powder sample

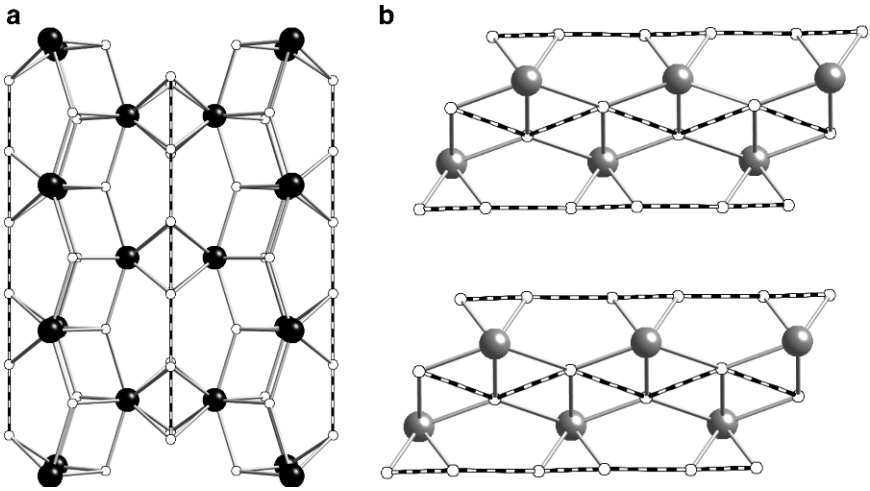

Fig. 37.34 *Comparison of the structures of* (*a*) UTe_2 *and* (*b*) $ZrSe_3$ (*U: black; Zr: gray; Se or Te: white*). *Te–Te and Se–Se bonds are shown as horizontal multi-banded bonds.*

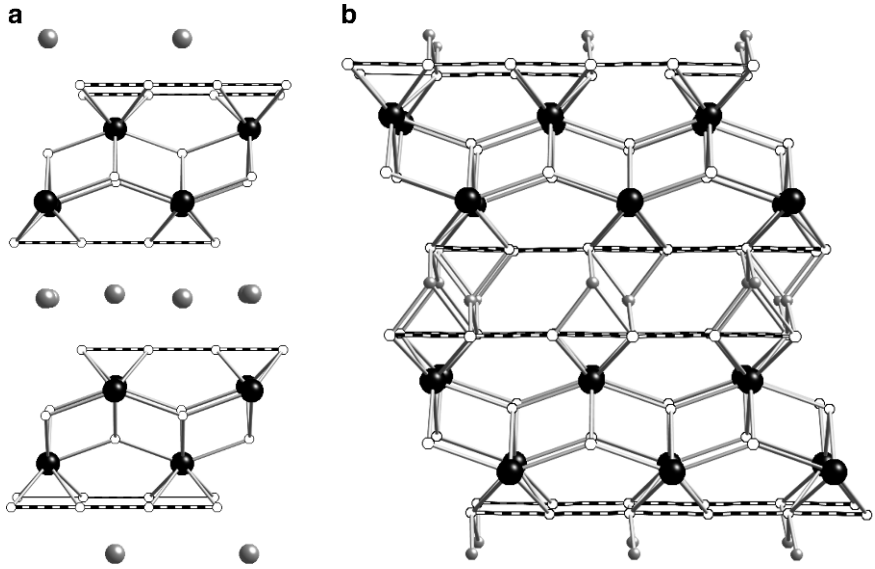

Fig. 37.35 *Comparison of the structures of the An_2AQ_6 compounds: (a) A = K, Cs, Tl; (b) A = Cu (An: black; A: gray; Q: white). Q−Q bonds are shown as horizontal multi-banded bonds.*

a formal oxidation state of +4 was assigned to U in KU_2Se_6 (Chan *et al.*, 2004). A comparison of KU_2Se_6 and $K_{0.91}U_{1.79}S_6$ (Mizoguchi *et al.*, 2006) offers further insight into the bonding in the An_2AQ_6 family. From charge balance the formal oxidation state of U is +4 in the latter compound. The electron responsible for the reduction of the Se−Se single bond in the Se_2^{2-} species in KU_2Se_6 cannot reduce the stronger S−S single bond in the S_2^{2-} species because of the relatively higher position of the S 3p σ* orbital compared to the Se 4p σ* orbital. Electron insertion into the S_2^{2-} dimer chain leading to a delocalized S chain with S−S distances longer than a normal single bond does not lower the total energy of the system as effectively as the formation of cationic vacancies. The structural difference between the sulfide and the selenide arises because the S valence states are more localized (anionic) than are the Se and Te states. Therefore, a compensation takes place via the formation of cationic vacancies that results in the observed formulation $K_{0.91}U_{1.79}S_6$. Apparently, the formation of cationic vacancies is also more facile than reduction of the U^{4+} ion.

37.3.15 An_2M_2Q compounds

Compounds of the type An_2N_2Q, where An = U, Th and Q = S, Se, Te, form from reactions of the binary chalcogenides with dinitrogen at 1,500–1,700°C

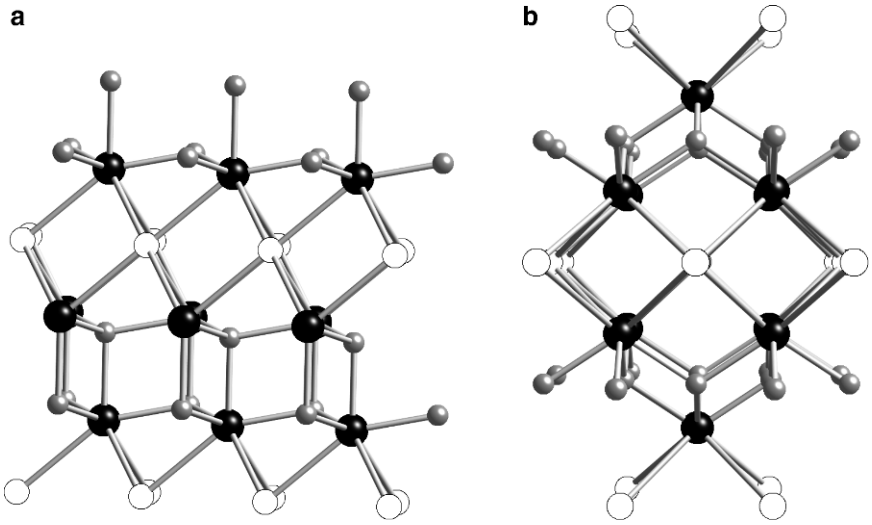

Fig. 37.36 *Comparison of the structures An_2N_2Q as viewed down the b-axis: (a) Q = S, Se, and (b) Q = Te (An: black; N: gray; Q: white).*

(Benz and Zachariasen, 1969). These compounds possess elegant structures that are closely related to the AnMQ family. There are two subgroups of the An_2N_2Q type, again as a function of ionic size (Benz and Zachariasen, 1970). When Q = S, Se the compounds adopt the Ce_2O_2S structure type, as shown in Fig. 37.36a. The An atoms have a capped triangular antiprismatic environment. Three Q atoms comprise one face of the prism, whereas four N atoms make up the opposite face and cap. The antiprisms share corners in one dimension and edges along the other to form slabs that stack by sharing corners and caps of the common faces. The Ce_2O_2S structure type cannot accommodate Te with its larger ionic radius. Thus, the compounds An_2N_2Te adopt a body-centered tetragonal structure, shown in Fig. 37.36b. Once again, An atoms are sandwiched between N and Te layers and are found in distorted square-antiprismatic sites. In this subgroup these antiprisms lack additional capping Q atoms and the An atom is only eight-coordinate. As expected, the An atoms also sit much closer to the N atoms than to the Q atoms and therefore the prisms are highly distorted.

The same structural subgroups are seen in the An_2O_2Q compounds. Thus, the compound Pu_2O_2Se (Zachariasen, 1949b) adopts the Ce_2O_2S structure, whereas the compound U_2O_2Te (Breeze *et al.*, 1971) adopts the An_2N_2Te structure.

The magnetic structures of U_2N_2S and U_2N_2Se (Leciejewicz *et al.*, 1975) and of U_2N_2Te (Leciejewicz *et al.*, 1977) have been determined from neutron diffraction studies of the powders. The magnetic moments were found to be 1.4, 2.3, and 2.50(5) μ_B, respectively. The magnetic cells of U_2N_2S and U_2N_2Se were

found to be the same as the crystallographic ones. U_2N_2Te shows a ferromagnetic alignment of the magnetic moments below 68 K with the magnetic direction forming an angle of 70(5)° with the tetragonal axis. From measurements of the magnetic susceptibilities it was determined that Pu_2O_2S and Pu_2O_2Se powders were antiferromagnetic with Néel temperatures of 28 and 34 K, respectively; both compounds were found to be semiconductors with band gaps of about 0.5 eV (Costantini *et al.*, 1983).

37.3.16 $An_2M_{10}Q_8$ compound

The only known compound of this stoichiometry is $Te_8[U_2Br_{10}]$ (Beck and Fischer, 2002). This compound, which was prepared by the reaction of $TeBr_4$, UBr_5, and $SiBr_4$ at 200°C, consists of one-dimensional $[Te_8^{2+}]_n$ cations and one-dimensional $[U_2Br_{10}^{2-}]_n$ anions. These ions are arranged in a simple tetragonal rod packing (Fig. 37.37). The formal oxidation state of U is +4.

37.3.17 An_3MQ_5 compounds

The isostructural compounds $U_3Ge_{0.7}Te_5$ and $U_3Sn_{0.5}Te_5$ (Tougait *et al.*, 2002) were prepared by heating U_3Te_5 with Ge or Sn at 850°C. In the structure there are both UTe_8 bicapped trigonal prisms and UTe_7 seven-octahedra. The three-dimensional packing of these polyhedra results in distorted hexagonal cavities where Ge or Sn reside (Fig. 37.38).

These compounds are hard ferromagnets with ordering temperature of 135 and 140 K for the Ge and Sn compounds, respectively. At low temperatures

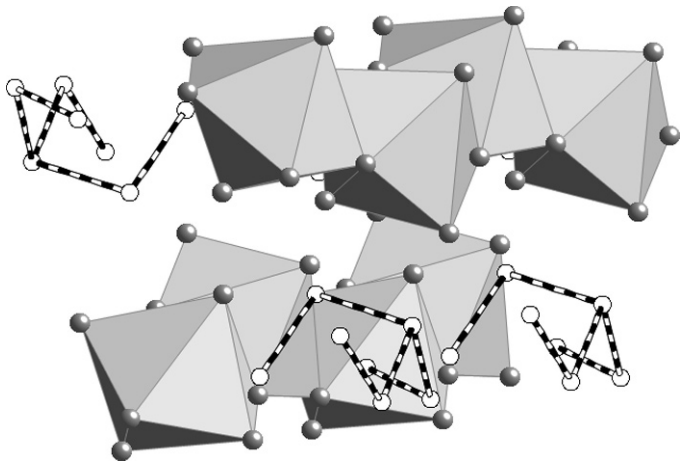

Fig. 37.37 *Structure of $Te_8[U_2Br_{10}]$ as viewed down* [101] (*UTe_7: gray polyhedra; Br: gray balls; Te: white balls*). *Te–Te bonds are shown as horizontal multi-banded bonds.*

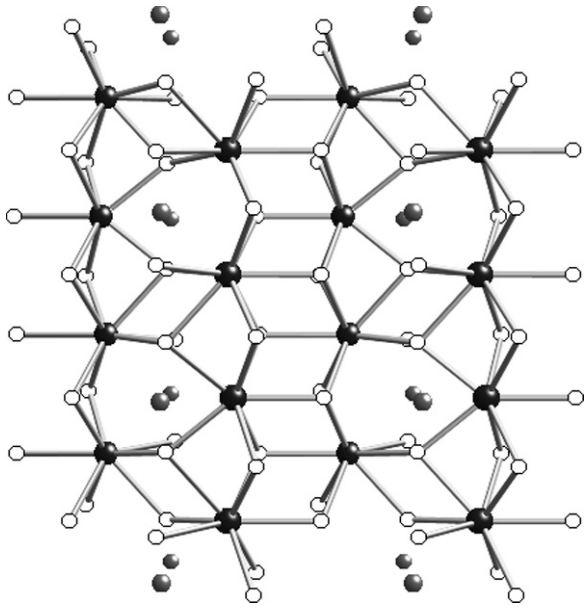

Fig. 37.38 *Structure of $U_3Ge_{0.7}Te_5$ as viewed down the a-axis* (*U: black; Ge: gray; Te: white*).

they display large magnetocrystalline anisotropy with origin on the domain wall and pinning at the magnetic domain boundaries.

37.3.18 An_3MQ_6 compounds

In addition to the $UScS_3$ (Julien *et al.*, 1978) and U_8ScQ_{17} (Q = S, Se) (Tien and Rodier, 1979), the compound U_3ScS_6 is known (Rodier and Tien, 1976). It forms from the reaction of UO_2 with Sc_2O_3 in a stream of H_2S at 1,350°C. The structure of U_3ScS_6 (Rodier and Tien, 1976) is shown in Fig. 37.39. Though overall it bears a close resemblance to the *Cmcm* $AnMQ_3$ compounds (Section 37.3.3), the U coordination environments are closer to those found in the $An_2M_2Q_5$ structures (Section 37.3.13). There are three crystallographically unique U atoms in U_3ScS_6; two are in bicapped trigonal-prismatic sites and the third is in a seven-coordinate capped octahedral site. ScS_6 octahedra are linked through edges to form infinite, though isolated, chains.

37.3.19 $An_3M_2Q_7$ compounds

The compounds $U_3Cu_2Q_7$ (Q = S, Se) (Daoudi *et al.*, 1996c) form from the reaction of the metal chalcogenide binaries at 600°C. The structure of $U_3Cu_2Q_7$ (Fig. 37.40) contains trigonal planar CuQ_3 units that stack along the corners of

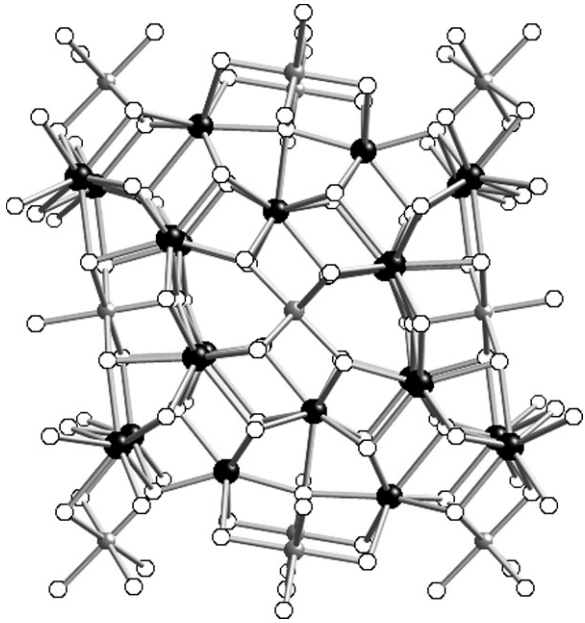

Fig. 37.39 *Structure of U_3ScS_6 as viewed down the c-axis* (*U: black; Sc: gray; S: white*).

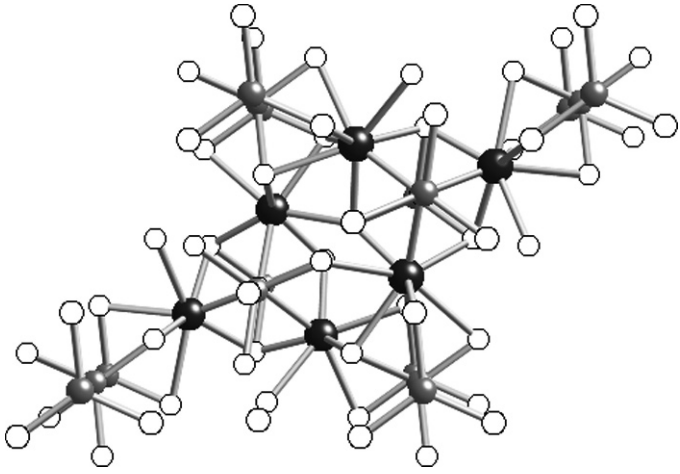

Fig. 37.40 *Structure of $U_3Cu_2Q_7$ as viewed down the c-axis* (*U: black; Cu: gray; Q: white*).

the unit cell. Double chains of UQ_8 polyhedra run through the middle of the unit cell, with CuQ_4 squashed tetrahedra filling in the holes between UQ_8 units. This structure is isotypic with La_3CuSiS_7, where SiS_4 and CuS_3 polyhedra are found (Daoudi *et al.*, 1996c).

37.3.20 $An_4M_4Q_3$ compound

The novel material $U_4O_4Te_3$ (Noel *et al.*, 1995) was prepared accidentally when U_3Te_4 powder was heated to 1,560°C in an alumina crucible. The structure of this unusual material is shown in Fig. 37.41. The structure is an intergrowth of the unit cell of U_2O_2Te (Breeze *et al.*, 1971) between two unit cells of UOTe (the PbFCl structure, Fig. 37.8b).

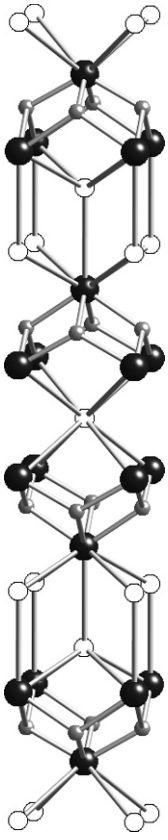

Fig. 37.41 *Structure of $U_4O_4Te_3$ as viewed approximately down the b-axis* (*U: black; O: gray; Te: white*).

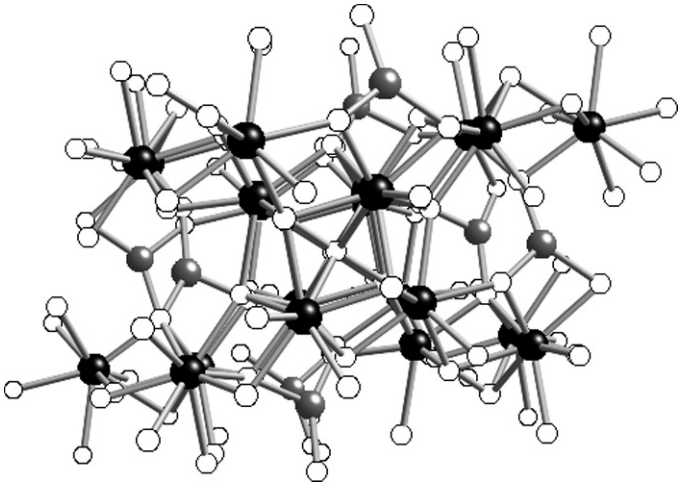

Fig. 37.42 *Structure of $U_6Cu_2S_{13}$ as viewed approximately down* [0$\bar{1}$0] (*U: black; Cu: gray; S: white*).

37.3.21 $An_6M_2Q_{13}$ compounds

The compounds $U_6Cu_2Q_{13}$ (Q = S, Se) (Noel, 1980) form from the reaction of the metal chalcogenide binaries at 800°C. The structure of $U_6Cu_2S_{13}$ (Noel and Potel, 1985) (Fig. 37.42) comprises layers of trigonal CuQ_3 units and dodecahedral and bicapped trigonal UQ_8 polyhedra; the layers alternate Cu−U−U−Cu. Magnetic susceptibility measurements on powders indicate that these compounds are Curie–Weiss paramagnetic above 70 and 40 K, respectively. No magnetic ordering is observed down to 4.2 K.

37.3.22 $An_6M_2Q_{15.5}$ compounds

Compounds of the type $U_6M_2Q_{15.5}$ (M = Rh, Ir; Q = S, Se) (Daoudi and Noel, 1996) form from reactions of UQ_2 with M and Q at temperatures near 1,100°C, but $U_6Rh_2S_{15.5}$ forms in the reaction of US_2 with Rh and S in a stream of H_2S at 1,400°C. These compounds crystallize with a three-dimensional channel structure built up of MQ_6 octahedra surrounded by UQ_8 bicapped trigonal prisms (Fig. 37.43).

37.3.23 An_8MQ_{17} compounds

Compounds of the type U_8MQ_{17} are formed at approximately 1,000–1,200°C from either stoichiometric reactions of the elements or from combinations of the binary metal chalcogenides. They are known for Q = S, Se and M = Mg, Sc−Ni

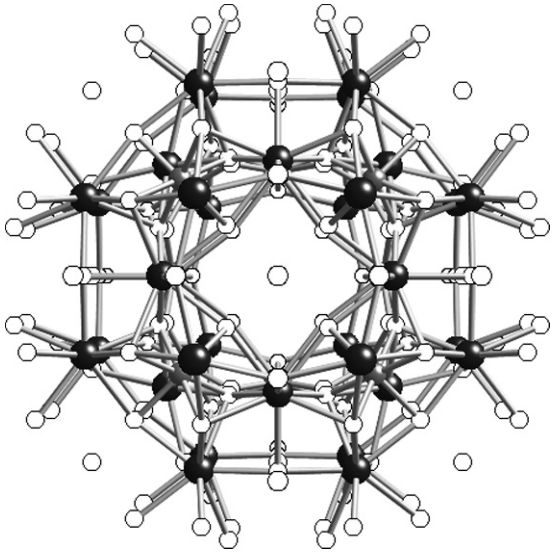

Fig. 37.43 *Structure of $U_6M_2Q_{15.5}$ as viewed down the c-axis* (*U: black; M = Rh, Ir: gray; Q = S, Se: white*).

(Noel *et al.*, 1971; Noel, 1973; Noel, 1974; Noel *et al.*, 1975a; Vovan and Rodier, 1979; Kohlmann *et al.*, 1997). No related Th compounds have been reported.

The U_8MQ_{17} compounds crystallize in the structure shown in Fig. 37.44. U atoms are located in three crystallographically distinct sites: one bicapped trigonal-prismatic and the other two highly deformed dodecahedral. MQ_6 octahedra sit at the corners of the unit cell and at the center of one face. They are isolated from each other by the various U polyhedra. Thus, the MQ_6 octahedra share no Q atoms with each other. The structure is built up from chains of the U polyhedra. The bicapped trigonal prisms share edges and caps to form infinite chains (P). The two distinct dodecahedra form edge-shared chains (D). These chains alternate P−D−P−D−P−. M atoms fill the octahedral holes formed by the chains.

37.4 QUATERNARY ACTINIDE CHALCOGENIDES

The introduction of additional elements increases the complexity of the structures in these materials. Synthetically this can be challenging, because simple binary and ternary compounds are thermodynamically favored and compete with the more complex compositions. Quaternary compounds with actinides have only recently been investigated. Therefore, the known quaternary actinide chalcogenide compounds are relatively few in number compared to the ternary

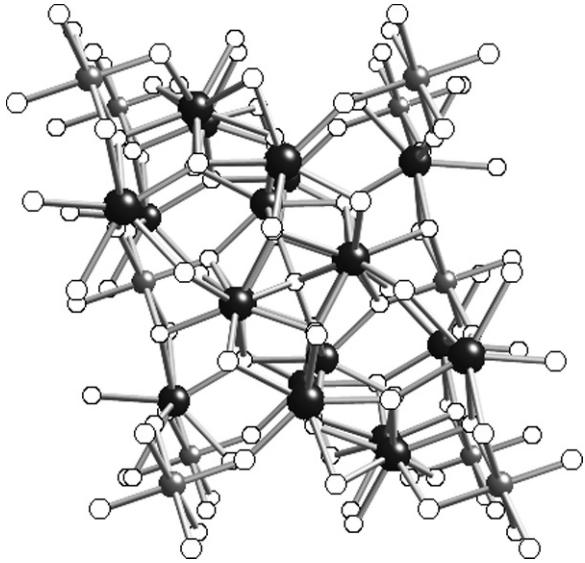

Fig. 37.44 *Structure of U_8MQ_{17} as viewed down the c-axis* (*U: black; M: gray; Q: white*).

and binary compounds. Quaternary compounds are known mainly for U and Th, but there are some examples of Pu-containing compounds. All quaternary actinide chalcogenides described below were isolated by reactive flux methods (Sunshine *et al.*, 1987; Kanatzidis and Sutorik, 1995), unless otherwise noted. The quaternary actinide chalcogenides with well-determined crystal structures are listed in Tables 37.4 and 37.5.

37.4.1 $AMAnQ_3$ compounds

Many quaternary actinide chalcogenide compounds have the general formula $AMAnQ_3$ (A = K, Rb, Cs; M = Cu, Ag; An = U, Th; Q = S, Se, Te) and adopt the layered $KZrCuS_3$ structure type (Mansuetto *et al.*, 1992). The structure of these materials is built from edge-shared AnQ_6 octahedra and MQ_4 tetrahedra, as illustrated for $RbCuUS_3$ in Fig. 37.45. The quaternary U chalcogenides with the $KZrCuS_3$ structure type are the compounds $KCuUS_3$, $RbCuUS_3$, $RbAgUS_3$, $CsCuUS_3$, $CsAgUS_3$, $RbAgUSe_3$, and $CsAgUSe_3$ (Yao *et al.*, 2008), as well as $KCuUSe_3$ (Sutorik *et al.*, 1996), $CsCuUSe_3$ (Huang *et al.*, 2001), and $CsCuUTe_3$ (Cody and Ibers, 1995). From charge balance considerations and the absence of short Q–Q distances, a formal oxidation state of +4 may be assigned for the U atoms in all these compounds.

Electrical conductivity versus temperature data revealed that $CsCuUS_3$ is a semiconductor with a band gap energy of ~0.3 eV (Yao *et al.*, 2008).

Table 37.4 *The known quaternary uranium chalcogenides.*

Compound	*References*	*Structure*	*Magnetism*	*Electrical properties*
$AMUQ_3$ (A = K, Rb, Cs; M = Cu, Ag; Q = S, Se, Te)	Cody and Ibers, 1995; Sutorik *et al.*, 1996; Huang *et al.*, 2001; Yao *et al.*, 2008	Layered	antiferromagnetic ($CsCuUS_3$) paramagnetic ($KCuUSe_3$)	semiconductor
AU_2SbQ_8 (Q = S,Se)	Choi and Kanatzidis, 1999	Layered	paramagnetic	n/a
$K_6Cu_{12}U_2S_{15}$	Sutorik *et al.*, 2000	Three-dimensional	paramagnetic	p-type metallic
$K_2Cu_3US_5$	Gray *et al.*, 2007	Layered	antiferromagnetic	n/a
$Cs_8U_5(P_3S_{10})_2(PS_4)_6$	Hess *et al.*, 2001	Three-dimensional	n/a	n/a
$A_{11}U_7(PS_4)_{13}$ (A = K, Rb)	Gieck and Tremel, 2002	Three-dimensional	antiferromagnetic	n/a
$K_5U(PS_4)_3$	Hess *et al.*, 2001	Discrete	n/a	n/a
$Ba_4Cr_2US_9$	Yao and Ibers, 2008	Chain	n/a	n/a
$Ba_2Cu_2US_5$	Zeng *et al.*, 2008	Layered	paramagnetic	n/a
$(UO)_2ErS_3$	Jaulmes *et al.*, 1986	Layered	n/a	n/a
$(UOS)_4LuS$	Jaulmes *et al.*, 1990	Layered	n/a	n/a
$Na_4(UO_2)Cu_2S_4$	Sutorik and Kanatzidis, 1997b	Layered	n/a	n/a
$Cs_4(UO_2)(S_2)_3$	Sutorik and Kanatzidis, 1997c	Discrete	n/a	n/a
$Na_4(UO_2)(S_2)_3Na_3S_4$	Sutorik and Kanatzidis, 1997c	Discrete	n/a	n/a
$Rb_4U_4P_4Se_{26}$	Chondroudis and Kanatzidis, 1997	Three-dimensional	paramagnetic	n/a
α-$K_2UP_3Se_9$	Chondroudis and Kanatzidis, 1996	Layered	antiferromagnetic	n/a
$Cs_2Hg_2USe_5$	Bugaris *et al.*, 2008	Layered	paramagnetic	semiconductor
$CsMUTe_5$ (M = Ti, Zr)	Cody and Ibers, 1995; Kim *et al.*, 2006	Layered	paramagnetic	semiconductor
$Cs_8Hf_5UTe_{30.6}$	Cody and Ibers, 1995	Chain	n/a	n/a

Table 37.5 *The known quaternary thorium and plutonium chalcogenides.*

Compound	*References*	*Structure*
$A_5Th(PS_4)_3$ (A = K, Rb, Cs)	Hess *et al.*, 2001	Discrete
$Cs_4Th_4P_4Se_{26}$	Briggs Piccoli *et al.*, 2001	Three-dimensional
α-$A_2ThP_3Se_9$ (A = K, Rb)	Briggs Piccoli *et al.*, 2000	Layered
β-$K_2ThP_3Se_9$	Briggs Piccoli *et al.*, 2002	Layered
$KCuThS_3$	Selby *et al.*, 2005	Layered
$K_2Cu_2ThS_4$	Selby *et al.*, 2005	Layered
$K_3Cu_3Th_2S_7$	Selby *et al.*, 2005	Layered
$Cs_4Th_4P_6S_{18}$	Chan *et al.*, 2005	Layered
$K_{10}Th_3(P_2S_7)_4(PS_4)_3$	Hess *et al.*, 2001	Layered
$KThSb_2Se_6$	Choi *et al.*, 1997	Three-dimensional
$Cs_4Th_2P_5Se_{17}$	Briggs Piccoli *et al.*, 2000	Chain
$Rb_7Th_2P_6Se_{21}$	Chan *et al.*, 2005	Chain
$K_3Pu(PS_4)_2$	Hess *et al.*, 2002	Chain
$APuP_2S_7$(A = K, Rb,Cs)	Hess *et al.*, 2002	Layered

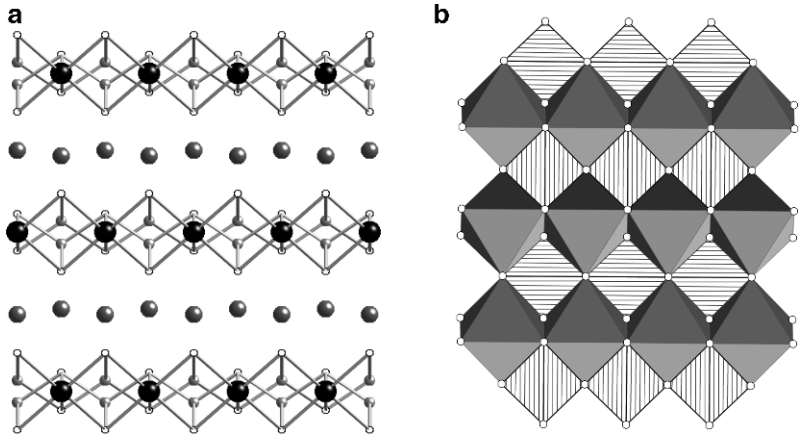

Fig. 37.45 (*a*) *View of the layers of* $RbCuUS_3$ *down the c-axis, with the* Rb^+ *ions intercalated between the layers* (*U: black; Cu: light gray; S: white; Rb: dark gray*); (*b*) *a single layer of* $RbCuUS_3$ (*US_6: gray polyhedra; CuS_4: striped polyhedra*).

An interesting theoretical study (periodic DFT spin band-structure calculations) was performed for $CsCuUS_3$ and $CsAgUS_3$. The results indicated an overall antiferromagnetic order for these compounds. The energetically-favored magnetic structure for both compounds consists of U-atom based spins aligned parallel within the layers and antiparallel between adjacent layers (Yao *et al.*, 2008).

The only example of a quaternary Th chalcogenide with the $KZrCuS_3$ structure type is the compound $KCuThS_3$ (Selby *et al.*, 2005). The structure of this compound in comparison to the structures of two other quaternary thorium sulfides is discussed in Section 37.4.17.

37.4.2 AU_2SbQ_8

The alkali chalcoantimonate U compounds KU_2SbSe_8 and RbU_2SbS_8 display a layered structure and crystallize in the polar noncentrosymmetric space group *Cm* (Choi and Kanatzidis, 1999). The U atoms adopt a bicapped trigonal prismatic coordination geometry (Fig. 37.46b). The coordination environment of U consists of two S_2^{2-} units forming the parallel edges of the prism and four S^{2-} units occupying the apex and capping positions. The trigonal prisms form chains along the *a*-axis by sharing their triangular faces. The chains share capping S atoms, thus forming sheets (Fig. 37.46a).

The structure of KU_2SbSe_8 is identical to that of RbU_2SbS_8 (Choi and Kanatzidis, 1999). However, these structures display different superstructures. The superstructure of RbU_2SbS_8 has a periodic arrangement of Rb and Sb along all the axes whereas that in KU_2SbSe_8 has well-ordered K and Sb atoms in every other layer but disordered K and Sb atoms in the remaining layers.

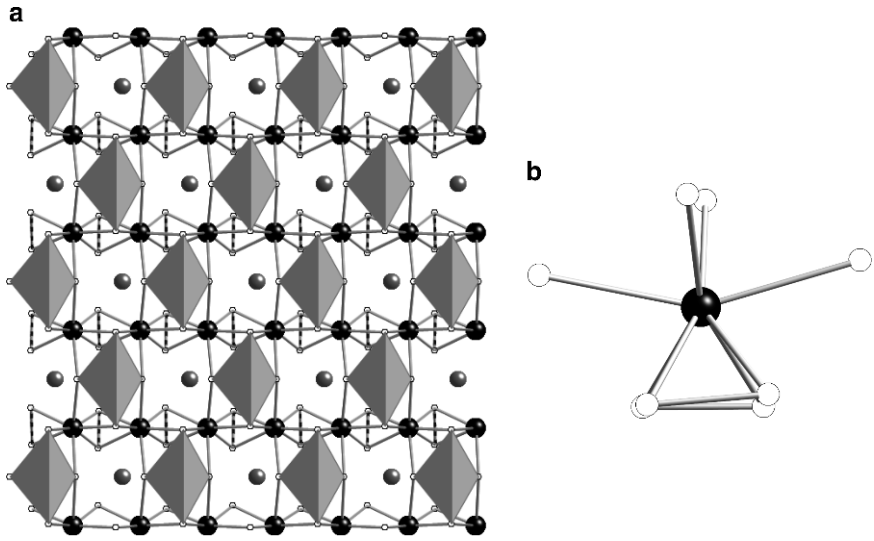

Fig. 37.46 (*a*) *The structure of* RbU_2SbS_8 *viewed down the c-axis* (SbS_4*: gray polyhedra; U: black; Rb: gray; S: white*); (*b*) *the U coordination environment. S–S bonds are shown as horizontal multi-banded bonds.*

RbU_2SbS_8 is a semiconductor with a band gap close to 1.4 eV. Magnetic susceptibility data indicated an effective magnetic moment ~3.2 μ_B, relatively close to the calculated value for U^{4+} (3.58 μ_B).

37.4.3 $K_6Cu_{12}U_2S_{15}$

An example of a quaternary uranium sulfide with a three-dimensional cubic structure is the compound $K_6Cu_{12}U_2S_{15}$ (Sutorik *et al.*, 2000). Its structure is constructed from US_6 octahedra interconnected through CuS_3 trigonal planar units. Straight columns of alternating US_6 and CuS_3 polyhedra are thus formed (Fig. 37.47). The three-dimensional framework is built by the interconnection of neighboring columns through S atoms of CuS_3 units (Fig. 37.47). Viewed parallel to the *a*-axis of the structure, small channels hosting K atoms are apparent. One of the many interesting features of this structure is the observed distance of 3.017(3) Å between neighboring U and Cu atoms. This short

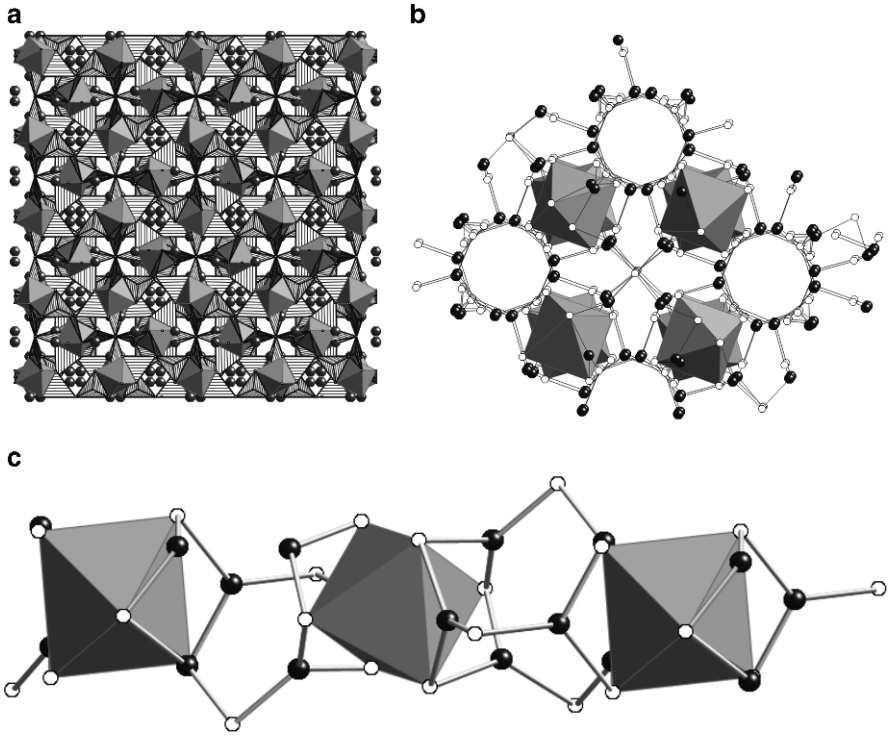

Fig. 37.47 (*a*) *View of the structure of* $K_6Cu_{12}U_2S_{15}$ *down the c-axis* (US_6*: gray polyhedra;* CuS_3*: striped polyhedra; K: black*); (*b*) *interconnection of four chains of* US_6/CuS_3 *polyhedra through* SCu_4 *units* (*S: white; Cu: black*); (*c*) *a single chain of* US_6/CuS_3 *polyhedra.*

distance is similar to that in the UCu_5 intermetallic compound (2.916 Å) (Baenziger *et al.*, 1950) and implies direct U−Cu bonding.

The isostructural compounds $Rb_6Cu_{12}U_2S_{15}$ and $Rb_6Cu_{12}U_2S_{15}$ have also been synthesized. The oxidation state of U in these compounds is puzzling and it is currently under investigation (Yao *et al.*, 2010).

37.4.4 $K_2Cu_3US_5$

$K_2Cu_3US_5$ is another quaternary compound in the system K/U/Cu/S (Gray *et al.*, 2007). It displays a new structure type crystallizing in the orthorhombic space group *Cmcm*. The structure of the material is layered, consisting of $^2_\infty[UCu_3S_5]^{2-}$ slabs (Fig. 37.48a). These slabs are made of edge-shared CuS_4 tetrahedra and US_6 octahedra. The octahedral-tetrahedral packing pattern for $K_2Cu_3US_5$ is *oct tet tet tet oct* (Fig. 37.48b) and is different from other known octahedral-tetrahedral packing patterns.

If the compound contains Cu in the +1 oxidation state, then charge balance is achieved with U in the +5 oxidation state. Magnetic susceptibility data revealed Curie–Weiss behavior in the temperature range 130–300 K with an effective magnetic moment of 2.45 μ_B, very close to the calculated value of 2.54 μ_B for U^{5+}. Bond valence calculations are also consistent with U^{5+}. No EPR signal from Cu^{2+} was detected, even at temperatures as low as 4.2 K, consistent with the presence of only Cu^{1+}. Hence, $K_2Cu_3US_5$ appears to be another rare example of a uranium chalcogenide in which the U has a formal oxidation state of +5.

37.4.5 $Cs_8U_5(P_3S_{10})_2(PS_4)_6$

The uranium chalcophosphate $Cs_8U_5(P_3S_{10})_2(PS_4)_6$ (Hess *et al.*, 2001) has a complex three-dimensional structure (Fig. 37.49a). In this structure the U atoms possess a +4 formal oxidation state and are eight-coordinated. The US_8 units can be described as bicapped trigonal prisms. The fundamental building block is a trimer, which consists of three U atoms each sharing two edges with the other two and two PS_4^{3-} units capping the top and bottom of the trimer (Fig. 37.49b). The trimers are connected with additional U atoms through PS_4^{2-} groups, thus forming a layer in the *ab* plane. One of the interesting features of this structure is the presence of a new chalcophosphate unit, namely the $[P_3S_{10}]^{5-}$ anion (Fig.37.49b). This unit comprises three corner-sharing PS_4 tetrahedra. It is the $[P_3S_{10}]^{5-}$ groups that connect the individual layers along the *c*-axis creating a three-dimensional structure with tunnels running along all crystallographic axes.

37.4.6 $A_{11}U_7(PS_4)_{13}$ (A = K, Rb)

The isostructural $A_{11}U_7(PS_4)_{13}$ (A = K, Rb) compounds (Gieck and Tremel, 2002) are another set of unusual quaternary uranium sulfides. The structure of

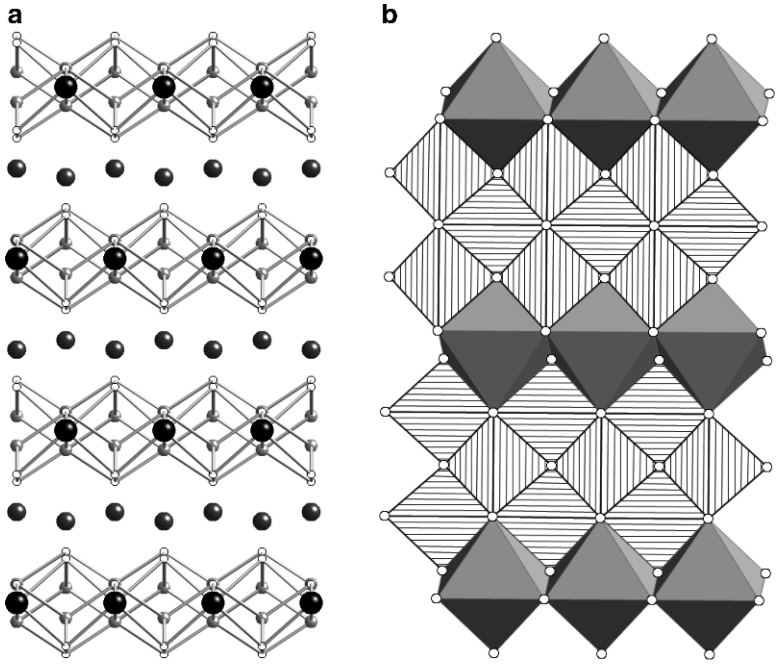

Fig. 37.48 (*a*) *View of the layers of* $K_2Cu_3US_5$ *down the c-axis, with the* K^+ *ions intercalated between the layers* (*U: black; Cu: light gray; S: white; K: dark gray*); (*b*) *a single layer of* $K_2Cu_3US_5$ (*US_6: gray polyhedra; CuS_4: striped polyhedra*).

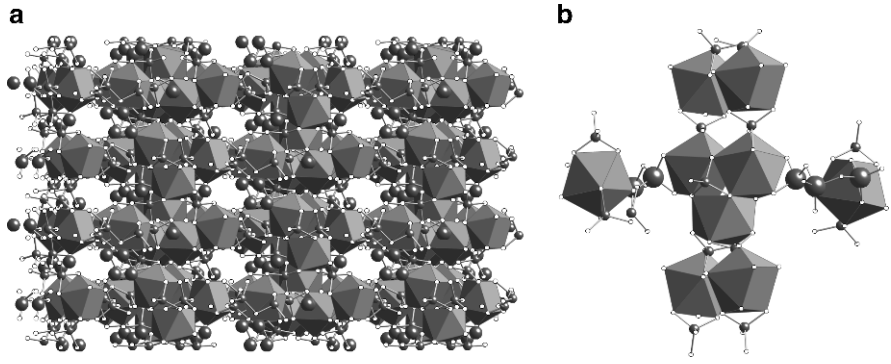

Fig. 37.49 (*a*) *View of the three-dimensional structure of* $Cs_8U_5(P_3S_{10})_2(PS_4)_6$ *down* $[\bar{1}01]$ *direction showing channels that contain* Cs^+ *ions* (*US_8: gray polyhedra; P: small black balls; S: white balls; Cs: large black balls*); (*b*) *the central trimer of* US_8 *polyhedra connected with additional polyhedra through* PS_4^{3-} *and* $P_3S_{10}^{5-}$ *units along the b- and c-axes respectively* (*P atoms of* PS_4^{3-}*: small black balls; P atoms of* $P_3S_{10}^{5-}$*: large black balls; S: white balls; US_8: gray polyhedra*).

these compounds is based on $U_7(PS_4)_{13}$ helices (Fig. 37.50). In each helix, U polyhedra are connected through double-bridging and chelating PS_4^{3-} groups (Fig. 37.50d,e). There are eight- and nine-coordinated U atoms in the structure. The US_8 polyhedra can be described as bicapped trigonal prisms (Fig. 37.50c); the US_9 polyhedra are tricapped trigonal prisms (Fig.37.50b). Four of the helices centered about the four-fold inversion axes (of the space group $I\bar{4}2d$) surround a relatively large pore with a diameter of ~5 Å that contains most of the A atoms (Fig. 37.50a). The connection of the helices creating this pore is made through PS_4^{3-} units, each of which bridges two helices. A second smaller pore, where also some of the A atoms are located, is formed by the interconnection of four helices through triply-connecting PS_4^{3-} groups. The remainder of

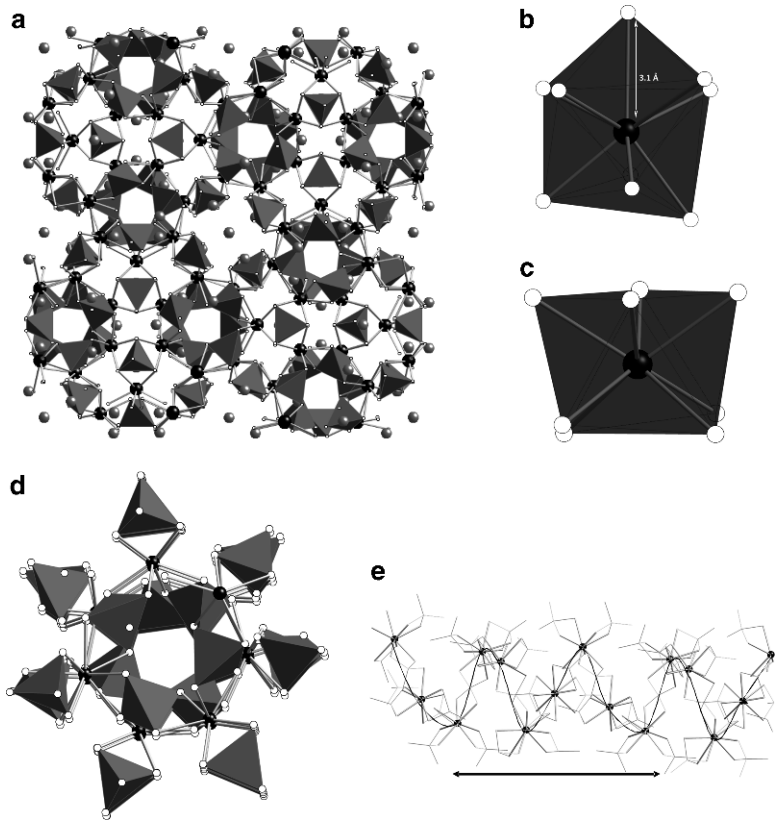

Fig. 37.50 (*a*) *View of the three-dimensional structure of* $K_{11}U_7(PS_4)_{13}$ *down the c-axis. Gray polyhedra represent* PS_4^{3-} *units* (*U: black; K: gray; S: white*), (*b*) US_9 *tricapped trigonal prisms;* (*c*) US_8 *bicapped trigonal prisms*, (*d*) $U_7(PS_4)_{13}$ *helices viewed down the c-axis;* (*e*) *the helices viewed along the c-axis* (*the arrow indicates the repeat distance*).

the A atoms are situated between PS_4^{3-} units within the helices. The oxidation state of the U in $A_{11}U_7(PS_4)_{13}$ should be +4, based on charge balance considerations.

Magnetic susceptibility studies for the K analogue show modified Curie–Weiss behavior in the temperature range 70–300 K and an antiferromagnetic transition around 60 K. The magnetic moment is 2.54 μ_B/U, substantially lower than the theoretical value for U^{4+} ions (3.58 μ_B). This large reduction of the magnetic moment was attributed to crystal field interactions.

37.4.7 $A_5An(PS_4)_3$ (A = K, Rb, Cs; An = U, Th)

$K_5U(PS_4)_3$ is the only example of a quaternary (non-oxo) uranium chalcogenide with molecular $[U_2(PS_4)_6]^{10-}$ dimers (Hess *et al.*, 2001). These dimers (Fig. 37.51a) are separated by K^+ ions. The U atoms are eight-coordinated in a dodecahedral geometry. The two U centers are bridged through two PS_4^{3-} units, and the coordination sphere of each U atom is completed by four S atoms provided by two face-capping PS_4^{3-} groups.

The diffuse reflectance UV-vis electronic spectrum of $K_5U(PS_4)_3$ contains a ligand-to-metal charge-transfer peak at ~1.7 eV, which is characteristic of U^{4+} ions (a similar absorption peak was also observed in the spectrum of $Cs_8U_5(P_3S_{10})_2(PS_4)_6$, Section 37.4.5).

$A_5Th(PS_4)_3$ (A = K, Rb, Cs) constitute compounds with a discrete dimeric structure (Hess *et al.*, 2001). The most striking difference between the structures of $A_5Th(PS_4)_3$ (A = K, Rb, Cs) and $K_5U(PS_4)_3$ is the coordination mode of one of the capping PS_4^{3-} units. In the Th compound this unit caps a triangular face of the nine-coordinated Th atoms (Fig. 37.51b), whereas the corresponding unit in the U compound is edge-bridging (Fig.37.51a).

37.4.8 $Ba_4Cr_2US_9$

$Ba_4Cr_2US_9$ (Yao and Ibers, 2008) represents the first chalcogenide compound in the perovskite-related $(A_3A'BQ_6)_m(A_3B_3Q_9)_n$ family (A = Ba; A′ = U; B = Cr; m = 3; n = 1). It crystallizes in the noncentrosymmetric trigonal space group *P*321. Its structure comprises $Cr_2US_9^{8-}$ chains consisting of face-sharing CrS_6 octahedra and US_6 trigonal prisms in the sequence *oct oct tp oct oct tp* (Fig. 37.52). Because there are no S–S bonds in the structure, a formal oxidation state of +4 was assigned to the U atoms.

37.4.9 $Ba_2Cu_2US_5$

The alkaline-earth chalcogenide $Ba_2Cu_2US_5$ was obtained in a two-step reaction from BaS, Cu_2S, and US_2 at 1,050°C for 4 d (Zeng *et al.*, 2008). $Ba_2Cu_2US_5$

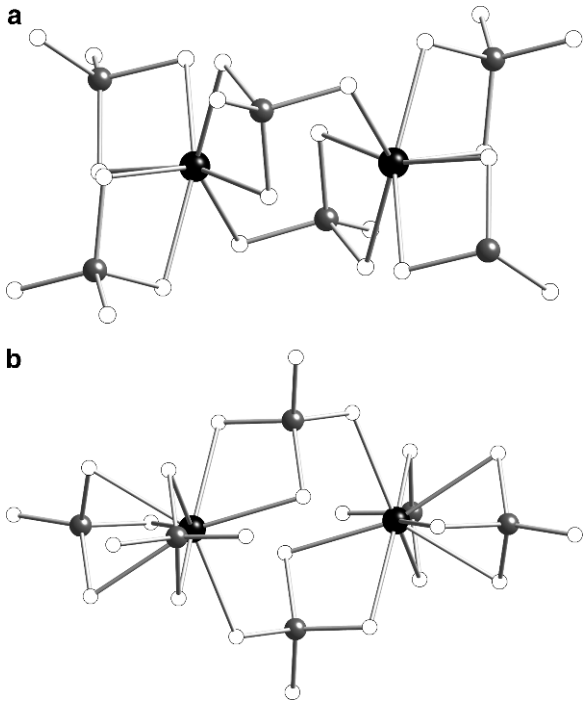

Fig. 37.51 (*a*) *The discrete binuclear compound* $K_5U(PS_4)_3$ (*U: black; P: dark gray; S: white;* K^+ *ions were omitted for clarity*); (*b*) *the discrete binuclear compound* $Cs_5Th(PS_4)_3$ (*Th: black; P: dark gray; S: white;* Cs^+ *ions were omitted for clarity*).

crystallizes in a new structure type in space group *C2/m* of the monoclinic system and features $^2_\infty[Cu_2US_5]^{4-}$ layers separated by Ba^{2+} ions, Fig.37.53a. The two-dimensional $^2_\infty[Cu_2US_5]^{4-}$ layer is built from US_6 octahedra and CuS_4 tetrahedra. The connectivity of the MS_n polyhedra within the layer in the [001] direction is *oct tet tet oct tet tet*, Fig.37.53b. A magnetic moment of 2.69(2) μ_B was obtained from the magnetic susceptibility data and no magnetic ordering was observed down to 2 K.

37.4.10 $(UO)_2ErS_3$, $(UOS)_4LuS$

The compounds characterized as $(UO)_2ErS_3$ (Jaulmes *et al.*, 1986) and $(UOS)_4LuS$ (Jaulmes *et al.*, 1990) were prepared by means of a high-temperature (1,800°C) solid-state reaction of UOS with ErS or LuS. In $(UO)_2ErS_3$, the U atoms are coordinated by four O and four S atoms (Fig. 37.54a). The structure is made of sheets of face-sharing UO_4S_4 polyhedra alternating with

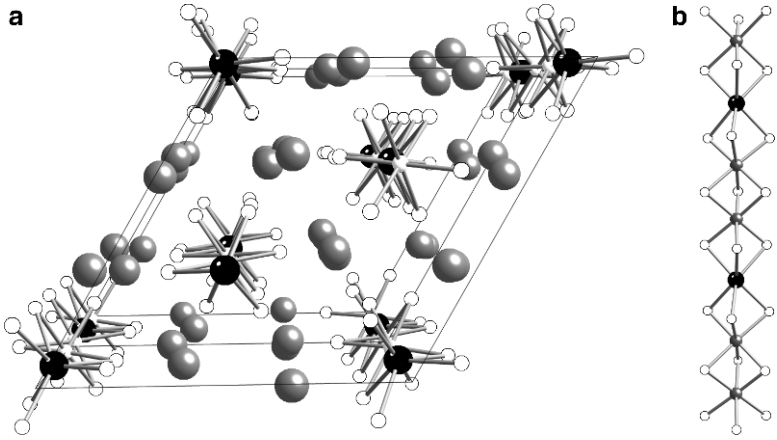

Fig. 37.52 (*a*) *View of the unit cell of* $Ba_4Cr_2US_9$ *down the c-axis;* (*b*) *view of a single chain of* $Ba_4Cr_2US_9$ *along the c-axis* (*U: black; Ba: large gray; Cr: small gray; S: white*).

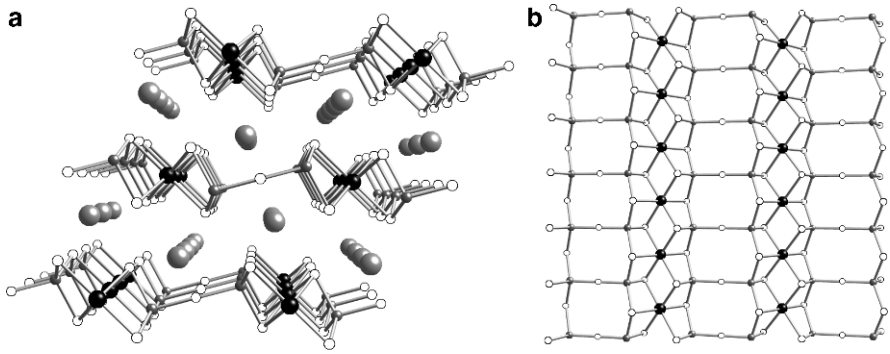

Fig. 37.53 (*a*) *View of the structure of* $Ba_2Cu_2US_5$ *down the b-axis;* (*b*) *view of a single layer of* $Ba_2Cu_2US_5$ *along the b-axis* (*U: black; Ba: large gray; Cu: small gray; S: white*).

sheets of ErS_6 octahedra. $(UOS)_4LuS$ displays a two-dimensional framework where two $(UOS)_2$ sheets alternate with (LuS) sheets (Fig. 37.54b). There are two crystallographically unique U atoms in this structure. One is eight-coordinated by four O and four S atoms whereas the other is nine-coordinated by four O and five S atoms.

For charge balance both compounds as formulated require mixed oxidation states for U, namely +4 and +3. However, the solution and refinement of single-crystal X-ray data collected for "$(UO)_2YbS_3$", prepared at 1,000°C, is identical

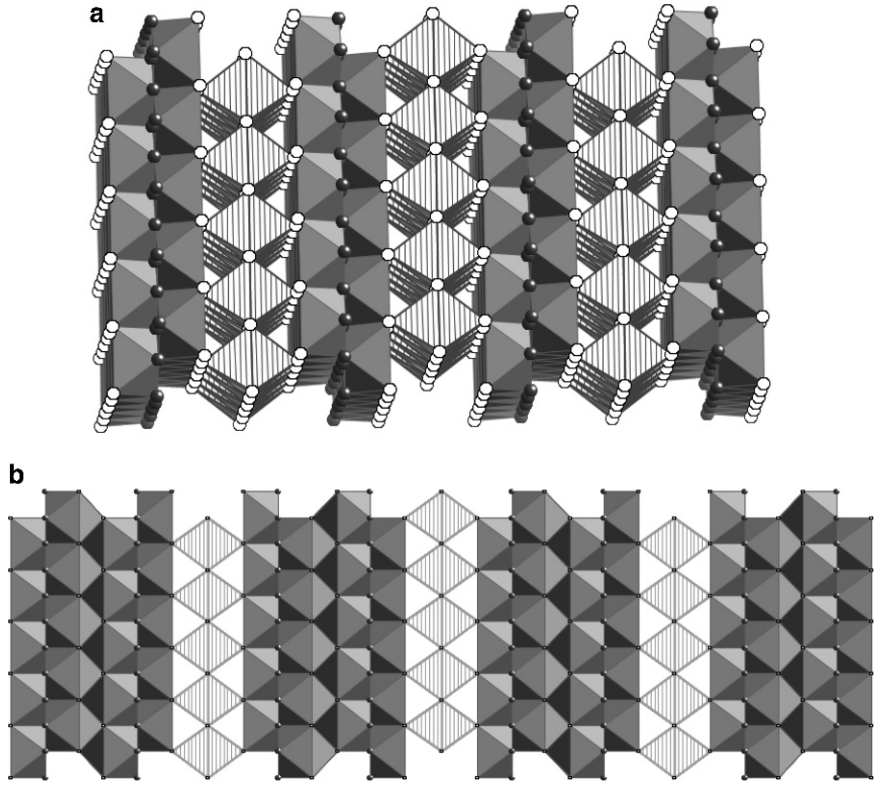

Fig. 37.54 (*a*) *The structure of* $(UO)_2ErS_3$ *made of alternating sheets of* UO_4S_4 *polyhedra and* ErS_6 *octahedra* (UO_4S_4*: gray polyhedra;* ErS_6*: striped polyhedra; O: dark gray balls; S: white balls*); (*b*) *the structure of* $(UOS)_4LuS$ *constructed by double sheets of* UO_4S_4 *and* UO_4S_5 *alternated by sheets of* LuS_6 *octahedra* (UO_4S_4 *and* UO_4S_5*: gray polyhedra;* LuS_6*: striped polyhedra; O: dark gray balls; S: white balls*).

with the earlier results save for the presence of Yb/U disorder (Jin *et al*., 2009). The actual formula is $(U_{0.5}Yb_{0.5}OS)_2YbS$; charge balance is achieved with Yb +3 and U solely in the +4 oxidation state.

37.4.11 $Na_4(UO_2)Cu_2S_4$, $Cs_4(UO_2)(S_2)_3$, $Na_4(UO_2)(S_2)_3{\cdot}Na_3S_4$

Three oxysulfides with U in its highest possible oxidation state of +6, namely the compounds $Na_4(UO_2)Cu_2S_4$, $Cs_4(UO_2)(S_2)_3$, and $Na_4(UO_2)(S_2)_3{\cdot}Na_3S_4$, have been reported. The isolation of these compounds from polychalcogenide fluxes indicates that the uranyl cation, UO_2^{2+}, can be chemically compatible with such fluxes to form strong U−S bonds. $Na_4(UO_2)Cu_2S_4$ is a layered material (Sutorik and Kanatzidis, 1997c). Its layers are constructed from UO_2^{2+} cations

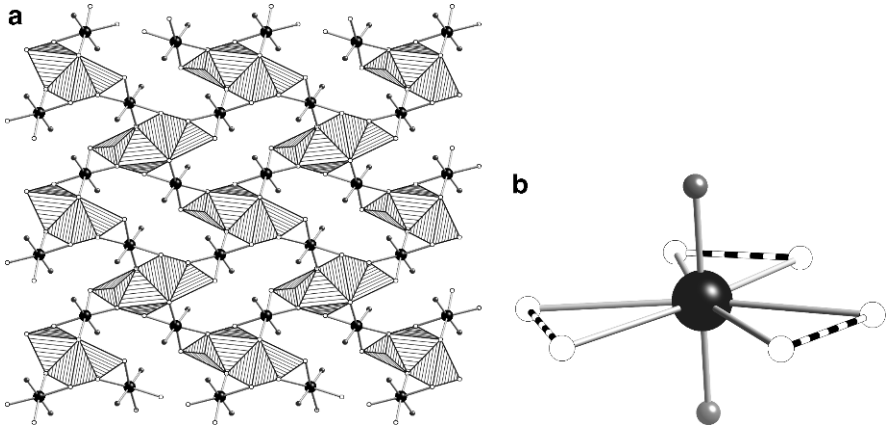

Fig. 37.55 (*a*) *View of a single layer of* $Na_4(UO_2)Cu_2S_4$ *down the a-axis* (CuS_4*: striped polyhedra; U: black balls; O: gray balls; S: white balls;* Na^+ *ions were omitted for clarity*); (*b*) *the structure of the mononuclear* $[(UO_2)(S_2)_3]^{4-}$ (*S–S bonds are shown as horizontal multi-banded bonds*).

and $Cu_4S_8^{12-}$ clusters, which provide the four S atoms that complete the octahedral coordination about U (Fig. 37.55a). The layers contain relatively large channels of approximate dimensions 6.4 Å × 9.3 Å. Interestingly, the U–Cu bonds are short (~3.1 Å) indicating partial bonding interactions between U and Cu atoms.

Both the $Cs_4(UO_2)(S_2)_3$ and $Na_4(UO_2)(S_2)_3{\cdot}Na_3S_4$ compounds (Sutorik and Kanatzidis, 1997a) contain the mononuclear discrete $[(UO_2)(S_2)_3]^{4-}$ anion (Fig. 37.55b). The U atom is connected with three η^2-S_2^{2-} units and two terminal O atoms. Considering a hypothetical atom at the midpoint of each η^2-S_2^{2-}unit, the coordination geometry of the U metal center may be viewed as trigonal bipyramidal.

37.4.12 $Rb_4U_4P_4Se_{26}$ and $Cs_4Th_4P_4Se_{26}$

Chalcophosphate anions are P/Q-containing anions with oxidized P atoms (usually in the +4 or +5 oxidation state). Examples are $[PSe_4]^{3-}$ and $[P_2Se_6]^{4-}$. The chalcophosphate $Rb_4U_4P_4Se_{26}$ (Chondroudis and Kanatzidis, 1997) has a three-dimensional structure Fig. 37.56a. The coordination environment of each U atom consists of two PSe_4^{3-} units, two chelating Se_2^{2-} groups, and one Se^{2-} unit. The overall coordination geometry for all U atoms is tricapped trigonal prismatic. Two U prisms form U_2Se_{14} dimers by sharing triangular faces. Neighboring dimers share edges, thus forming chains along [100] (Fig. 37.56b). The three-dimensional framework is constructed by the cross linking of these chains at four sides by PSe_4^{3-}groups (Fig. 37.56a). There are

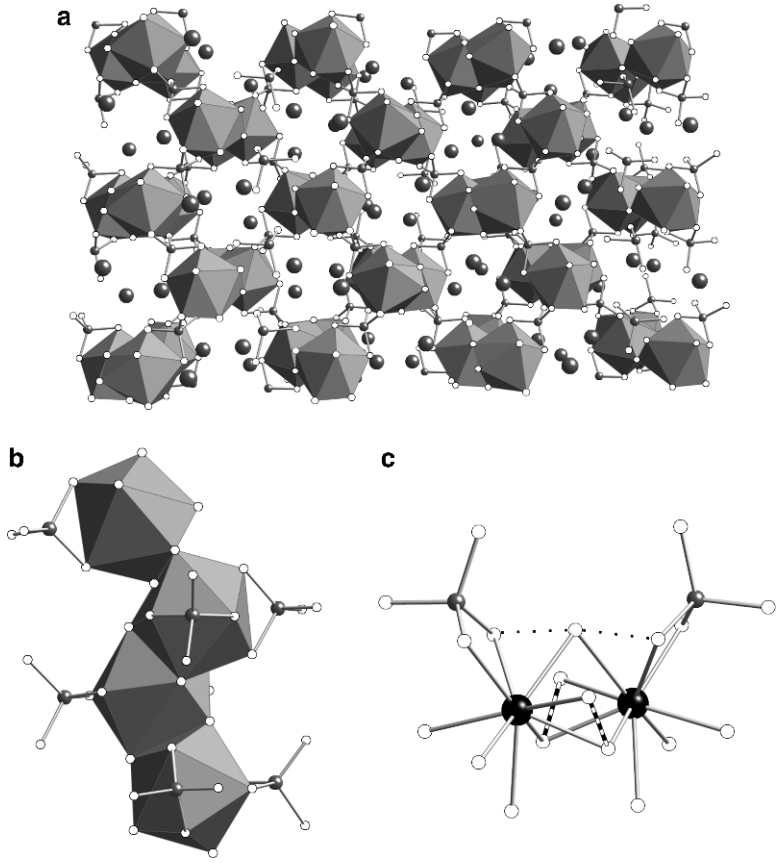

Fig. 37.56 (*a*) *View of the three-dimensional structure of* $Rb_4U_4P_4Se_{26}$ *down the b-axis* (USe_9*: gray polyhedra; Rb: large gray balls; P: small gray balls; Se: white balls*); (*b*) *representation of a chain of* USe_9 *prisms running along a-axis;* (*c*) *view of a dimer of Th atoms* (*large black balls*) *in* $Cs_4Th_4P_4Se_{26}$ *showing the* $P_2Se_9^{6-}$ *unit made of two* PSe_4^{3-} *units* (*P: gray; Se: white*) *joined by one Se atom. Se–Se short interactions are shown as horizontal multi-banded bonds, whereas the longer Se–Se interactions in the* $P_2Se_9^{6-}$ *unit are shown as dotted lines.*

relatively large cavities of 7 Å × 5 Å along [010]. The Rb atoms located in these cavities are disordered and easily exchangeable by smaller Li atoms. The formula $Rb_4U_4P_4Se_{26}$ is charge-balanced with U in the +5 oxidation state. The compound shows Curie–Weiss behavior in the temperature range 70–300 K. The derived effective magnetic moment is 1.85 μ_B, lower than the theoretical value for U^{5+} (2.54 μ_B). Additional studies ought to be conducted to verify or rule out the presence of U in an oxidation state of +5. This is a very unusual

oxidation state for U in solid-state chalcogenides, but it is not unknown (see Section 37.4.4). The diffuse reflectance mid-IR spectrum of $Rb_4U_4P_4Se_{26}$ showed a broad peak at ~3,900 cm^{-1} that was assigned an f^1-f^1 transition.

The analogous $Cs_4Th_4P_4Se_{26}$ compound displays a three-dimensional framework structure (Briggs Piccoli *et al.*, 2001), identical to the structure of $Rb_4U_4P_4Se_{26}$. The formula $[Cs_2Th_2(P_2Se_9)(Se_2)_2]_2$ seems to be charge-balanced only with the Th atoms in the +3 oxidation state (considering a charge of −4 for the P_2Se_9 unit). However, magnetic measurements revealed that the compound is diamagnetic, thus supporting the presence of Th^{4+} centers. It was claimed that the extra two electrons needed for the charge balance are located on the central Se atom of a dimeric $P_2Se_9^{6-}$ unit (Fig. 37.56c). This unit was not considered in the above description of the structure of $Rb_4U_4P_4Se_{26}$, because the central Se of this group is separated by 2.64–2.65 Å from the closest Se atoms of the two corner PS_4 units. According to the VSEPR model, the presence of an extra pair of electrons in the central Se atom of the $P_2Se_9^{6-}$ unit would induce a trigonal bipyramidal geometry for this Se atom and consequently, a linear Se−Se−Se moiety. Indeed, the Se−Se−Se angle is ~171°. Clearly, in view of the Th results the formal oxidation state of U in $Rb_4U_4P_4Se_{26}$ presents an interesting puzzle.

37.4.13 $K_2UP_3Se_9$ and $A_2ThP_3Se_9$ (A = K, Rb)

Two polymorphs of $K_2AnP_3Se_9$ are known. α-$K_2UP_3Se_9$ (Chondroudis and Kanatzidis, 1996) is another example of a layered material (Fig. 37.57a, b). It contains two crystallographically unique U atoms that are coordinated by nine Se atoms in a tricapped trigonal prismatic geometry (Fig. 37.57c, d). All Se atoms are provided by $P_2Se_6^{4-}$ units. The basic building block of the structure is a U_2Se_{14} dimer that is formed by face sharing of two individual USe_9 polyhedra (Fig. 37.57c, d). Each dimer shares its two apical corners with two adjacent dimers, thus forming chains running along the *c*-axis (Fig. 37.57b). The chains are interconnected through $P_2Se_6^{4-}$ units to form layers (Fig. 37.56a, b). There are several bonding modes of the $P_2Se_6^{4-}$ bridges in this structure, which serve to stitch the U_2Se_{14} dimers into a chain (Fig. 37.57c, d). The α-$A_2ThP_3Se_9$ (A = K, Rb) compounds (Briggs Piccoli *et al.*, 2000) are isostructural to α-$K_2U_3P_3Se_9$.

$K_2UP_3Se_9$ shows Curie–Weiss behavior above 100 K and an effective magnetic moment of 3.72 μ_B, a value consistent with the presence of the U^{4+} cation. Below 100 K an antiferromagnetic order was observed.

The compound β-$K_2ThP_3Se_9$ is also known (Briggs Piccoli *et al.*, 2002). It also is a layered structure. The Th atoms coordinate with nine Se atoms (all provided by $P_2Se_6^{4-}$ units) in a tricapped-trigonal prismatic geometry (Fig. 37.58a, b). The $ThSe_9$ units are corner sharing along the *b*-axis and are arranged in a zigzag fashion. To form the layer, the chains of the $ThSe_9$ polyhedra are joined through $P_2Se_6^{4-}$ groups (Fig. 37.58b). The interconnection of the $ThSe_9$ chains creates a

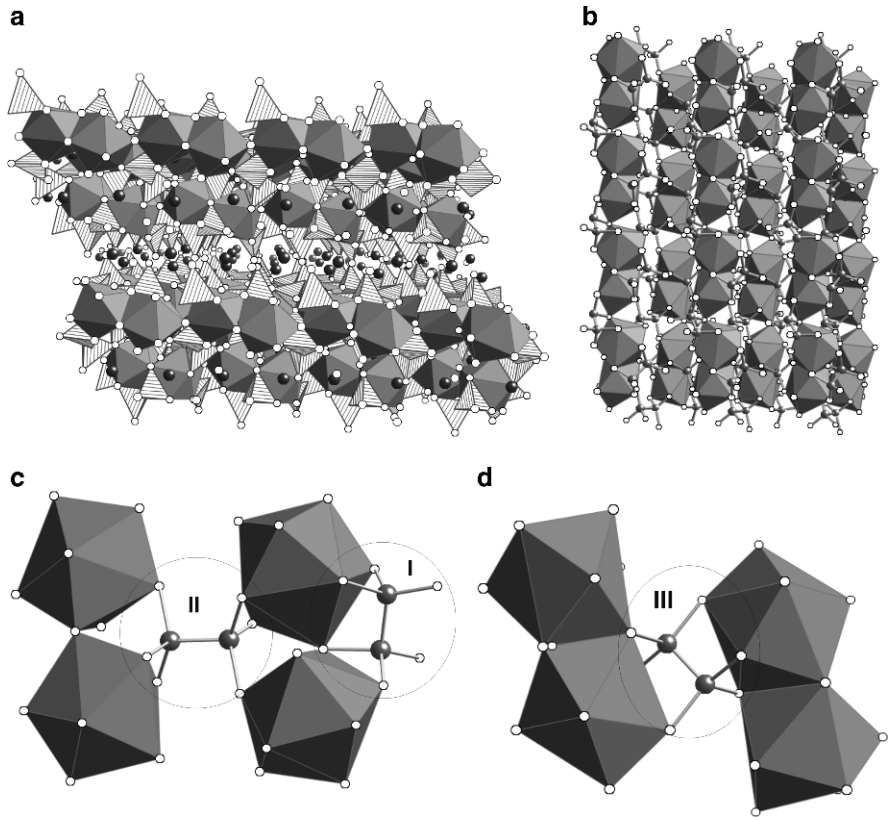

Fig. 37.57 (*a*) *The structure of* $K_2UP_3Se_9$ *viewed down the a-axis* (USe_9*: gray polyhedra;* PSe_4*: striped polyhedra; K: black balls*); (*b*) *a single layer of* $K_2UP_3Se_9$ *viewed down the b-axis* (USe_9*: gray polyhedra; P: gray balls; Se: white balls*); (*c*) *representation of the binding modes I and II for the* $P_2Se_6^{4-}$ *groups* (USe_9*: gray polyhedra; P: gray balls; Se: white balls*); (*d*) *representation of the binding mode III for the* $P_2Se_6^{4-}$ *groups* (USe_9*: gray polyhedra; P: gray balls; S: white balls*).

layer with relatively large openings (4 Å × 11.5 Å). Note that both α- and *β*-polymorphs were found in the same reaction products, indicating a possible equilibrium between these two phases. Both compounds are based on the same selenophosphate building blocks and display the same coordination geometry for the Th atoms. However, the α-phase displays a dense layered structure, whereas the structure of the *β*-phase is based on corrugated layers.

37.4.14 $Cs_2Hg_2USe_5$

The compound $Cs_2Hg_2USe_5$ was obtained from the solid-state reaction of U, HgSe, Cs_2Se_3, Se, and CsI (as flux) at 850°C (Bugaris *et al.*, 2009). This material

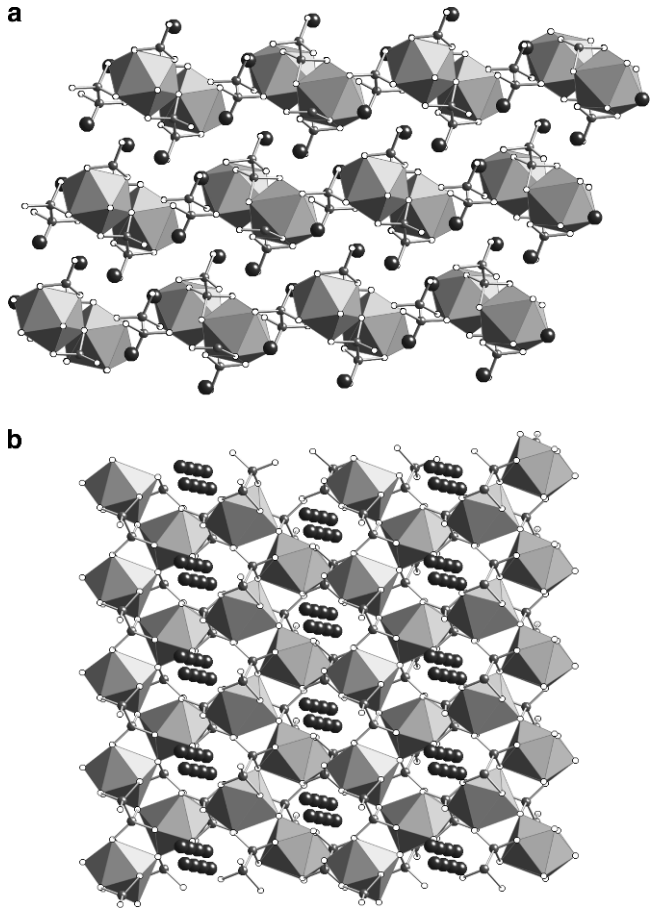

Fig. 37.58 (*a*) *The layered structure of β-$K_2ThP_3Se_9$ viewed down the b-axis;* (*b*) *a single layer of β-$K_2ThP_3Se_9$ viewed down the a-axis* (*$ThSe_9$: gray polyhedra; P: gray balls; K: black balls; Se: white balls*).

crystallizes in a new structure type in space group $P2/n$ of the monoclinic system. The structure contains $^{2}_{\infty}[Hg_2USe_5]^{2-}$ layers separated by Cs^+ cations (Fig. 37.59a). Within the layers are distorted $HgSe_4$ tetrahedra and regular USe_6 octahedra (Fig. 37.59b). In the temperature range of 17–300 K $Cs_2Hg_2USe_5$ displays Curie–Weiss behavior with $\mu_{eff} = 3.82(2)\ \mu_B$. The compound exhibits semiconducting behavior in the [010] direction; the conductivity at 298 K is 3×10^{-3} S/cm. Formal oxidation states of Cs/Hg/U/Se may be assigned as +1/+2/+4/−2, respectively.

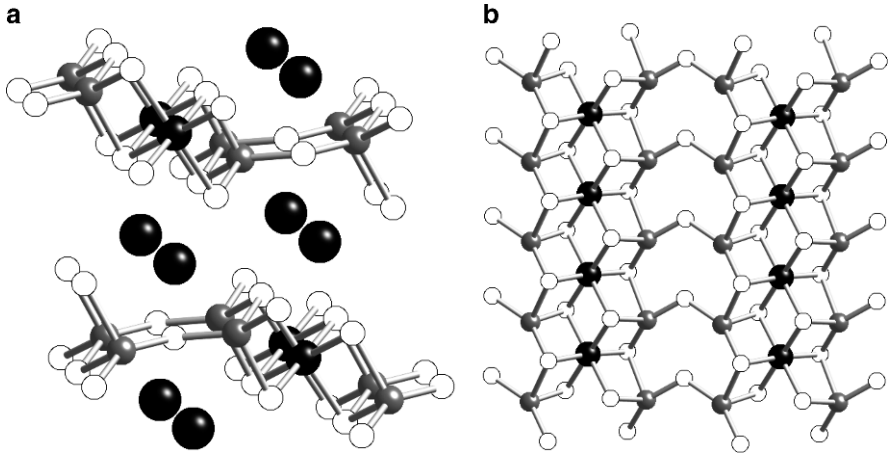

Fig. 37.59 (*a*) *View of the structure of* $Cs_2Hg_2USe_5$ *down the b-axis;* (*Cs: black non bonded; U: black bonded; Hg: gray; Se: white*) (*b*) *view of a single layer of* $Cs_2Hg_2USe_5$ *down the c-axis.*

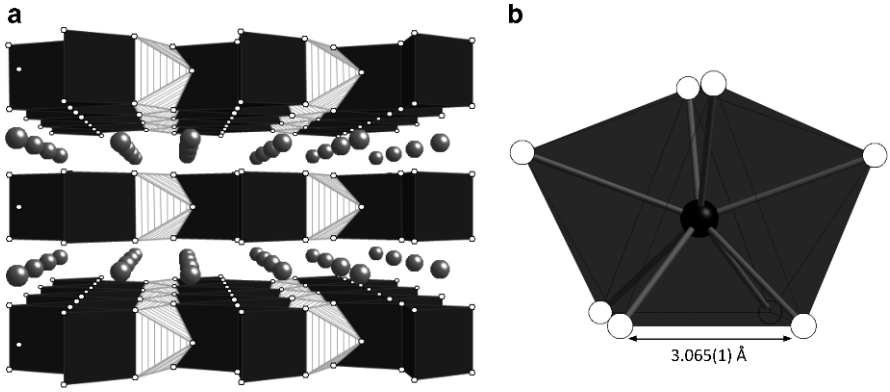

Fig. 37.60 (*a*) *View of the layered structure of* $CsTiUTe_5$ *down the a-axis* (*UTe_8: black polyhedra; $TiTe_6$: striped polyhedra; Te: white balls; Cs: gray balls*); (*b*) *the UTe_8 bicapped trigonal prism with indication of the short* [3.065(1) Å] *Te–Te interactions.*

37.4.15 $CsMUTe_5$ (M = Ti, Zr)

$CsMUTe_5$ (M = Ti, Zr) compounds have a layered structure that is built from UTe_8 bicapped trigonal prisms that share a common edge and $TiTe_6$ octahedra that share faces (Cody and Ibers, 1995; Kim *et al.*, 2006) (Fig. 37.60a). The Te–Te interactions (3.065(1) Å) observed within the layers are longer than a single bond (Fig.37.60b). This chain of short Te–Te interactions could induce

high conductivity in the material; however, the room-temperature conductivity measured along the direction of the Te–Te chain is low ($1.2(9) \times 10^{-3}$ $\Omega^{-1}cm^{-1}$). $CsTiUTe_5$ is paramagnetic with an effective magnetic moment of 2.23 μ_B, close to the calculated value for U^{5+} (2.54 μ_B). Again given the rarity of U^{5+} species in chalcogenide chemistry, additional characterization of the oxidation state is desirable.

37.4.16 $Cs_8Hf_5UTe_{30.6}$

$Cs_8Hf_5UTe_{30.6}$ (Cody and Ibers, 1995) consists of $Hf_3Te_{15.6}^{4-}$ and $Hf_2UTe_{15}^{4-}$ chains (Fig. 37.61). The U atoms adopt an eightfold coordination. The Te–Te distances in this compound are very short (2.70–3.07 Å) and therefore simple electron counting and oxidation-state formalisms are difficult to apply.

37.4.17 $KCuThS_3$, $K_2Cu_2ThS_4$, $K_3Cu_3Th_2S_7$

$KCuThS_3$, $K_2Cu_2ThS_4$, and $K_3Cu_3Th_2S_7$ are layered compounds (Selby *et al.*, 2005). $KCuThS_3$ is isostructural to $KZrCuS_3$ whereas the other two compounds

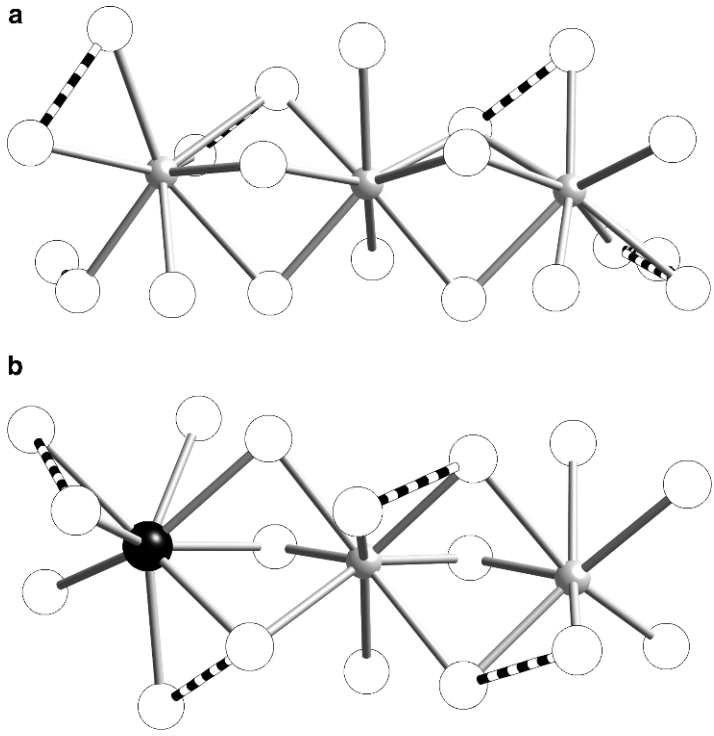

Fig. 37.61 (*a*) *The* $[Hf_3Te_{15.6}]^{4-}$ *chain* (*Hf: gray; Te: white*); (*b*) *The* $[Hf_2UTe_{15}]^{4-}$ *chain* (*U: black*). *Te–Te bonds are shown as horizontal multi-banded bonds.*

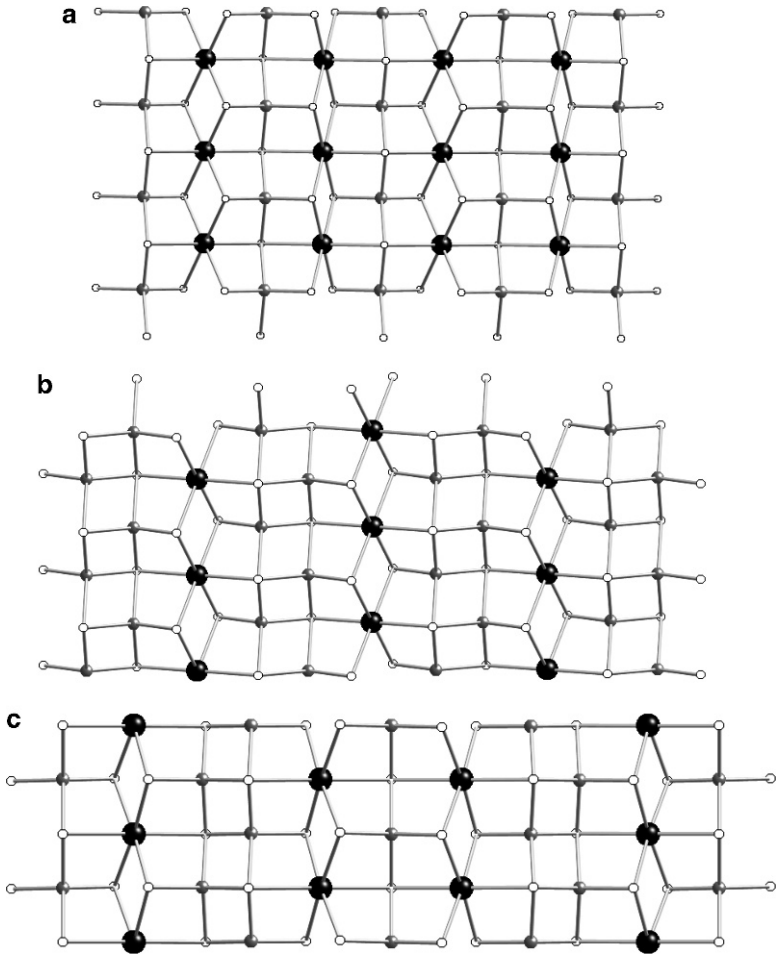

Fig. 37.62 *View of the layered structures of* (*a*) *$KCuThS_3$*, (*b*) *$K_2Cu_2ThS_4$*, *and* (*c*) *$K_3Cu_3Th_2S_7$* (*Th: black; Cu: dark gray; S: white balls; K^+ were omitted for clarity*).

have closely related structures. There is an interesting relationship among the structures of the three materials. Each layer of $KCuThS_3$ is built from alternating single lines of ThS_6 octahedra and CuS_4 tetrahedra (Fig. 37.62a), whereas the layer of $K_2Cu_2ThS_4$ consists of alternating single threads of ThS_6 octahedra and double threads of CuS_4 tetrahedra (Fig. 37.62b). A hybrid of the structures of $KCuThS_3$ and $K_2Cu_2ThS_4$ is the structure of $K_3Cu_3Th_2S_7$. It is composed of single and double threads of CuS_4 tetrahedra separated by threads of ThS_6 octahedra (Fig. 37.62c).

$KCuThS_3$, $K_2Cu_2ThS_4$, and $K_3Cu_3Th_2S_7$ are semiconductors with band gaps of 2.95, 2.17, and 2.49 eV, respectively. These band gaps were rationalized on

the basis of the continuity of the CuS_4 framework; Th^{4+} with an $5f^0$ electronic configuration was deemed less important in influencing the band gaps of these compounds. $K_2Cu_2ThS_4$ with double threads of CuS_4 tetrahedra displays more extended Cu−S interactions and consequently more diffuse bands and a smaller band gap than the other compounds. $KCuThS_3$ with only single threads of CuS_4 tetrahedra contains the least diffuse bands and the lowest band gap energy, whereas $K_3Cu_3Th_2S_7$, which contains both single and double threads of CuS_4 tetrahedra, shows an intermediate band gap.

37.4.18 $Cs_4Th_4P_6S_{18}$

$Cs_4Th_4P_6S_{18}$ has a layered structure (Chan *et al.*, 2005), Fig. 37.63a. Two crystallographically unique Th centers can be found. One of them is coordinated to

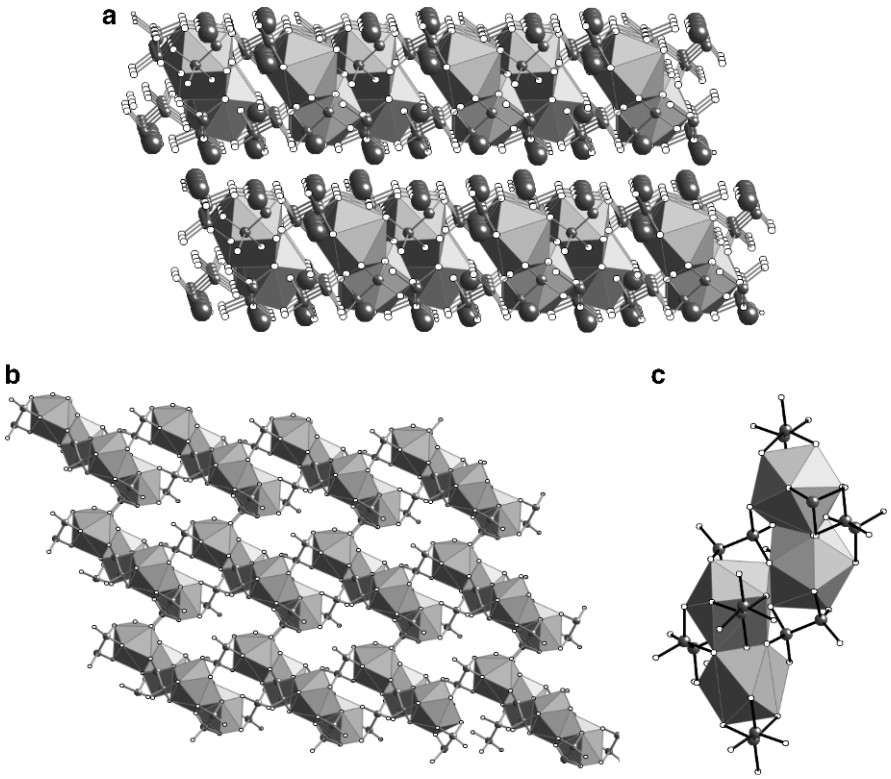

Fig. 37.63 (*a*) *View of the structure of* $Cs_4Th_4P_6S_{18}$ *down the c-axis;* (*b*) *representation of a layer of* $Cs_4Th_4P_6S_{18}$ *showing the connectivity of tetramers of* ThS_9 *and* ThS_{10} *units through* $P_2S_6^{4-}$ *groups;* (*c*) *the tetramer of two* ThS_{10} *units* (*core of the tetramer*) *and two* ThS_9 *units* (*edges of the tetramer*) (*ThS_9 and ThS_{10}: gray polyhedra; P: small gray balls; S: white balls; Cs: large black balls*).

ten S atoms in a sphenocoronal geometry. The second is bound to nine S atoms in a distorted tricapped trigonal prism. All S atoms are provided by $P_2S_6^{4-}$ groups. The building block in this structure is a tetramer of Th polyhedra (Fig.37.63b). Each tetramer contains two 10- and two 9-coordinated Th atoms. The ten-coordinated Th atoms constitute the core of this tetramer and are edge-shared, whereas the nine-coordinated Th atoms cap the tetramer and each shares a triangular face with each of the ten-coordinated Th centers. To form the layers, the individual tetramers are linked through $P_2S_6^{4-}$ groups (Fig.37.63c).

37.4.19 $K_{10}Th_3(P_2S_7)_4(PS_4)_3$

$K_{10}Th_3(P_2S_7)_4(PS_4)_3$ displays a layered structure (Hess *et al.*, 2001). It contains two crystallographically independent Th atoms (Th1, Th2), both coordinated with eight S atoms in a dodecahedral geometry. Adjacent Th2 atoms are bridged through $P_2S_7^{4-}$ units, whereas Th2 atoms are connected with Th1 centers by either $P_2S_7^{4-}$ or PS_4^{3-} groups. A single layer of $K_{10}Th_3(P_2S_7)_4(PS_4)_3$ comprises two intertwined chains with the arrangement Th2-P_2S_7-Th1-PS_4-Th2 (Fig. 37.64). The intertwined chains create channels running along the *b*-axis.

37.4.20 $KThSb_2Se_6$

$KThSb_2Se_6$ displays an interesting three-dimensional structure (Fig. 37.65a) with K atoms filling tunnels running parallel to the *a*-axis (Choi *et al.*, 1997). It contains nine-coordinated Th^{4+} atoms in a tricapped trigonal prismatic geometry. A notable feature of the structure is the presence of double chains of Th atoms running parallel to [100] (Fig. 37.65b). The single chains comprise $ThSe_6$ prisms sharing opposite triangular faces and are bridged through Se_2^{2-} groups to form the double chains. Interestingly, each Se_2^{2-}unit is bound to four Th atoms. The double chains are separated by $[Sb_4Se_{10}]_n$ blocks (Fig. 37.65a). The Sb atoms are coordinated with six Se atoms in a distorted octahedral geometry and the $SbSe_6$ octahedra are connected to each other by edge sharing.

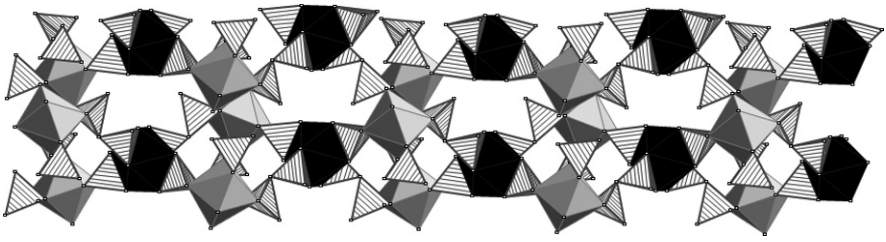

Fig. 37.64 *View of a single layer* $K_{10}Th_3(P_2S_7)_4(PS_4)_3$ *down* [101] (*ThS_8: black polyhedra; Th_2S_8: gray polyhedra; P−S units: striped polyhedra*).

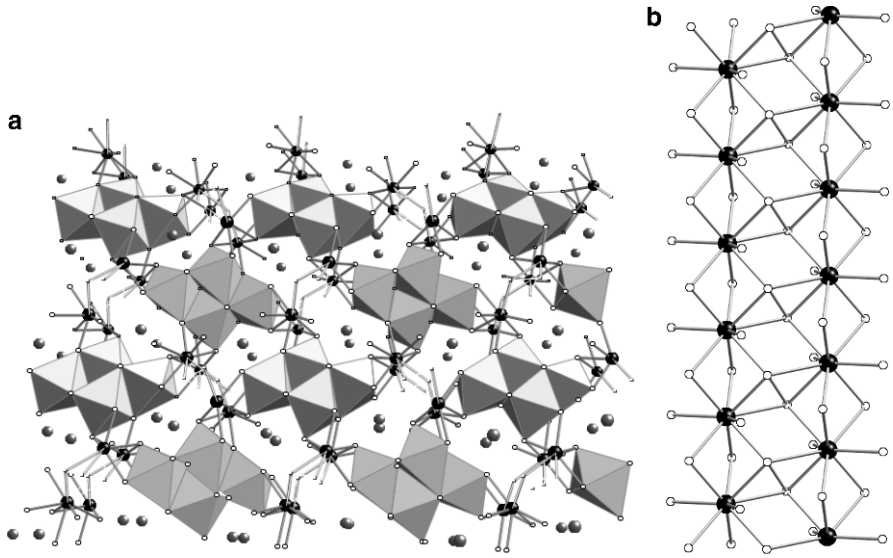

Fig. 37.65 (*a*) *View of the structure of* $KThSb_2Se_6$ *down the a-axis;* (*b*) *representation of the double chain of* $ThSe_6$ *prisms running parallel to the a-axis* (SbS_6*: gray polyhedra; K: dark gray balls; Th: black balls; Se: white balls*).

37.4.21 $Cs_4Th_2P_5Se_{17}$

$Cs_4Th_2P_5Se_{17}$ displays a structure (Briggs Piccoli *et al.*, 2000) with similarities to that of the $A_2ThP_3Se_9$ (A = K, Rb) compounds (Section 37.4.13). The structure of $Cs_4Th_2P_5Se_{17}$ is also based on dimers of Th polyhedra sharing triangular faces that are connected by adjacent dimers through their apical Se atoms to form chains (Fig. 37.66a, b). Unlike the structure of $A_2ThP_3Se_9$ in which all Th centers are nine-coordinated, the structure of $Cs_4Th_2P_5Se_{17}$ contains both eight- and nine-coordinated Th atoms. The eight-coordinated Th atom adopts a bicapped trigonal prismatic geometry. The nine-coordinated Th center does not display a coordination geometry similar to that of the Th atoms in $A_2ThP_3Se_9$. Rather the coordination environment around the nine-coordinated Th atoms includes an η^2-Se_2^{2-} unit. If we consider the Se_2^{2-}group to occupy a single coordination site, then the overall coordination geometry of the nine-coordinated Th atom can be described as bicapped trigonal prismatic (Fig. 37.66c).

37.4.22 $Rb_7Th_2P_6Se_{21}$

$Rb_7Th_2P_6Se_{21}$ has a one-dimensional chain structure (Chan *et al.*, 2005). Each of the two crystallographically unique Th atoms (Th1 and Th2) is coordinated by eight Se atoms in a distorted bicapped trigonal prismatic geometry. Th1 and Th2 polyhedra share one Se atom and they are further connected through

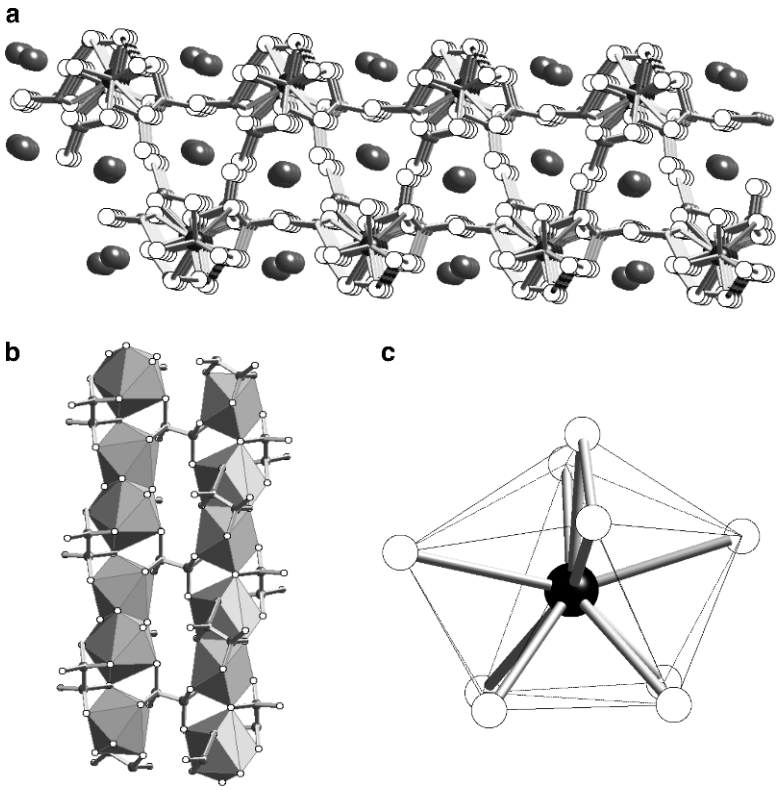

Fig. 37.66 (*a*) *View of the structure of* $Cs_4Th_2P_5Se_{17}$ *down the a-axis* ($ThSe_8$ *and* $ThSe_9$*: gray polyhedra; P: small dark gray balls; Se: white balls; Cs: large dark gray balls*); (*b*) *the chains of Th polyhedra connected by* $P_2Se_6^{4-}$ *units;* (*c*) *the nine-coordinated Th atom* (*black ball*) *in bicapped trigonal-prismatic geometry.*

threefold coordination of two PSe_4^{3-} units. By bridging adjacent Th1-Th1 polyhedra through two PSe_4^{3-} groups, a tetramer of Th polyhedra is created. The chain is then formed by the interconnection of neighboring tetramers through $P_2Se_6^{4-}$ groups (Fig. 37.67).

37.4.23 $K_3Pu(PS_4)_2$

$K_3Pu(PS_4)_2$ has a chain structure (Fig. 37.68) (Hess *et al.*, 2002). It contains PuS_8 bicapped trigonal prisms. Each PuS_8 polyhedron shares two of its edges with two other PuS_8 polyhedra to form $Pu(PS_4)_2^{3-}$ chains. All S atoms belong to PS_4^{3-} units. These share three of their S atoms with the Pu centers leaving the fourth S atom available for ionic interactions with the K atoms. The Pu center has a formal oxidation state of +3.

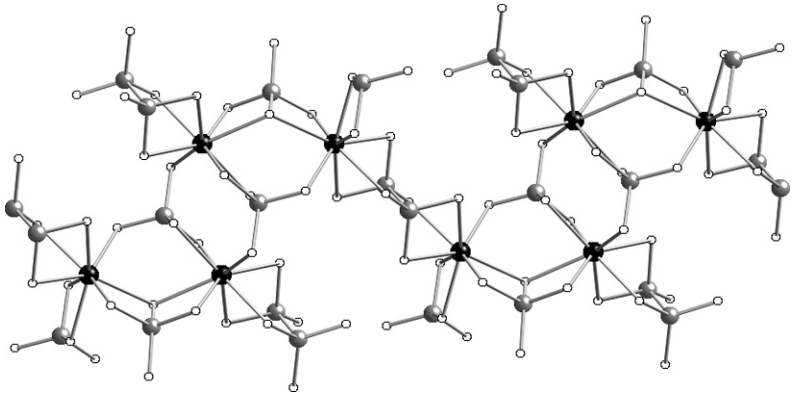

Fig. 37.67 *The chain structure of $Rb_7Th_2P_6Se_{21}$ (Th: black; P: gray; Se: white).*

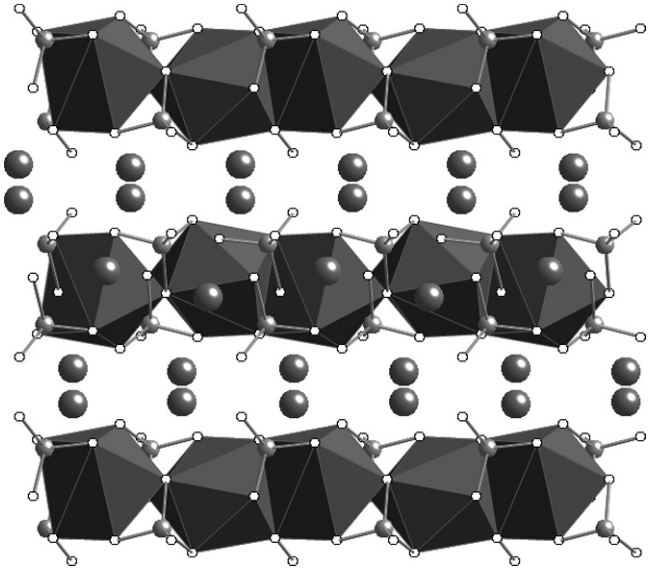

Fig. 37.68 *The structure of $K_3Pu(PS_4)_2$ viewed down the c-axis (PuS_8: black polyhedra; P: gray balls; S: white balls; K: black balls).*

37.4.24 $APuP_2S_7$ (A = K, Rb, Cs)

The $APuP_2S_7$ (A = K, Rb, Cs) compounds are isostructural and display a layered structure (Fig. 37.69a, b) (Hess *et al.*, 2002). The Pu atoms are coordinated with eight S atoms, provided by the $P_2S_7^{4-}$ units, in a distorted square

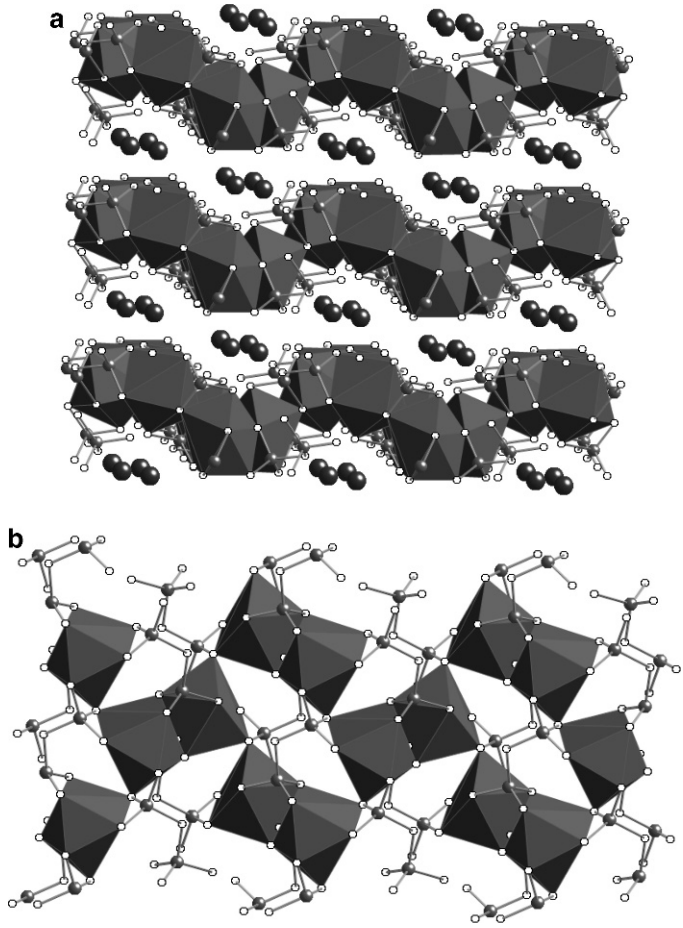

Fig. 37.69 (*a*) *The structure of* $KPuP_2S_7$ *viewed down the c-axis;* (*b*) *a single layer of* $KPuP_2S_7$ *viewed down the a-axis* (*PuS_8: black polyhedra; P: gray balls; S: white balls; K: black balls*).

antiprismatic geometry. The fundamental building block of the structure is a dimer of PuS_8 polyhedra sharing one edge. The dimers are linked through corner-sharing PuS_8 units. In addition, the $P_2S_7^{4-}$ groups further connect the PuS_8 polyhedra in a chelate fashion. Corrugated layers with channels running perpendicular to the layer are formed by the arrangement of the corner- and edge-sharing PuS_8 polyhedra and the multidentate $P_2S_7^{4-}$ groups. The formal oxidation state of Pu is +3 from charge balance and the optical transitions seen in the diffuse reflectance spectra of these materials.

LIST OF ABBREVIATIONS

An	actinide
DFT	density functional theory
EXAFS	extended X-ray absorption fine structure
°C	degree Celsius
e	electron
eV	electron volt
EPR	electron paramagnetic resonance
IR	infrared
K	kelvin
M	elements N−Bi, Si−Pb, metal
oct	octahedron
Q	chalcogen: S, Se, or Te
T_c	Curie temperature
T_N	Néel temperature
tet	tetrahedron
tp	trigonal prism
UV	Ultraviolet
VIS	visible
VSEPR	valence shell electron pair repulsion
XPS	X-ray photoelectron spectroscopy
μ_B	Bohr magneton

ACKNOWLEDGMENT

JAI acknowledges the support of the U.S. Department of Energy, Basic Energy Sciences, Chemical Sciences, Biosciences, and Geosciences Division and Division of Materials Sciences and Engineering grant ER-15522. MGK acknowledges the support from the National Science Foundation, Division of Materials Research.

REFERENCES

Amoretti, G., Blaise, A., Bogé, M., Bonnisseau, D., Burlet, P., Collard, J. M., Fournier, J. M., Quézel, S., Rossat-Mignod J. (1989) *J. Magn. Magn. Mater.*, **79**, 207–24.

Amoretti, G., Blaise, A., Bonnet, M., Caciuffo, R., Erdos, P., Noel, H., Santini P. (1995) *J. Magn. Magn. Mater.*, **139**, 339–46.

Amoretti, G., Blaise, A., Burlet, P., Gordon, J. E., and Troc, R. (1986). *J. Less-Common Met.*, **121**, 233–48.

Amoretti, G., Calestani, G., and Giori, D. C. (1984). *Z. Naturforsch. A.*, **39**, 778–82.

Baenziger, N. C., Rundle R. E., Snow, A. I., Wilson, A. S., (1950), *Acta Crystallogr.*, **3**, 34–40.

Bazan, C. and Zygmunt, A. (1972). *Phys. Status Solidi A*, **12**, 649–53.

Beck, H. P. and Dausch, W. (1988). *Z. Naturforsch. B*, **43**, 1547–50.
Beck, H. P. and Dausch, W. (1989a). *Z. Anorg. Allg. Chem.*, **571**, 162–4.
Beck, H. P. and Dausch, W. (1989b). *J. Solid State Chem.*, **80**, 32–9
Beck, J. and Fischer, A. (2002). *Z. Anorg. Allg. Chem.*, **628**, 369–72.
Ben Salem, A., Meerschaut, A., and Rouxel, J. (1984). *Cr. Hebd. Acad. Sci., II*, **299**, 617–9.
Benz, R. and Zachariasen, W. H. (1969). *Acta Crystallogr.*, **B25**, 294–6.
Benz, R. and Zachariasen, W. H. (1970). *Acta Crystallogr.*, **B26**, 823–7.
Blaise, A., Lagnier, R., Wojakowski, A., Zygmunt, A., and Mortimer, M. J. (1980). *J. Low Temp. Phys.*, **41**, 61–72.
Breeze, E. W., Brett, N. H., and White, J. (1971). *J. Nucl. Mater.*, **39**, 157–65.
Briggs Piccoli, P. M., Abney, K. D., and Dorhout, P. K. (2002). *J. Nucl. Sci. Technol.*, **3**, 611–5.
Briggs Piccoli, P. M., Abney, K. D., Schnoover, J. R., and Dorhout, P. K. (2000). *Inorg. Chem.*, **39**, 2970–6.
Briggs Piccoli, P. M., Abney, K. D., Schoonover, J. D., and Dorhout, P. K. (2001). *Inorg. Chem.*, **40**, 4871–5.
Brochu, R., Padiou, J., and Grandjean, D. (1970b). *Cr. Acad. Sci. C. Chim.*, **271**, 642–3.
Brochu, R., Padiou, J., and Prigent, J. (1970a). *Cr. Acad. Sci. C. Chim.*, **270**, 809–10.
Brochu, R., Padiou, J., and Prigent, J. (1972). *Cr. Acad. Sci. C. Chim.*, **274**, 959–61.
Bugaris, D. E., Wells, D. M., and Ibers, J. A. (2009). *J. Solid State Chem.*, **182**, 1017–20.
Busch, G. and Vogt, O. (1978). *J. Less-Common Met.*, **62**, 335–42.
Chan, B. C., Hess, R. F., Feng, P. L., Abney, K. D., and Dorhout, P. K. (2005). *Inorg. Chem.*, **44**, 2106–13.
Chan, B. C., Hulvey, Z., Abney, K. D., and Dorhout, P. K. (2004). *Inorg. Chem.*, **43**, 2453–5.
Chenevier, B., Wolfers, P., Bacmann, M., and Noel, H. (1981). *Cr. Acad. Sci. II B*, **293**, 649–52.
Chevrel, R., Sergent, M., and Prigent, J. (1971). *J. Solid State Chem.*, **3**, 515–9.
Choi, K. S., Iordanidis, L., Chondroudis, K., and Kanatzidis, M. G. (1997). *Inorg. Chem.*, **36**, 3804–5.
Choi, K. S. and Kanatzidis, M. G. (1999). *Chem. Mater.*, **11**, 2613–8.
Choi, K. S., Patschke, R., Billinge, S. J. L., Waner, M. J., Dantus, M., and Kanatzidis, M. G. (1998). *J. Am. Chem. Soc.*, **120**, 10706–14.
Chondroudis, K. and Kanatzidis, M. G. (1996). *Cr. Hebd. Acad. Sci., II.* **322**, 887–94.
Chondroudis, K. and Kanatzidis, M. G. (1997). *J. Am. Chem. Soc.*, **119**, 2574–5.
Cody, J. A. and Ibers, J. A. (1995). *Inorg. Chem.* **34**, 3165–72.
Cody, J. A. and Ibers, J. A. (1996). *Inorg. Chem.* **35**, 3836–8.
Conradson, S. D., Abney, K. D., Begg, B. D., Brady, E. D., Clark, D. L., Den Auwer, C., Ding, M., Dorhout, P. K., Espinosa-Faller, F. J., Gordon, P. L., Haire, R. G., Hess, N. J., Hess, R. F., Keogh, D. W., Lander, G. H., Lupinetti, A. J., Morales, L. A., Neu, M. P., Palmer, P. D., Paviet-Hartmann, P., Reilly, S. D., Runde, W. H., Tait, C. D., Veirs, D. K., and Wastin, F. (2004a). *Inorg. Chem.* **43**, 116–31.
Conradson, S. D., Begg, B. D., Clark, D. L., Den Auwer, C., Ding, M., Dorhout, P. K., Espinosa-Faller, F. J., Gordon, P. L., Haire, R. G., Hess, N. J., Hess, R. F., Keogh, D. W., Morales, L. A., Neu, M. P., Paviet-Hartmann, P., Runde, W., Tait, C. D., Veirs, D. K., and Villella, P. M. (2004b). *J. Am Chem. Soc.*, **126**, 13443–58.

Conradson, S. D., Begg, B. D., Clark, D. L., Den Auwer, C., Ding, M., Dorhout, P. K., Espinosa-Faller, F. J., Gordon, P. L., Haire, R. G., Hess, N. J., Hess, R. F., Webster Keogh, D., Lander, G. H., Manara, D., Morales, L. A., Neu, M. P., Paviet-Hartmann, P., Rebizant, J., Rondinella, V. V., Runde, W., Tait, C. D., Veirs, D. K., Villella, P. M., and Wastin, F. (2005). *J. Solid State Chem.*, **178**, 521–35.

Costantini, J. M., Damien, D., De Novion, C. H., Blaise, A., Cousson, A., Abazli, H., and Pages, M. (1983). *J. Solid State Chem.* **47**, 210–18.

d'Eye, R. W. M. (1953). *J. Chem. Soc.*, **1953**, 1670–2.

d'Eye, R. W. M. and Sellman, P. G. (1954). *J. Chem. Soc.*, **1954**, 3760–6.

d'Eye, R. W. M., Sellman, P. G., and Murray, J. R. (1952). *J. Chem. Soc.*, **1952**, 2555–62.

Dabos-Seignon, S., Benedict, U., Heathman, S., Spirlet, J. C., and Pages, M. (1990). *J. Less-Common Met.*, **160**, 35–52.

Damien, D. (1973). *Inorg. Nucl. Chem. Lett.* **9**, 453–6.

Damien, D. (1974). *J. Inorg. Nucl. Chem.* **36**, 307–8.

Damien, D., de Novion, C. H., and Gal, J. (1981). *Solid State Commun*. **38**, 443–40

Daoudi, A., Lamire, M., Levet, J. C., and Noel, H. (1996c). *J. Solid State Chem.*, **123**, 331–6.

Daoudi, A., Levet, J. C., Potel, M., and Noel, H. (1996a). *Mater. Res. Bull.*, **31**, 1213–8.

Daoudi, A. and Noel, H. (1985). *J. Solid State Chem.* **60**, 131–4.

Daoudi, A. and Noel, H. (1986a). *Inorg. Chim. Acta.*, **117**, 183–5.

Daoudi, A. and Noel, H. (1986b). *J. Less-Common Met.*, **115**, 253–9.

Daoudi, A. and Noel, H. (1987). *Inorg. Chim. Acta*, **140**, 93–5.

Daoudi, A. and Noel, H. (1989). *J. Less-Common Met.*, **153**, 293–8.

Daoudi, A. and Noel, H. (1996). *J. Alloy. Compd.* **233**, 169–73.

Daoudi, A., Potel, M., and Noel, H. (1996b). *J. Alloy. Compd.* **232**, 180–5.

Dell, R. M., Carney, R. F. A., and Allbutt, M. (1967). Application, GB Patent No. 1060130.

de Novion, C. H., Damien, D., and Hubert, H. (1981). *J. Solid State Chem*. **39**, 360–7

Do, J., Kim, J., Lah, S., and Yun, H. (1993) *Bull. Korean Chem. Soc.*, **14**, 678–681.

Ellert, G. V., Kuz'micheva, G. M., Eliseev, A. A., Slovyanskikh, V. K., and Morozov, S. P. (1974). *Zh. Neorg. Khim.*, **19**, 2834–8.

Ferro, R. (1954). *Z. Anorg. Allg. Chem.*, **275**, 320–6.

Ferro, R. (1955). *Atti Accad. Nazl. Lin.*, **18**, 641–4.

Furuseth, S., Brattas, L., and Kjekshus, A. (1975). *Acta Chem. Scand. A*. **29**, 623–31.

Furuseth, S. and Fjellvag, H. (1991). *Acta Chem. Scand. A*. **45**, 694–7.

Gieck, C. and Tremel, W. (2002). *Chem. Eur. J.* **8**, 2980–7.

Gray, D. L., Backus, L. A., von Nidda, H. A. K., Skanthakumar, S., Loidl, A., Soderholm, L., and Ibers, J. A. (2007). *Inorg. Chem.* **46**, 6992–6.

Haessler, M., de Novion, C. H., and Damien, D. (1976). *Plutonium 1975*, *Proc. Int. Conf.*, **1975**, 649–57.

Handwerk, J. H. and Kruger, O. L. (1971). *Nucl. Eng. Des.*, **17**, 397–408.

Handwerk, J. H., White, G. D., and Shalek, P. D. (1965). Application, US Patent No. 3194745.

Haneveld, A. J. K. and Jellinek, F. (1964). *J. Inorg. Nucl. Chem.* **26**, 1127–8.

Haneveld, A. J. K. and Jellinek, F. (1969). *J. Less-Common Met.*, **18**, 123–9.

Henkie, Z., Cichorek, T., Pietraszko, A., Fabrowski, R., Wojakowski, A., Kuzhel, B. S., Kepinski, L., Krajczyk, L., Gukasov, A., and Wisniewski, P. (1998). *J. Phys. Chem. Solids.* **59**, 385–93.

Hess, R. F., Abney, K. D., Burris, J. L., Hochheimer, H. D., and Dorhout, P. K. (2001). *Inorg. Chem.* **40**, 2851–9.

Hess, R. F., Gordon, P. L., Tait, C. D., Abney, K. D., and Dorhout, P. K. (2002). *J. Am. Chem. Soc.*, **124(7)**, 1327–33.

Huang, F. Q. and Ibers, J. A. (2001). *J. Solid State Chem.*, **159**, 186–90.

Huang, F. Q., Mitchell, K. and Ibers, J. A. (2001). *Inorg. Chem.* **40**, 5123–6.

Hulliger, F. (1968). *J. Less-Common Met.*, **16**, 113–17.

Ijjaali, I., Mitchell, K., Huang, F. Q., and Ibers, J. A. (2004). *J. Solid State Chem.*, **177**, 257–61.

Jaulmes, S., Julien-Pouzol, M., Dugue, J., Laruelle, P., Vovan, T., and Guittard, M. (1990). *Acta Crystallogr. C.* **46**, 1205–7.

Jaulmes, S., Julien-Pouzol, M., Guittard, M., Vovan, T., Laruelle, P., and Flahaut, J. (1986). *Acta Crystallogr. C.* **42**, 1109–11.

Jin, G. B., Choi, E. S., and Ibers, J. A. (2009). *Inorg. Chem.* **48**, 8227–32.

Julien, R., Rodier, N., and Tien, V. (1978). *Acta Crystallogr.* **B34**, 2612–4.

Julien-Pouzol, M., Jaulmes, S., Mazurier, A., and Guittard, M. (1981). *Acta Crystallogr.* **B37**, 1901–3

Kaczorowski, D., Noel, H., Potel, M., and Zygmunt, A. (1994). *J. Phys. Chem. Solids.* **55**, 1363–7.

Kaczorowski, D., Poettgen, R., Gajek, Z., Zygmunt, A., and Jeitschko, W. (1993). *J. Phys. Chem. Solids.* **54**, 723–31.

Kanatzidis, M. G. and Sutorik, A. C. (1995). *Progr. Inorg. Chem.* **43,** 151–265.

Khodadad, P. (1959). *Cr. Hebd. Acad. Sci.* **249**, 694–6.

Khodadad, P. (1961). *Compt. Rend.* **253**, 1575–7.

Kikuchi, A. and Fukuda, K. (1974). *Creep strength of the uranium monocarbide containing small quantity of uranium monosulfide*, Japan At. Energy Res. Inst.,Tokyo, Japan.

Kim, J. Y., Gray, D. L. and Ibers, J. A. (2006). *Acta Crystallogr.* **E62**, I124–I125.

Kohlmann, H. and Beck, H. P. (1997). *Z. Anorg. Allg. Chem.* **623**, 785–90.

Kohlmann, H. and Beck, H. P. (1999). *Z. Kristallogr.*, **214**, 341–5.

Kohlmann, H., Stöwe, K., and Beck, H. P. (1997). *Z. Anorg. Allg. Chem.* **623**, 897–900.

Komac, M., Golic, L., Kolar, D., and Brcic, B. S. (1971). *J. Less-Common Met.* **24**, 121–8.

Kruger, O. L. and Moser, J. B. (1967). *J. Phys. Chem. Solids* **28**, 2321–5.

Kwak, J. E., Gray, D. L., Yun, H. and Ibers, J. A. (2006). *Acta Crystallogr.* **E62**, I86–I87.

Leciejewicz, J., Zolnierek, Z., Ligenza, S., Troc, R., and Ptasiewicz, H. (1975). *J. Phys. C Solid State* **8**, 1697–704.

Leciejewicz, J., Zolnierek, Z., and Troc, R. (1977). *Solid State Commun.* **22**, 697–9.

Leciejewicz, J. and Zygmunt, A. (1972). *Phys. Status Solidi A*, **13**, 657–60.

Lelieveld, R. and Ijdo, D. J. W. (1980). *Acta Crystallogr.* **B36**, 2223–6.

Lovell, G. H. B. and Van Tets, A. (1979). *J. Nucl. Mater.* **79**, 277–301.

Lovell, G. H. B., Van Tets, A., and Britz, E. J. (1973). *J. Nucl. Mater.* **48**, 74–8.

Mansuetto, M. F., Jobic, S., Ng, H. P., and Ibers, J. A. (1993). *Acta Crystallogr. C* **49**, 1584–5.

Mansuetto, M. F., Keane, P. M., and Ibers, J. A. (1992). *J. Solid State Chem.*, **101**, 257–64.
Marcon, J. P. and Pascard, R. (1966). *Cr. Acad. Sci. C. Chim.* **262**, 1679–81.
Mattenberger, K., Scherrer, L., and Vogt, O. (1984). *J. Cryst. Growth.* **67**, 467–71.
Mattenberger, K. and Vogt, O. (1992). *Phys. Scr.* **T45**, 103–9.
Mitchell, A. W. and Lam, D. J. (1970). **37**, 349–52.
Mitchell, A. W. and Lam, D. J. (1971). *J. Nucl. Mater.* **39**, 219–23.
Mizoguchi, H., Gray, D., Huang, F. Q., and Ibers, J. A. (2006). *Inorg. Chem.* **45**, 3307–11.
Mooney-Slater, R. C. L. (1977). *Z. Kristallogr. Krist.*, **120**, 278–85.
Moseley, P. T., Brown, D., and Whittaker, B. (1972). *Acta Crystallogr.* **B28**, 1816–21.
Narducci, A. A. and Ibers, J. A. (1998a). *Chem. Mater.* **10**, 2811–23.
Narducci, A. A. and Ibers, J. A. (1998b). *Inorg. Chem.* **37**, 3798–801.
Narducci, A. A. and Ibers, J. A. (2000). *Inorg. Chem.* **39**, 688–91.
Neimark, L. A. and Carlander, R. (1964). *IMD Special Rep. Ser.*, **10**, 753–64.
Noel, H. (1973). *C. R. Acad. Sci. C. Chim* **277**, 463–4.
Noel, H. (1974). *C. R. Acad. Sci. C. Chim.* **279**, 513–15.
Noel, H. (1980). *J. Less-Common Met.* **72**, 45–9.
Noel, H. (1984). *Mater. Res. Bull.*, **19**, 1171–5.
Noel, H. (1985a). *Physica B and C*, **130**, 499–500
Noel, H. (1985b). *Inorg. Chim. Acta*, **109**, 205–7.
Noel, H. (1986). *J. Less-Common Met.*, **121**, 265–70.
Noel, H. and le Marouille, J. Y. (1984). *J. Solid State Chem.* **52**, 197–202
Noel, H. and Levet, J. C. (1989). *J. Solid State Chem.* **79**, 28–33.
Noel, H. and Padiou, J. (1976a). *Acta Crystallogr.* **B32**, 1593–5.
Noel, H. and Padiou, J. (1976b). *Acta Crystallogr.* **B32**, 605–6.
Noel, H., Padiou, J., and Prigent, J. (1971). *Cr. Acad. Sci. C. Chim.* **272**, 206–8.
Noel, H., Padiou, J., and Prigent, J. (1975b). *Cr. Acad. Sci. C. Chim.* **280**, 123–6.
Noel, H. and Potel, M. (1982). *Acta Crystallogr.* **B38**, 2444–5.
Noel, H. and Potel, M. (1985). *J. Less-Common Met.*, **113**, 11–5.
Noel, H., Potel, M., and Padiou, J. (1975a). *Acta Crystallogr.*, **B31**, 2634–7.
Noel, H., Potel, M., Shlyk, L., Kaczorowski, D., and Troc, R. (1995). *J. Alloy. Compd.*, **217**, 94–6.
Noel, H., Potel, M., Troc, R., and Shlyk, L. (1996). *J. Solid State Chem.* **126**, 22–6.
Noel, H. and Prigent, J. (1980). *Physica B and C*, **102**, 372–9.
Olsen, J. S., Gerward, L., Benedict, U., Luo, H., and Vogt, O. (1988). *High Temp. - High Press.* **20**, 553–9.
Padiou, J. and Guillevi.J. (1969). *Cr. Acad. Sci. C. Chim.* **268**, 822–4.
Pearson, W. B. (1985). *Z. Kristallogr.*, **171**, 23–39.
Pietraszko, D. and Lukaszewicz, K. (1975). *Bull. Acad. Pol. Sci. Chim.*, **23(4)**, 337–40.
Potel, M., Brochu, R., and Padiou, J. (1975). *Mater. Res. Bull.*, **10**, 205–8.
Potel, M., Brochu, R., Padiou, J., and Grandjea.D. (1972). *CR. Acad. Sci. C. Chim.* **275**, 1419–21.
Ptasiewicz-Bak, H., Leciejewicz, J., and Zygmunt, A. (1978). *Phys. Status Solidi A*, **47**, 349–56.
Rocker, F. and Tremel, W. (2001). *Z. Anorg. Allg. Chem.* **627**, 1305–8.
Rodier, N. and Tien, V. (1976). *Acta Crystallogr.* **B32**, 2705–7.

Sato, N., Nakajima, T., Yamada, K., and Fujino, T. (1999). *Korean J. Ceram.* **5**, 348–52.
Selby, H. D., Chan, B. C., Hess, R. F., Abney, K. D., and Dorhout, P. K. (2005). *Inorg. Chem.*, **44(18)**, 6463–9.
Shlyk, L., Stepien-Damm, J., Troc, R., and Kaczorowski, D. (1995a). *J Alloys Compds.*, **219**, 264–6.
Shlyk, L., Troc, R., and Kaczorowski, D. (1995b). *J. Magn. Magn. Mater.*, **140–144**, 1435–6.
Simon, A., Peters, K., and Peters, E. M. (1982). *Z. Anorg. Allg. Chem.*, **491**, 295–300.
Slovyanskikh, V. K., Kuznetsov, N. T., and Gracheva, N. V. (1984). *Zh. Neorg. Khim.*, **29**, 1676–8.
Stocks, K., Eulenberger, G., and Hahn, H. (1981). *Z. Anorg. Allg. Chem.*, **472**, 139–48.
Stöwe, K. (1996a). *Z. Anorg. Allg. Chem.*, **622**, 1419–22.
Stöwe, K. (1996b). *Z. Anorg. Allg. Chem.*, **622**, 1423–7.
Stöwe, K. (1997). *Z. Anorg. Allg. Chem.*, **623**, 749–54.
Stöwe, K. and Appel-Colbus, S. (1999). *Z. Anorg. Allg. Chem.*, **625**, 1647–51.
Sunshine, S. A., Kang, D., and Ibers, J. A. (1987). *J. Am. Chem. Soc.*, **109**, 6202–4.
Suski, W., Gibinski, T., Wojakowski, A., and Czopnik, A. (1972). *Phys. Stat. Solidi A*, **9**, 653–8.
Sutorik, A. C., Albritton-Thomas, J., Hogan, T., Kannewurf, C. R., and Kanatzidis, M. G. (1996). *Chem. Mater.*, **8**, 751–61.
Sutorik, A. C. and Kanatzidis, M. G. (1997a). *Polyhedron*, **16**, 3921–7.
Sutorik, A. C. and Kanatzidis, M. G. (1997b). *Chem. Mater.*, **9**, 387–98.
Sutorik, A. C. and Kanatzidis, M. G. (1997c). *J. Am. Chem. Soc.*, **119**, 7901–2.
Sutorik, A. C., Patschke, R., Schindler, J., Kannewurf, C. R., and Kanatzidis, M. G. (2000). *Chem. Eur. J.*, **6**, 1601–7.
Szytula, A. and Suski, W. (1973). *Acta Phys. Polonica*, *A*, **43**, 631–2.
Tien, V., Guittard, M., Flahaut, J., and Rodier, N. (1975). *Mater. Res. Bull.*, **10**, 547–54.
Tougait, O., Andre, G., Bouree, F., and Noel, H. (2001). *J. Alloy. Compd.*, **317–318**, 227–32.
Tougait, O., Daoudi, A., Potel, M., and Noel, H. (1997b). *Mater. Res. Bull.*, **32(9)**, 1239–45.
Tougait, O., Potel, M., Levet, J. C., and Noel, H. (1998a). *Eur. J. Solid State Inorg. Chem.*, **35**, 67–76.
Tougait, O., Potel, M., and Noel, H. (1998b). *Inorg. Chem.*, **37**, 5088–91.
Tougait, O., Potel, M., and Noel, H. (1998c). *J. Solid State Chem.*, **139**, 356–61.
Tougait, O., Potel, M., and Noel, H. (2002). *J. Solid State Chem.*, **168**, 217–23.
Tougait, O., Potel, M., Padiou, J., and Noel, H. (1997a). *J. Alloy. Compd.*, **262–263**, 320–4.
Troc, R., Kaczorowski, D., Shlyk, L., Potel, M., and Noel, H. (1994). *J. Phys. Chem. Solids*, **55(9)**, 815–23.
Trzebiatowski, W., Niemiec, J., and Sepichowska, A. (1961). *Bull. Acad. Pol. Sci. Chim.*, **9**, 373–7.
Van Lierde, W. and Bressers, J. (1966). *J. Appl. Phys.*, **37**, 444.
Vogt, O., Mattenberger, K., and Lohle, J. (2001). *J. Magn. Magn. Mater.*, **231**, 199–212.
Vovan, T. and Rodier, N. (1979). *Cr. Acad. Sci. C. Chim.*, **289**, 17–20.
Wastin, F., Spirlet, J. C., and Rebizant, J. (1995). *J. Alloy. Compd.*, **219**, 232–7.

Wawryk, R., Wojakowski, A., Pietraszko, A., and Henkie, Z. (2005). *Solid State Commun.*, **133**, 295–300.
Wedgwood, F. A. and Kuznietz, M. (1972). *J. Phys. C Solid State*, **5**, 3012–20.
Wells, D. M., Skanthakumar, S., Soderholm, L., Ibers, J. A. (2009) *Acta Crystallogr.*, **E65**, i14.
Wolfers, P. and Fillion, G. (1977). *Physica B and C*, **86**, 896–8.
Wu, E. J., Pell, M. A., and Ibers, J. A. (1997). *J. Alloy. Compd.*, **255**, 106–9.
Yao, J. and Ibers, J. A. (2008). *Anorg. Allg. Chem.*, **634**, 1645–7.
Yao, J., Malliakas, C. D., Jin, G. B., Wells, D. M., Balasubramanian, M., Kanatzidis, M. G., and Ibers, J. A. (2010). Unpublished.
Yao, J., Wells, D. M., Chan, G. H., Zeng, H.-Y., Ellis, D. E., Van Duyne, R. P., and Ibers, J. A. (2008). *Inorg. Chem.*, **47**, 6873–9.
Yoshihara, K., Kanno, M., and Mukaibo, T. (1967). *J. Nucl. Sci. Technol.-T*, **4**, 578–81.
Zachariasen, W. H. (1949a). *Acta Crystallogr.*, **2**, 288–91.
Zachariasen, W. H. (1949b). *Acta Crystallogr.*, **2**, 57–60
Zachariasen, W. H. (1949c). *Acta Crystallogr.*, **2**, 60–2.
Zachariasen, W. H. (1949d). *Acta Crystallogr.*, **2**, 291–6.
Zeng, H. Y., Yao, J., and Ibers, J. A. (2008). *J. Solid State Chem.*, **181**, 552–5.
Zogal, O. J. and Zygmunt, A. (1982). *J. Magn. Magn. Mater.*, **27**, 293–7.
Zumbusch, M. (1940). *Z. Anorg. Allg. Chem.*, **243**, 322–9.
Zygmunt, A., Ligenza, S., Ptasiewicz, H., and Leciejewicz, J. (1974a). *Phys. Status Solidi A*, **25**, 77–80
Zygmunt, A., Murasik, A., Ligenza, S., and Leciejew.J. (1974b). *Phys. Status Solidi A*, **22**, 75–9.